UNIVERSITEIT VAN PRETORIA
UNIVERSITY OF PRETORIA
YUNIBESITHI YA PRETORIA

EXPERIMENTAL INVESTIGATION AND MODEL DEVELOPMENT FOR THE THERMAL CONDUCTIVITY OF GLYCEROL-BASED NANOFLUIDS

by

Ntumba TSHIMANGA

Submitted in partial fulfilment of the requirements for the degree

MASTER OF SCIENCE (Mechanical Engineering)

in the

Faculty of Engineering, Built Environment and Information Technology

University of Pretoria

2016

ABSTRACT

Title: Experimental investigation and model development for thermal conductivity of glycerol-based nanofluids

Student: Ntumba Tshimanga

Supervisors: Dr Mohsen Sharifpur and Prof Josua P Meyer

Department: Mechanical and Aeronautical Engineering

University: University of Pretoria

Degree: Master of Science

Glycerol has historically been used as an antifreeze fluid to facilitate heat transfer in the automotive and air conditioning and refrigeration industries. It has also been used as a lubricant in the processing of food and the production of pharmaceuticals and cosmetics. Although a lot of work has been done recently to evaluate the potential to enhance heat transfer using nanoparticles mixed with a base fluid to form a nanofluid, no work has been done on using glycerol as a base fluid. Therefore the purpose of this study was to investigate the effect of nanoparticle volume fraction, nanoparticle size and temperature on the thermal conductivity of stable glycerol-based nanofluids. Two types of metal oxide nanoparticles were considered namely MgO and α-Al_2O_3. The particle sizes of the MgO ranged from 21 nm to 119 nm and for the α-Al_2O_3 it ranged from 31 nm to 134 nm. The thermal conductivities were determined by experimental measurements and with analytical and empirical models. The thermal conductivity measurements were taken at temperatures ranging from 20˚C to 45˚C, for nanofluids prepared at volume fractions ranging from 0.5% to 4%. The nanofluids were prepared

with a two-step method that included ultrasound mixing to ensure the nanoparticles were fully dispersed and deagglomerated in the glycerol. The experimental results showed that both the α-Al_2O_3-glycerol and MgO-glycerol nanofluids had substantially higher thermal conductivity than the base fluid. It was also found that at room temperature, the effective thermal conductivity remains almost constant for at least 50 hours. The maximum thermal conductivity enhancement for the α-Al_2O_3-glycerol nanofluids was observed for a 4% volume fraction to be 19.5% for a nanoparticle size of 31 nm. For the MgO-glycerol nanofluids the maximum thermal conductivity enhancements were also for a volume fraction of 4%, however, the enhancement was 18% for a particle size of 21 nm. Furthermore, the thermal conductivities as function of nanoparticle size, volume fraction and temperature, of the two nanofluids were investigated. It was found that the thermal conductivities of the α-Al_2O_3-glycerol nanofluids were significantly more dependent on particle size than the MgO-glycerol nanofluids. Furthermore, it was found that no equations exist at present that can accurately predict the thermal conductivity of glycerol based nanofluids and therefore new empirical equations correlations were developed.

Keywords: *Nanofluids, thermal conductivity, glycerol, nanoparticle size, volume fraction, temperature, stability.*

DEDICATION

To my wife, Joelle Muteba, and

children, Joedy, Jessica, Joy and Joshua.

ACKNOWLEDGEMENTS

I would like to express my greatest gratitude to the following people for their assistance, support and encouragement during my studies:

Firstly, I thank my supervisor, Dr Mohsen Sharifpur, for his enormous consideration, encouragement, unsheakable patience, constructive suggestions, guidance and consistent support throughout my research. It has been a real privilege to work with him.

My special thanks go to the Head of the Department of Mechanical and Aeronautical Engineering at the University of Pretoria, Professor Josua P. Meyer, who accepted me in the thermoflow research group, provided me with the financial support and co-supervised my dissertation. It has been an honour working under his supervision.

I am grateful for the help, support and assistance that I have received from the nanofluid research group members, Saheed, Dr Mehrabi, Dr Nwosu, Gaettan, Sanama, Inegbedion, Mahdavi and Hadi during the dissertation work. I would also like to thank my office colleague and friend, Gerard Muteba, for his useful comments and encouragement.

I am extending my exceptional thanks to my lovely wife, Joelle Muteba Mbuyi, for her love, encouragement and support during my dissertation work. I would also like to thank my others two daughters, Patricia Muteba and Monique Yowa, for their supports.

Lastly, I would like to thank my parents, brothers and sisters, brothers-in-law, sisters-in-law and friends for their encouragement and support during my studies.

TABLE OF CONTENTS

LIST OF FIGURES

LIST OF TABLES

NOMENCLATURE

A_p	Projected area of nanoparticle, m^2
$circ$	Circularity
d	Diameter, m
D	Einstein diffusion coefficient
F	F-statistic
h	Non-locality characteristic length, m
$\hbar$	Ratio, $\hbar = \frac{r}{h}$
k	Thermal conductivity (W/mK)
K	A shape factor
$\Im 1$	Ratio, $\Im 1 = \frac{1}{\hbar} + \arctan(\hbar) - \frac{\pi}{2}$
$\Im 2$	Ratio, $\Im 2 = \arctan(\hbar) + \frac{\hbar}{1+\hbar^2} + \frac{8\hbar}{(1+\hbar^2)^2} + \frac{8\hbar^3}{(1+\hbar^2)^3} - \frac{\pi}{2}$
m	Matrix
p	p-value
P	Outline perimeter of nanoparticle, m
Pr	Prandtl number
r	Radius, m
R	Coefficient of correlation
Re	Reynolds number
R_k	Interfacial resistance, Km^2W^{-1}
SSA	Specific surface area, m^2

T	Temperature, ˚C
t	Time, s
$t_{v,p}$	Weighing function for ν degree of freedom and P% of probability
u	Uncertainty
u_B	Bias error
u_p	Precision or random error
wt.	Weight fraction of the species
W	Weight, kg

Greek symbols

α	Nanoparticle Biot number
β	Full-width at half maximum, rad
ε	Fraction of liquid volume that travels with a nanoparticle
γ	Ratio between the thermal conductivity of nanolayer and thermal conductivity of particle
δ	Nanolayer thickness
θ	Diffraction angle, rad
κ	Boltzmann's constant, J/K
λ	X-ray wavelength, Å
μ	Viscosity, N.s/m^2
v	Velocity, m/s
ξ	Ratio, $\xi = \frac{k_p - k_f}{3(\Im 1 k_p - \Im 2 k_f)}$

ρ	Density, kg/m^3
σ_1	Ratio, $\sigma_1 = \left(1 + \frac{\delta}{r_p}\right)$
σ_2	Ratio, $\sigma_2 = \left(1 + \frac{\delta}{2r_p}\right)$
ς	Ratio, $\left(1 - \frac{k_f}{k_{pe}}\right)$
τ_D	Time necessary for nanoparticle of diameter d_p to cover the distance equal to its size, s
ϕ	Volume fraction
ϕ_e	Equivalent volume fraction, $\phi_e = \phi(1 + \chi)^3$
χ	Ratio between the nanolayer thickness and particle radius
ω	Volume ratio of spherical nanoparticle and complex nanoparticle

Subscripts

$cryst$	Crystallite
eff	Effective
f	Fluid
fr	Freezing point of the base liquid
gly	Glycerol
$layer$	Nanolayer
m	Matrix
p	Particle
pe	Equivalent particle

TCR	Thermal conductivity ratio
10	10% of nanoparticles have diameter less than
50	Mean of particle diameter distribution
90	90% of nanoparticles have diameter less than

Abbreviations

ASTM	American Society for Testing and Materials
CFD	Computational fluid dynamics
CGPA	Cumulative grade point average
CSIR	Council for Scientific and Industrial Research
DEM	Differential effective medium
EEDSM	Energy efficiency and demand-side management
EG	Ethylene glycol
FWHM	Full width at half maximum
IEEE	Institute of Electrical and Electronics Engineers
IRT	Institutional Research Theme
MgO	Magnesium oxide
MG	Maxwell-Garnett
NAC	National Aerospace Centre
NRF	National Research Foundation
S	Sample
TCR	Thermal conductivity ratio
VIF	Variance inflation factor

W	Water
XRD	X-ray powder diffraction
XRF	X-ray fluorescence spectroscopy

PUBLICATIONS IN JOURNALS AND CONFERENCE PROCEEDINGS

Articles in peer-reviewed journals:

1. N. Tshimanga, M. Sharifpur and J. P. Meyer, "Experimental investigation and model development for thermal conductivity of glycerol-MgO nanofluids", *International Journal of Heat Transfer Engineering*, HTE 7414, 2015 **(accepted).**

2. N. Tshimanga, M. Sharifpur and J. P. Meyer, "Experimental investigation and model development for thermal conductivity of glycerol-Al_2O_3 nanofluids", *International Communications in Heat and Mass Transfer*, 2015 (**under preparation).**

Conference papers:

1. M. Sharifpur, T. Ntumba, J.P. Meyer, Parametric analysis of effective thermal conductivity models for nanofluids, *Proceedings of the ASME 2012 International Mechanical Engineering Congress and Exposition,* American Society of Mechanical Engineers, IMECE2012-85093, 2012, pp. 1-11.

2. J.P. Meyer, P. N. Nwosu, M. Sharifpur, T. Ntumba, Parametric analysis of effective viscosity models for nanofluids, *Proceedings of the ASME 2012 International Mechanical Engineering Congress and Exposition,* American Society of Mechanical Engineers, IMECE2012-93200, 2012, pp. 1149-1157.

3. N. Tshimanga, M. Sharifpur and J. P. Meyer, "The effect of sonication time on effective thermal conductivity of glycerol-MgO based nanofluids", *Proceedings of the 15th International Heat Transfer Conference*, IHTC15-8595, August 10-15, 2014, Kyoto, Japan.

CHAPTER 1: INTRODUCTION

1.1 Background

Water is one of the best choices for liquid cooling applications due to its availability, low viscosity, acceptable heat capacity and thermal conductivity. However, in the cold weather regions, water alone is less desired because of the freezing point at 0 ˚C. Instead, an ethylene glycol and water mixture (60:40 wt.) is widely used for the heat-transfer fluid in building heating systems, geothermal heat and cooling systems, automobiles and heat exchangers [1-3]. Glycerol is commonly known as an additive in many creams and lotions to keep the skin soft and moisturised. It was historically used as an antifreeze for a broad range of mechanical equipment during the winter period to prevent freezing of aqueous heat transfer fluids before being replaced by ethylene glycol in the 1930s due to cost considerations.

Nowadays, glycerol, being more environmentally friendly than ethylene glycol, is being examined by the ASTM International Committee D15 in order to use it in automotive applications [4]. The situation is due to a surplus production of glycerol in the global market since 2004 from biodiesel. The biodiesel production produces 10% (w/w) of glycerol; thus 4 billion gallons of crude glycerol are expected by 2016 for the projected 47 billion gallons of biodiesel. This situation could impact on the cost-effective return of glycerol as antifreeze. In 2007, the price per pound of crude glycerol in the USA decreased from $0.25 to $0.05 [5]. The price of refined glycerol per ton fell from $2 000 in 1995 to $1 000 in 1998. It recovered to $1 500 in 2000, then decreased to about $900. In 2012 and early 2013, the price was $838 to $1014/ton and $900/ton respectively. Thus, new opportunities for glycerol are considered in various industries.

A total of 2 million ton of glycerol has been produced annually since 2011. It was about 200 000 ton in 2003, 600 000 ton in 2006, more than 2 million in 2011 and 2012 [6]. The estimated usage of the global refined glycerol in 2015 is 2 million ton compared with 0.8 million in 2009 (see Figure 1.1). The global production of crude glycerol is expected to be 6 million ton by 2025.

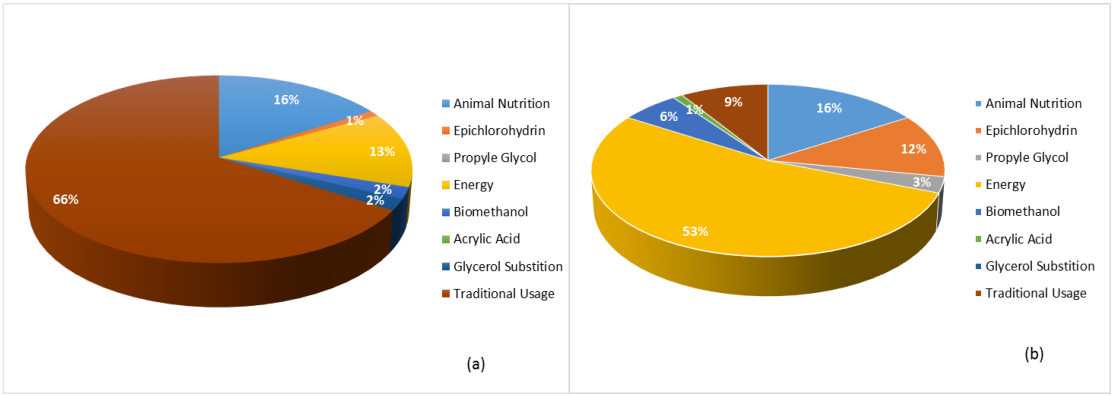

Figure 1.1: Previous and future glycerol application [6]

The automobile industry uses nanofluids not only as a coolant but also as fuel additive, lubricant, shock absorber and refrigerant. Lubricants with suspended nanoparticles improve the load capacity, reduce the wear resistance and friction between the moving components of vehicles, and consequently, improve their lifetime. Nanofluids as a shock absorber in modern cars absorb more vibrations and provide a comfortable ride [3, 7, 8]. Oil coolant-based nanofluids increase the maximum engine power, maximum torque and improve the fuel efficiency [9].

Glycerol is often used as a lubricant not only because of its high viscosity but also for its ability to better remain fluid at low temperatures and resist oxidation than oil. Glycerol is suggested rather than mineral oils for oxygen compressor, pumps and

bearings exposed to gasoline and benzene as well as where there is contact with the lubricant in the food, pharmaceutical and cosmetic manufacturing and other machinery where the purity is of paramount importance. It is used as plasticisers of heat casings and special types of papers (glassine and greaseproof paper). Glycerol is also used as an ingredient in cough medicine, anaesthetics, for ear treatment and as bacteriological culture media [10].

1.2 Motivation

In view of the interest in glycerol, especially in the automotive industry and food, pharmaceutical and cosmetic manufacturing, it was deemed necessary to study the applicability of glycerol-based nanofluids for heat transfer applications.

The literature review relevant to this dissertation reveals the lack of reported data on the thermal conductivity of glycerol-based nanofluids. Therefore, this research explains the factors influence on the thermal conductivity of metal oxide-based glycerol nanofluids.

1.3 Objectives of the present research

The goals of the research presented in this dissertation are:

- to measure the effective thermal conductivity of glycerol-based nanofluids from 20 ˚C to 45 ˚C, prepared with various nanoparticles including MgO and α-Al_2O_3 at volume fractions ranging from 0.5% to 4% and particle sizes between 21 nm and 119 nm for the MgO and 31 nm and 134 nm for the α-Al_2O_3 respectively;

- to statistically analyse the effect of measurable parameters such as the volume fraction, diameter, temperature and elapsed time after preparation on the thermal conductivity ratio of glycerol nanofluids;
- to compare the obtained experimental data with the predicted values from available theoretical and empirical models which may work for glycerol-based nanofluids;
- to develop a new empirical correlation for the thermal conductivity of glycerol-based nanofluids with measurable variables.

1.4 Method, scope and limitations

The work experimentally investigated the effect of parameters (volume fraction, diameter, temperature and elapsed time after preparation) on the thermal conductivity ratio of glycerol-based nanofluids, and the development of a new mathematical model for predictive purposes for glycerol-based nanofluids. The glycerol was mixed with various particles, including MgO and α-Al_2O_3 having particle sizes ranging from 21 nm to 119 nm for the MgO and 31 nm to 134 nm for the α-Al_2O_3 respectively.

The effective thermal conductivity of glycerol-based nanofluids was measured in the laboratory with KD2 Pro thermal conductivity probe (Decagon Device, US). Because of the limitation of the KD2 Pro, the investigation was carried out between 20 ˚C and 45 ˚C at particle volume fractions between 0.5% and 4%.

The stability of glycerol-based nanofluid samples was evaluated for a high-volume fraction (4%) of nanoparticles. Thirty minutes after sonication, the effective thermal conductivity was measured for various particle sizes at one-hour step, up to 50 hours.

The experimental data of thermal conductivity were compared with the predicted values of some existing theoretical and empirical models which may work for glycerol-based nanofluids such as the Maxwell, Bruggeman, effective medium theory, Shaker *et al.*, Vajjha *et al.* and Corcione models. A multivariate regression analysis was conducted to evaluate the impact of involved parameters on the thermal conductivity of glycerol nanofluids. Thus, new empirical correlations for MgO and α-Al_2O_3-glycerol-based nanofluids were developed.

1.5 Organisation of the dissertation

The dissertation consists of six chapters and appendices. Chapter 1 presents the background, objectives, scope limitations, motivation and organisation of the study. Chapter 2 deals with the literature review relevant to the thermal conductivity of nanofluids. The literature review discusses the experimental results of the thermal conductivity of nanofluids and the mechanisms involved in the enhancement of the thermal conductivity of nanofluids. The chapter also presents the available experimental correlations for and models of the thermal conductivity of nanofluids. Chapter 3 deals with the investigated materials of the study, their physical characterisation and the nanofluid preparation. The chapter also offers the experimental set-up, the validation of the experimental data and the uncertainty calculation with additional information in Appendix A. Chapter 4 discusses the thermal conductivity of α-Al_2O_3-glycerol-based nanofluid results for each independent parameter (volume fraction, temperature, nanoparticle size and glycerol properties) influencing the thermal conductivity of nanofluids. The chapter also presents and develops the new correlations for the thermal conductivity of α-Al_2O_3-glycerol-based nanofluids. A regression

analysis is conducted to determine how the measurable variables jointly influence the TCR of α-Al_2O_3-glycerol-based nanofluids. The additional information of regression analysis is presented in Appendix B. Chapter 5 deals with all the work described in Chapter 4 but applied to MgO-glycerol-based nanofluid. Chapter 6 presents the summary of the investigation, conclusions from the study and the recommendations for future work.

CHAPTER 2: LITERATURE REVIEW

2.1 Introduction

This chapter deals with the literature review relevant to the thermal conductivity of nanofluids. It presents the experimental results of the thermal conductivity of nanofluids suspended with distinct nanoparticles viz metal, metal oxides, ceramic oxides and carbon nanotubes. The nanoparticles were prepared with different liquid coolants such as water, ethylene glycol, a mixture of water and ethylene glycol at various proportions, engine oil and transformer oil, at various sonication times and conditions. The chapter also presents the mechanisms involved in the enhancement of the thermal conductivity of nanofluids and the available experimental correlations for and models of the thermal conductivity of nanofluids.

2.2 Experimental results of the thermal conductivity of nanofluid

2.2.1 Introduction

The publications dealing with nanofluids reveal that the thermal conductivity of nanofluids is influenced by several parameters, such as the nanoparticle volume fraction, temperature, particle size, thermal conductivity of the nanoparticle, thermal conductivity of the base fluid, settlement time, sonication time, viscosity of base fluid and pH of the nanofluid [11-30].

2.2.2 Effect of nanoparticle volume fraction

Masuda *et al.* [31] presented the first experimental data for the thermal conductivity of nanofluids. The nanofluids were prepared with water as a base fluid and three types of nanoparticles, namely Al_2O_3 (13 nm), SiO_2 (12 nm) and TiO_2 (27 nm). The

experimental data were carried in the temperature range of 31.85 ˚C to 86.85 ˚C and the particle volume fraction ranged from 1.3% to 4.3%. They reported a linear increase in the thermal conductivity of nanofluid with volume fraction, which reached the maximum enhancement of 32.4%, 10.8% and 1.1 for Al_2O_3, TiO_2 and SiO_2 respectively, at 31.85 ˚C. They also state that the thermal conductivity ratio of nanofluids decreases with temperature increase.

Lee *et al.* [31, 32] measured the thermal conductivity of nanofluids prepared with CuO (23.6 nm) and Al_2O_3 (38.4 nm) in both base fluids, water and ethylene glycol. They reported an increase in the thermal conductivity of nanofluid with volume fraction for both CuO and Al_2O_3 suspended in water or EG. The maximum increase of 18% and 23% in thermal conductivity was observed respectively for CuO-EG and Al_2O_3-EG nanofluids of the maximum volume fraction (4%) at room temperature, while it was 12% and 10% for CuO-water and Al_2O_3-water-based nanofluids.

In a recent study, Ghanbarpour *et al.* [33] experimentally measured the thermal conductivity of water-based Al_2O_3 nanofluids. Nanoparticles of spherical shape and an average size of about 75 nm were investigated at a mass concentration ranging from 3% to 50% and temperature range of 293 K to 323 K. They observed that the thermal conductivity increased non-linearly with nanoparticle concentration, but linearly with a rise in temperature. The thermal conductivity enhancements were in the range of 1.1% to 87%. In addition, they depicted that at high-mass concentration, the thermal conductivity ratio had a decreasing slope with temperature. The nanoparticle agglomeration possibly occurred because of an increase in nanoparticle number and motion.

2.2.3 Effect of temperature

Li and Peterson [34] measured the effect of volume fraction and temperature on the thermal conductivity of Al_2O_3-distilled water and CuO-distilled water nanofluids. The average diameters of Al_2O_3 and CuO were 29 nm and 36 nm respectively. The nanofluids prepared at a volume fraction of 2% to 10% were analysed at a temperature range of 27.5 ˚C to 34.7 ˚C. A maximum enhancement of 51% was observed for the CuO-water nanofluid at the maximum temperature.

Das *et al.* [32] measured the thermal conductivity of Al_2O_3 or CuO-water nanofluids with temperatures ranging from 21˚C to 51˚C and particle volume fraction ranging from 1% to 4%. They depicted an increase in thermal conductivity with an increase in both volume fraction and temperature. The thermal conductivity of 4% Al_2O_3-water nanofluids increased from 9.4% to 24.3% when the temperature rose from 21 ˚C to 51 ˚C, whereas it increased from 6.5% to 29% and from 14% to 36% for 1% and 4% CuO-EG nanofluids respectively for the same temperature range.

2.2.4 Effect of particle size

Vajjha and Das [1] experimentally investigated the thermal conductivity of three nanofluids containing aluminium oxide, copper oxide and zinc oxide dispersed in an ethylene glycol and water mixture (60:40 %wt.) over a temperature range of 298-363K for nanoparticle volume fraction ranging from 1% to 10%. The results showed an increase in the thermal conductivity ratio with an increase in volume fraction and temperature and a decrease in nanoparticle size.

2.2.5 Effect of nanoparticle thermal conductivity

Mostafizur *et al.* [11] also measured the thermal conductivity of three different methanol-based nanofluids for temperatures ranging from 1 ˚C to 20 ˚C and volume fraction ranging from 0.005% to 0.15%. The sonication of two hours was used to improve the dispersion of the mixture of Al_2O_3-methanol, SiO_2-methanol and TiO_2-methanol nanofluids with average particle diameter of 13, 5-15 and 21 nm respectively. The thermal conductivity of Al_2O_3, SiO_2 and TiO_2 nanoparticles was 40, 8.4 and 1.2 W/mK respectively. They found that the thermal conductivity ratio of the nanofluids increased with a rise in nanoparticle volume fraction, temperature and thermal conductivity of the nanoparticle. Al_2O_3 nanoparticles dispersed in methanol gave greater enhancement of thermal conductivity than that of the SiO_2 and TiO_2 nanoparticles. At 20 ˚C, for 0.15% volume fraction of Al_2O_3, SiO_2 and TiO_2 nanoparticles, the thermal conductivity enhancement was 29.41%, 23.033% and 24.51% respectively.

Xie *et al.* [35] measured thermal conductivity via a transient hot-wire apparatus of five kinds of oxide nanoparticles (MgO, TiO_2, ZnO, Al_2O_3 and SiO_2) with a mean diameter of about 20 nm prepared with different volume fractions (05%-5%) in ethylene glycol (EG). The thermal conductivity of MgO, TiO_2, ZnO, Al_2O_3 and SiO_2 nanoparticles was 40, 8.4, 13, 36 and 10.4 W/mK respectively. Two distinct suspension methods (stirring and sonication) were applied in preparing their nanofluid samples in three hours' time. They concluded that the thermal conductivity of nanofluids could be enhanced by up to 40.6% for MgO, 27.2% for TiO2, 26.8% for ZnO, 28.2% for Al_2O_3 and 25.3% for SiO_2 at 5% volume fraction nanoparticle at 30 °C. They also observed an increase in thermal

conductivity ratio with increasing nanoparticle volume fraction for all five kinds of oxide nanoparticles and a very weak dependence of temperature of 5% MgO-EG nanofluids from 10 °C to 60 °C.

2.2.6 Effect of sonication time

Kole and Dey [36] conducted an experimental study in order to investigate the thermal conductivity of 3.75% volume fraction of ZnO-ethylene glycol nanofluid for sonication time ranging from four to 100 hours. They state that the effective thermal conductivity increases from ~21% at four hours and reaches a peak of ~40% at around 60 hours, and then decreases to ~35% at 100 hours. Kole and Dey also found that the thermal conductivity ratio of ZnO-EG nanofluids (0.5%-3.75%) increased linearly with an increasing ZnO volume fraction from 12% to ~40%.

Khedkar *et al.* [37] investigated the effect of ultrasonication time ranging from 20 minutes to 160 minutes on the effective thermal conductivity of different volume fractions (2%, 4% and 5%) of CuO nanoparticles dispersed in both water and monoethylene glycol. Their results indicate that the water-based nanofluids show a similar trend at different volume fractions, whereas the monoethylene glycol illustrates the same pattern only for 4% and 5% ZnO volume fraction. It was observed that the thermal conductivity increased up to an optimum time of 80 minutes for water-based nanofluids and 60 minutes for monoethylene glycol-based nanofluids. It started decreasing afterwards. An optimum time of 60 to 80 minutes was found for 2% volume fraction of ZnO-monoethylene glycol. In addition, they proved that the thermal conductivity ratio of CuO-water and CuO-monoethylene glycol increased with increasing volume fraction. The thermal conductivity of water-CuO-based nanofluids

increased by ~6 to 32%, while an increment of ~4 to 21% was noted for monoethylene glycol-CuO nanofluids at volume fractions ranging from 1% to 7.5%.

2.2.7 Effect of the thermal conductivity of base fluid

Sundar *et al.* [38] dispersed Al_2O_3 nanoparticles of volume concentrations ranging from 0.3% to 1.5% in different base fluids. The experiment was carried out in the temperature range of 20 ˚C to 60 ˚C for 20:80%, 40:60% and 60:40% by weight of ethylene glycol and water mixtures respectively. The thermal conductivity of base fluids was 0.492, 0.404 and 0.334 W/mK for 20:80% EG/W, 40:60% EG/W and 60:40% EG/W respectively. They experimentally showed that the thermal conductivity of nanofluids increased with increasing volume concentrations, temperatures and the thermal conductivity of the base fluid. The highest enhancement of 32.26% was observed at 60 °C, for 1.5% volume concentration of 20:80% ethylene glycol-water-based Al_2O_3 nanofluids compared with the base fluid, whereas the Al_2O_3-EG/W (40:60%) and Al_2O_3-EG/W (60:40%) showed 30.51% and 27.42% of enhancement respectively. The estimated crystallite size of Al_2O_3 was 36 nm, whereas the average diameter of diluted Al_2O_3/40:60% EG-water mixture measured with Malvern ZSNanoS analyser was 30 nm.

2.2.8 Effect of settlement time

Xi *et al.* [21] examined the influence of settlement time on the thermal conductivity ratio of MgO-ethylene glycol (5% vol.) nanofluids after three hours of sonication. They demonstrated that the thermal conductivity decreased with elapsed time in the first six hours and became constant afterwards up to 25 hours, $(k_p \,/\, k_f)$ decreasing with less than 3%.

Khedkar *et al.* [32] investigated the influence of elapsed time ranging from 0 to 30 minutes of both CuO-monoethylene glycol and CuO-water nanofluids at 3% volume fraction. After 80 minutes of sonication time, they found that, initially, the thermal conductivity decreased as the time elapsed up to 10 minutes. Afterwards, it was almost unchanged. The same observation was demonstrated for water-based nanofluids [21, 37]. This effect is more noticeable for water-based nanofluids prepared without surfactants than for those prepared with surfactants.

2.2.9 Summary of experimental studies of the thermal conductivity of nanofluids

Table 2.1 summarises the experimental results of the thermal conductivity of nanofluids.

Table 2.1: Summary of experimental studies of thermal conductivity enhancement

Investigator (year)	Particle type	Base fluid	Particle volume fraction (%)	Particle size (nm)	Temperature (˚C)	Maximum enhancement (%)
Masuda *et al.* (1993)	Al_2O_3	Water	1.3 - 4.3	13	31.85 - 86.85	32.4
	SiO_2	Water	1.1 - 2.4	12	31.85 - 86.85	1.1
	TiO_2	Water	3.1 - 4.3	27	31.85 - 86.85	10.8
Lee *et al.* (1999)	Al_2O_3	Water	1 - 4.3	38	Room	10
	Al_2O_3	EG	1 - 5	38	Room	18
	CuO	Water	1 - 3.5	23.6	Room	12
	CuO	EG	1 - 4	23.6	Room	23
Das *et al.* (2003)	Al_2O_3	Water	1 - 4	38.4	21 - 51	24
	CuO	Water	1 - 4	28.6	21 - 51	36
Li and Peterson (2006)	Al_2O_3	Water	2 - 10	36	27.5 - 34.7	29
	CuO	Water	2 - 6	29	28.9 - 33.4	51
Vajjha and Das (2009)	Al_2O_3	Water/EG	1 - 10	53	25 - 90	69
	ZnO	Water/EG	1 - 7	29 and 77	25 - 90	48.5
	CuO	Water/EG	1 - 6	29	25 - 90	60
Xie *et al.* (2010)	MgO	EG	0.5 - 5	20	10 - 60	40.6
	Al_2O_3	EG	0.5 - 5	20	10 - 60	28.2
	TiO_2	EG	0.5 - 5	20	10 - 60	27.2
	ZnO	EG	0.5 - 5	20	10 - 60	26.8
	SiO_2	EG	0.5 - 5	20	10 - 60	25.3

Kole and Dey (2012)	ZnO	EG	0.5 - 3.75	< 50	10 - 70	> 40
Khedkar *et al.* (2012)	CuO	Water	1 - 7.5	30	26	32
	CuO	MonoEG	1 - 7.5	30	26	21
Ghanbarpour *et al.* (2014)	Al_2O_3	Water	3 - 50[a]	75	20 - 50	87
Mostafizur *et al.* (2014)	Al_2O_3	Methanol	0.005 - 0.15	13	1 - 20	29.41
	SiO_2	Methanol	0.005 - 0.15	5 -15	1 - 20	23.033
	TiO_2	Methanol	0.005 - 0.15	21	1 - 20	24.51
Sundar *et al.* (2014)	Al_2O_3	20:80 EG/Water	0.3 - 1.5	30	20 - 60	32.26
	Al_2O_3	40:60 EG/Water	0.3 - 1.5	30	20 - 60	30.51
	Al_2O_3	60:40 EG/Water	0.3 - 1.5	30	20 – 60	27.42

2.3 Mechanisms of enhancement of heat transfer in nanofluids

2.3.1 Introduction

Pang *et al.* [39] report that various works of literature present different mechanisms of enhancement of heat transfer in nanofluids. Xue and Li [40] also present five reasons for the thermal conductivity enhancement of nanofluids viz. the suspended solids increase the surface area and the heat capacity of the base fluid, the suspended solids increase the effective thermal conductivity of the base fluid, the interaction and collision among nanoparticles, fluid and the low passage surface are intensified, the mixing fluctuation and turbulence of the base fluid are intensified, the dispersion of nanoparticles flattens the transverse temperature gradient of the fluid. Keblinski and co-workers [39-43] offer four possible mechanisms that may enhance the thermal conductivity of stationary nanofluids, namely the Brownian motion of the nanoparticle, molecular-level layering of the liquid at the liquid/interface, the nature of the heat transfer in the nanofluids, and the effect of the nanoparticle clustering.

2.3.2 Brownian motion

The collision of suspended particles in the base fluid enhances the thermal conductivity of nanofluid by direct particle-particle heat transport. The Stokes-Einstein formula defines the particle diffusion constant (D), which describes the Brownian motion:

$$D = \frac{\kappa T}{3\pi\mu_f d_p} \tag{2.1}$$

where κ is the Boltzmann constant, T is the temperature of the nanofluid in Kelvin, μ_f is the viscosity of the base fluid and d_p is the nanoparticle diameter in nanometre.

The heat diffusion in the base fluid time (τ_f) and particle motion time (τ_D) are relevant parameters that can describe the effect of Brownian motion on the thermal conductivity enhancement of the nanofluid:

$$\tau_D = \frac{d_p^2}{6D} = \frac{\pi \mu_f d_p^3}{2\kappa T} \tag{2.2}$$

$$\tau_f = \frac{d_p^2}{6\chi} = \frac{\rho_f C_p d_p^2}{6k_f} \tag{2.3}$$

where τ_D is the time necessary for nanoparticle of diameter d_p (nm) to cover the distance equal to its size in the base fluid of viscosity μ_f (kg/m.s), τ_f is the required time to move heat in the base fluid at the same distance as τ_D, T is the nanofluid temperature in K, D is the Einstein diffusion coefficient, κ is the Boltzmann's constant and χ is the thermometric conductivity given by equation (2.4):

$$\chi = \frac{k}{\rho C_p} \tag{2.4}$$

where k is the thermal conductivity, ρ is the density and C_p is the specific heat.

They show that at room temperature τ_D and τ_f are about $2 * 10^{-7}$ s and $4 * 10^{-10}$ respectively, for water-based nanofluid prepared with nanoparticle of 10 nm diameter. The τ_D and τ_f ratios of 500 mean that the Brownian diffusion is much slower than the thermal diffusion. Keblinski and co-workers conclude that the Brownian motion can also indirectly yield to the particle clustering.

2.3.3 Molecular-level layering of the liquid at the liquid-solid interface

The thermal conductivity enhancement of nanofluids is enhanced by the formation of a nanolayer at the solid-liquid interface. The layering of base fluid around solids is assumed to have higher thermal conductivity than the base fluid due to the well-ordered atomic structure of the layering. Keblinski *et al.* show that the nanolayer theory alone cannot explain the enhancement of the thermal conductivity of nanofluids.

2.3.4 Nature of the heat transfer in nanofluids

The heat transport in nanoparticles occurs by ballistic and very fast diffusion phonons. The thermal conductivity of nanofluids is enhanced when a ballistic phonon occurring in the nanoparticles reaches a nearby nanoparticle through the base fluid. The phenomenon above occurs in nanofluid even at a very low volume fraction of the nanoparticle as the distances between nanoparticles are very small. In addition, the Brownian motion's incidence decreases the distance between nanoparticles, consequently improving the phonon heat transport in nanofluid.

2.3.5 Effect of the nanoparticle clustering

The nanoparticle clustering or aggregation could positively or negatively affect the thermal conductivity of nanofluids. The clustering improves the k_{eff} when the formed nanoparticle of the cluster is separated with a thin nanolayer that facilitates the heat transport among nanoparticles. In contrast, it decreases the k_{eff} when a nanolayer of nil thickness isolates the nanoparticle cluster. The impact of the clustering phenomenon on the thermal conductivity increases with the decrease in the packing fraction of highly conductive clusters. Keblinski *et al.* define the packing fraction as the ratio volume of the nanoparticles in the cluster to the total volume of the cluster. The clustering may

result in the sedimentation of heavy clusters or the settling of light particles out of the base fluid.

2.4 Mathematical and experimental models of the thermal conductivity of nanofluids

2.4.1 Introduction

According to the literature, a wide range of experimental and theoretical studies was conducted to model the thermal conductivity of nanofluids [23, 36-42]. The models of the thermal conductivity of nanofluids are either new models or an improvement on the old two-phase flow mixture models [19, 26, 31, 44-46].

2.4.2 Thermal conductivity models

Table 2.3 in Section 2.4.3 provides the proposed reported models for effective thermal conductivity, together with their investigators, which are sorted according to the year of publication. There are more than 30 experimental correlations and theoretical models that can be used to estimate the effective thermal conductivity ratio of different nanofluids [39]. They include the following models: Maxwell [40], Bruggeman [47], Maxwell-Garnett (M-G) [48], effective medium [49], Yu and Choi [50], C.H. Chon *et al.* [1], Li and Peterson [34], Prasher *et al.* [51], Feng *et al.* [52], Vajjha and Das [1], Akbari *et al.* [53], Sitprasert *et al.* [31] and Khanafer, Vafai [54], Corcione [55], Yiamsawasd and Wongwises [56] and Shaker [57]. The most important parameters for choosing these models were the citation and the fact that they had to be recent works. A brief explanation of each follows:

Although the Maxwell model [40, 58] was reported when nobody had yet investigated nanoscience, it remains one of the most representative models of the early studies. It is applied to solid-liquid mixtures of relatively large particles (micro-/mini-sized spherical) suspended in the base fluid. It is the basis relation of many recent models for the effective thermal conductivity of nanofluids. The model was based on the solution of the heat conduction equation through a stationary random suspension of spheres. The effective thermal conductivity (k_{eff}) depends on the thermal conductivity of the spherical particle (k_p), base fluid (k_f) and a particle volume fraction of suspension (ϕ). The Maxwell formula gives a good result for well-dispersed non-interacting spherical-shaped particles with low particle volume concentrations and negligible thermal resistance at the particle fluid interface. The model fails to predict a good match with experimental results for a high solid concentration, as well as the effect of different parameters involved, especially the particle size of nanoparticles, even in low particle volume concentrations.

For the low and high particle volume concentrations, Bruggeman [47] proposes the implicit formula for the effective thermal conductivity of spherical particles randomly distributed in the base fluid. The model is based on the differential effective medium (DEM) theory to estimate the effective thermal conductivity of composites at any particle concentration (low or high). The model can be used for particle percolation in suspensions. It analyses the interactions among randomly distributed particles and it predicts a good match with some experimental results for low and high solid concentration where the particle size is not a concern. This model provides the same result as the Maxwell model for a low solid concentration. The measured thermal

conductivity of nanofluids is much higher than the predicted value of the Bruggeman model [59].

The Maxwell-Garnett (MG) [48] model has been successfully applied to explaining the thermal conductivity of solid-solid composites at small volume fractions. This model includes the impact of nanosized particles and interfacial resistance (R_K). The magnitude of R_K, between nanoparticles and different matrices, ranges from small values $\approx 0.77x10^{-8}$ Km^2 W^{-1} to high values $\approx 20x10^{-8}$ Km^2 W^{-1}. The MG model is applied whenever the thermal conductivity of the base fluid is much less than the thermal conductivity of the nanoparticle. Prasher *et al.* [51] show that the MG model underpredicts the data of Lee *et al.* [31, 32] for Al_2O_3 of 38.4 nm at room temperature for both water and EG mixture. The MG model also completely fails to explain the enhancement of k_{eff} in nanofluids with temperatures in the range of 293 K to 323 K, when the volume concentration of Al_2O_3 of 38 nm is 1% and 4%.

The Yu and Choi [50] model is a modified version of the Maxwell equation for the effective thermal conductivity of a solid-liquid mixture which considers the nanolayer influence. The renovated Maxwell model is limited to suspensions with no agglomeration of particles. Yu and Choi's model predicts the experimental data (Cu-EG and CuO-EG) of Lee *et al.* and Eastman quite well. They state that the thermal conductivity enhancement for a 1% copper particle in ethylene glycol nanofluid is strongly dependent on the thickness of the nanolayer (δ). However, it is almost invariant to the thermal conductivity of the nanolayer when $k_{layer} > 10\, k_f$. This mechanism is most effective when the nanoparticle diameters are less than 10 nm for a 1% copper particle in ethylene glycol nanofluid. They considered a nanolayer thickness

of 2 nm. Xie *et al.* [60] show that the Yu and Choi model with k_{layer} equal to $5k_f$ predicts quite well the experimental data of CuO-EG nanofluid. Eastman *et al.* used the transient hot-wire method to measure the thermal conductivity of copper and copper oxide-EG mixtures in the temperature range from 290 K to 310 K at atmospheric pressure [61].

The Chon *et al.* [1] model is an experimental correlation for the thermal conductivity of Al_2O_3 nanofluids as a function of the nanoparticle size, molecular diameter, Prandtl number and Reynolds number of the base fluid. The correlation comes from the linear regression scheme applied to the experimental data by using the Buckingham-Pi theorem. The mean-free path for the base fluid (l_f) uses 0.17 nm for water as a base fluid. The Brownian motion of the suspended nanoparticle is the most important factor in the enhancement of the thermal conductivity of nanofluids. Vajjha and Das state that the model of Chon *et al.* underpredicts the value of effective thermal conductivity of CuO-water at lower temperatures.

Li and Peterson [34] developed two correlations for predicting the thermal conductivity of Al_2O_3-distilled water and CuO-distilled water nanofluids. These equations were based on the linear regression analysis of the temperature of nanofluid and particle volume fraction. The CuO and Al_2O_3 nanoparticles of the average diameter of 29 nm and 36 nm were mixed with water at volume fraction range of 2% to -10% for Al_2O_3 and 2-6% for CuO respectively. These correlations were valid for a temperature range of 27.5 ˚C to 34.7 ˚C and 28.9 ˚C to 33.4 ˚C for Al_2O_3 and CuO respectively. They emphasise that the particle volume fraction dependence of effective thermal

conductivity is much higher than the temperature dependence as well as that the volume fraction dependence is more pronounced with increasing temperature.

The Prasher *et al.* model is called the multisphere Brownian model (MSBM) [51]. The model is a combination of the MG conduction model and the convection caused by the Brownian movement of the nanoparticles, which reduces to the MG model for large particle sizes. Prasher *et al.* show that the model predicts the right trend for CuO-water of the Das *et al.* (2003) mixture with respect to different parameters such as nanoparticle volume fraction, nanoparticle diameter and temperature (293-323 K) for the following parameters: $R_k = 0.77x10^{-8}$ m^2 w^{-1}, m = 2.35 for ϕ = 4% and m = 2.05 for ϕ = 1%. A = 40000; a good trend for the alumina-oil base fluid when R_k is set to $1.2x10^{-8}$ Km^2W^{-1}. The m-value has a significant influence on the MSBM model. Prasher *et al.* show that the best value of m is 2.5% ± 15% for nanofluid with water as a base fluid.

Li and Kleinstreuer [62] state that the model cannot predict the thermal conductivity enhancement trend for the experimental results of Li and Peterson. However, it well predicts the thermal conductivity enhancement trend for the experimental results of Li and Peterson S.K Das, Chon *et al.* and Prasher.

The Feng *et al.* model [52] takes into account the contributions from both the nanolayer at the solid-liquid interface (first part of the equation) and the agglomeration of nanoparticles in contact, which forms the clusters (second part of the equation). The first part of the equation is the renovated Maxwell model developed by Yu and Choi [50]. Feng *et al.* demonstrate that the theoretical predictions of the effective thermal conductivities of nanofluids are in good agreement with the available experimental data

of Das [32], Lee [31, 32] and Xie *et al.* [52] for δ = 1 nm, $k_{layer} = 2k_f$. Kole and Dey [63] confirm that the model validates the experimental data of the thermal conductivity of TiO_2-water nanofluid, reported by Duangthongsuk and Wongwises [59] within 1.2%, with δ = 2 nm and $k_{layer} = 3k_f$. However, it underpredicts the data of Eastman *et al.* (1997) and Masuda *et al.* (1993). Kole and Dey also confirm that, if the thermal conductivity enhancement is within 15%, Feng's model successfully explains the observed effective thermal conductivity of oxide-based nanofluids.

Vajjha and Das [1] developed a correlation that was an improvement on the Koo and Kleinstreuer model derived from a broader data set (133), obtained from three nanofluids (Al_2O_3, CuO and ZnO). The model incorporates the classic Maxwell model and the Brownian motion effect to account for the thermal conductivity of nanofluids as a function of temperature, particle volume concentration, the properties of nanoparticles and the base fluid. The function is the same for all three nanofluids. The ε correlation is the same for Al_2O_3 and ZnO but differs slightly for CuO (see Table 2.3). The applicable range is at a temperature of 298 to 363 K and 29 nm to 77 nm for the particle size respectively. This correlation gives an accurate prediction of the thermal conductivity of different nanofluids (Al_2O_3, ZnO and CuO) over a broad range of concentrations (1%-10%) and temperatures (298-363K).

Sitprasert *et al.* and co-workers [31] modified the model proposed by Leong *et al.* by including the effect of temperature on the thermal conductivity and thickness of nanolayer. It is applied to the thermal conductivity of nanofluids for both no-flowing and flowing fluids. The expressions for the interfacial layer thickness δ and the thermal conductivity of the interfacial layer [64] were found using the experimental data of

Masuda *et al.* [31], Eastman *et al.*, Pak and Cho, Lee *et al.* [31, 32], Das *et al.* [32], Chon *et al.* and Li and Peterson [34]. The model makes good predictions of the effective thermal conductivity ratio with volume fraction and temperature of nanofluids for both non-flowing and flowing fluids.

Khanafer and Vafai [54] developed general correlations for the effective thermal conductivity and viscosity of nanofluids based on the pertinent experimental data in terms of the volume fraction, particle diameter, temperature and the base fluid physical properties. Their correlation is valid for the effective thermal conductivity of Al_2O_3-water nanofluid at the temperature range of 20 °C $\leq T \leq$ 70 °C and nanoparticle diameter 11 nm $\leq d_p \leq$ 150 nm. The effective dynamic viscosity of nanofluid, expressed in m.Pa.s, is valid at the temperature range of 20 °C $\leq T \leq$ 70 °C, volume fraction 1% $\leq \phi \leq$ 9 % and nanoparticle diameter 13 nm $\leq d_p \leq$ 131 nm. The dynamic viscosity of water is expressed in Pa.s. The effective thermal conductivity of nanofluids increases with a rise in temperature and volume fraction and decreases with an increase in the particle diameter.

Akbari *et al.* [53] developed a thermal conductivity model for five nanofluids, namely Al_2O_3-water, Al_2O_3-EG, CuO-water, CuO-EG and Cu-water. The model is an improvement on the Nan *et al.* equation of effective thermal conductivity of nanofluid taking into consideration the Brownian motion and clustering. Akbari and co-workers considered the fractal model to evaluate the size, size distribution and number of clusters. They determined the parameters *B*, *C* and *G* of the model as $B = 0$, $C = 1$ and $G = 20 * 10^5$ from the published experimental data (see Table 2.3).

The effective medium model [49] predicts the thermal conductivity ratio for highly conducting spherical particles. In this model, the particles are assumed to be immobile.

In 2011, Corcione [55, 65] developed an empirical correlation for the thermal conductivity ratio from experimental data relative to nanofluids consisting of alumina, copper oxide, titania and copper nanoparticles suspended in water or EG. The correlation is valid for nanoparticles in the range of temperatures 21 $^{\circ}$C to 51°C, volume fraction 2% to 9% and nanoparticle diameter 10 nm to 150 nm. The correlation was obtained by the way of regression analysis with a 1.86% standard deviation of error.

Shaker *et al.* [57] recently proposed an extended Maxwell model for the thermal conductivity of nanofluids. They modified the classic model of Maxwell by taking into account the non-local heat transfer rising due to the small characteristic length in nanofluids. They compared the novel model predictions and the experimental data of each given nanofluid to determine the non-locality characteristic parameter (h). They depicted that it was equal to 8 and 11 for alumina-EG and alumina-water nanofluids respectively. The model is valid for spherical nanoparticles suspended in the base fluid and can be modified also to account for non-spherical nanoparticle suspension. The model well predicts the experimental results of both alumina-water and alumina-EG nanofluids at volume fraction ranging from 0.05% to 5.5% and nanoparticle size between 10 nm and 150 nm with a maximum error of 5%.

Yiamsawasd and Wongwises [56] proposed a correlation for the predicting thermal conductivity of the Al_2O_3 and TiO_2 nanoparticles suspended in both base fluids, water and ethylene glycol-water mixture (20/80% wt.). This correlation is valid for a volume

fraction ranging from 1% to 8% over the temperature ranging from 15 °C to 65 °C. The correlation takes into account the effects of volume fraction, temperature and thermal conductivity of nanoparticles and base fluid. Wongwises and co-worker state that the correlation can also predict other base fluids. The coefficients *A*, *B* and *C* are given in Table 2.2. The model was derived from TiO_2 and Al_2O_3 nanoparticles of average diameter of 21 nm and 120 nm respectively.

Table 2.2: Coefficients in the correlation for different nanofluids

Nanofluids	**Coefficients**				**Max. error**	**Avg. error**
	A	***B***	***C***	***D***		
Al_2O_3	0.945867	0.073528	0.036168	-0.00585	2.74%	1.23%
TiO_2	0.916205	0.066817	0.018789	0.016229	2.28%	1.11%

In summary, each mathematical model or correlation predicts its value of the thermal conductivity ratio of the nanofluids for the same value of the given parameters [30, 44]. However, it gives a good prediction of the thermal conductivity of specific nanofluids in certain given conditions.

2.4.3 Summary of thermal conductivity models

In this section, the thermal conductivity models discussed in Section 2.4.2 are summarised in Table 2.3. The columns of the table consist of the authors that did the investigation, the mathematical or correlation model, applied types of particles and base fluids, particle size, volume fraction and temperature. The entries are arranged according to the date of publication.

Table 2.3: Summary of thermal conductivity models

Investigator (Year)	Model	Particles/ Fluids	Diameter	Volume fraction (%)	Temperature (˚C)
Maxwell (1881)	$\frac{k_{eff}}{k_f} = \frac{k_p + 2k_f + 2(k_p - k_f)\phi}{k_p + 2k_f + (k_p - k_f)\phi}$		Large particles (micro-/mini-size)	Low solid concentration	
Bruggeman (1935)	$\phi\left(\frac{k_p - k_{eff}}{k_p + 2k_{eff}}\right) + (1-\phi)\left(\frac{k_f - k_{eff}}{k_f + 2k_{eff}}\right) = 0$			Low and high solid concentration	
Nan *et al.* (1927)	$\frac{k_{eff}}{k_f} = \frac{[k_p(1+2\alpha) + 2k_f] - 2\phi[k_f - k_p(1-\alpha)]}{[k_p(1+2\alpha) + 2k_f] + \phi[k_f - k_p(1-\alpha)]}$ with $\alpha = \frac{2R_k k_f}{d_p}$	diamond - ZnS	0.5 µm -4µm	10 - 40	Room
Maxwell-Garnett (M-G) (1997)	$\frac{k_{eff}}{k_f} = \frac{[(1+2\alpha) + 2\phi(1-\alpha)]}{[(1+2\alpha) - \phi(1-\alpha)]}$ with $\alpha = \frac{2R_k k_f}{d_p}$			Low solid concentration	

Yu & Choi (2003)	$\frac{k_{eff}}{k_f} = \frac{k_{pe} + 2k_f + 2(k_{pe} - k_f)(1-\chi)^3\phi}{k_{pe} + 2k_f - (k_{pe} - k_f)(1-\chi)^3\phi}$ with $k_{pe} = \frac{[2(1-\gamma) + (1+\chi)^3(1+2\gamma)\gamma]}{[-(1-\gamma) + (1+\chi)^3(1+2\gamma)]} k_p$ and $\gamma = \frac{k_{layer}}{k_p}$, $\chi = \frac{\delta}{r_p}$				
Xue and Xu (2005)	$\left(1 - \frac{\phi}{\omega}\right)\left(\frac{k_{eff} - k_f}{2k_{eff} + k_f}\right) + \frac{\phi}{\omega}\left[\frac{\left[\begin{matrix}(k_{eff} - k_{layer})(2k_{layer} + k_p) - \\ \omega(k_p - k_{layer})(2k_{layer} + k_{eff})\end{matrix}\right]}{\left[\begin{matrix}(2k_{eff} + k_{fayer})(2k_{layer} + k_p) + \\ 2\omega(k_p - k_{layer})(k_{layer} - k_{eff})\end{matrix}\right]}\right] = 0$ with $\omega = \left[\frac{r_p}{r_p + \delta}\right]^3$	Cu-water CuO-EG	- 	1 – 4 1 - 4	-

Li & Peterson (2006)	$\frac{(k_{eff} - k_f)}{k_f} = 0.764481\phi + 0.018688867T - 0.462147175$ with $R^2 = 0.9171$	Al_2O_3-water	36 nm	2 - 10	27.5 - 34.7
Li & Peterson (2006)	$\frac{(k_{eff} - k_f)}{k_f} = 3.761088\phi + 0.017924T - 0.30734$ with $R^2 = 0.9078$	CuO-water	29 nm	2 - 6	28.9 – 33.4

Prasher *et al.* (2006)	$\frac{k_{eff}}{k_f} = (1 + ARe^m Pr^{0.333}\phi)\begin{bmatrix}[k_p(1+2\alpha)+k_m]+ \\ \frac{2\phi[k_p(1-\alpha)-k_m]}{[k_p(1+2\alpha)+k_m]-} \\ \phi[k_p(1-\alpha)-k_m]\end{bmatrix}$	Al_2O_3-EG (Xie *et al.*, 2002)	15, 26, 60.4, 302 nm	1 - 5	-
		Al_2O_3-EG (Lee *et al.*, 1999)	38.4 nm	1 - 4	Room
	with	CuO-EG (Lee *et al.*, 1999)	23.6 nm	1 - 3.5	Room
	$\alpha = \frac{2R_k k_f}{d_p}$, $k_m = k_f(1 + ARe^m Pr^{0.333}\phi)$	Cu-EG (Eastman *et al.*, 2001)	6 nm	0.05 - 0.55	-
		CuO-water (Das *et al.*, 2003)	28.6 nm	1 - 4	21 - 51

Feng *et al.* (2007)	$\frac{k_{eff}}{k_f} = (1-\phi_e)k_{eff,R-M} + \phi_e\left[\left(1-\frac{3}{2}\phi_e\right)+\frac{3\phi_e}{\varsigma}\left[\frac{1}{\varsigma}ln\frac{r_p+\delta}{(r_p+\delta)(1-\varsigma)}-1\right]\right]$ with $k_{eff,R-M} = \frac{k_{pe}+2k_f+2(k_{pe}-k_f)(1-\chi)^3\phi}{k_{pe}+2k_f-(k_{pe}-k_f)(1-\chi)^3\phi}$, $\phi_e = \phi(1+\chi)^3$, $\varsigma = 1-\frac{k_f}{k_{pe}}$	Al_2O_3-water (Lee *et al.*, 1999)	38.4 nm	1 - 4	Room
		Al_2O_3-EG(Lee *et al.*, 1999)	38.4 nm	1 - 5	Room
		Al_2O_3-water (Xie *et al.*, 2002)	60.4 nm	1.8 - 5	-
		CuO-water (Lee *et al.*, 1999)	23.6nm	1 - 3.5	Room
		CuO-water (Das *et al.*, 2003)	28.6 nm	1 - 4	21 – 51
		Al_2O_3-EG (Xie *et al.*, 2002)	15 nm	1.8 - 5	-
		Al_2O_3-EG (Xie *et al.*, 2002)	26 nm	1.8 - 5	-
		CuO-EG (Lee *et al.*, 1999)	23.8 nm	1 - 3.5	Room

Sitprasert *et al.* (2009)	$$k_{eff} = \frac{(k_p - k_{layer})\phi k_{layer}[2\sigma_2^3 - \sigma_1^3 + 1] + (k_p + 2k_{layer})\sigma_2^3[\phi\sigma_1^3(k_{layer} - k_f) + k_f]}{\sigma_2^3(k_p + 2k_{layer}) - (k_p - k_{layer})\phi[\sigma_2^3 + \sigma_1^3 - 1]}$$ with $\sigma_1 = 1 + \frac{\delta}{r_p}$, $\sigma_2 = 1 + \frac{\delta}{2r_p}$, $\delta = 0.01(T - 273)r_p^{0.35}$, $k_{layer} = C\frac{\delta}{r_p}k_f$, $C = 30$ for Al_2O_3, $C = 110$ for CuO	Al_2O_3-water (Masuda *et al.*, 1993)	13 nm	1.3 - 4.3	Room
		Al_2O_3-water (Pak & Cho, 1998)	13 nm	1.3 - 4.3	Room
		Al_2O_3-water (Eastman *et al.*, 1997)	33 nm	1-5	Room
		Al_2O_3-water (Lee *et al.*, 1999)	38.4 nm	1-4	Room
		Al_2O_3-water (Das *et al.*, 2003)	38.4 nm	1-4.5	Room
		Al_2O_3-water (Chon *et al.*, 2005)	11, 47, 150 nm	1	21 - 70
		Al_2O_3-water (Chon *et al.*, 2005)	38.4 & 47 nm	4	21 - 70
		CuO-water (Li & Peterson, 2006)	29 nm	4 - 6	28.9 – 34.7
		CuO-water (Eastman *et al.*, 1997)	35 nm	1 - 5	Room

Vajjha & Das (2009)	$k_{eff} = k_{eff,Maxwell} + 5x10^4 \epsilon \phi \rho_p C_{pf} \sqrt{\frac{\kappa T}{\rho_p d_p}} f(T,\phi)$ where $k_{eff,Maxwell} = \frac{k_p + 2k_f + 2(k_p - k_f)\phi}{k_p + 2k_f + (k_p - k_f)\phi} k_f$ and $f(T,\phi) = (2.8217 * 10^{-2}\phi + 3.917 * 10^{-3})\left(\frac{T}{T_0}\right) + (-3.0669 * 10^{-2}\phi - 3.91123 * 10^{-3})$, $\epsilon = 8.4407(100\phi)^{-1.07304}$ for Al_2O_3 and ZnO, $\epsilon = 9.881(100\phi)^{-0.9446}$ for CuO, $T_0 = 273K$	Al_2O_3-EG/water (60:40)	53	1 - 10	25 - 90
		ZnO-EG/water (60:40)	29 and 79	1 - 7	25 - 90
		CuO-EG/water (60:40)	29	1 - 6	25 - 90

Corcione (2011)	$\frac{k_{eff}}{k_f} = 1 + 4.4Re_p^{0.4}Pr_f^{0.66}\left(\frac{T}{T_{fr}}\right)^{10}\left(\frac{k_p}{k_f}\right)^{0.66}$ where $Re_p = \frac{2\rho_f \kappa T}{\pi {\mu_f}^2 d_p}$, $Pr_f = \frac{\mu_f C_{pf}}{k_f}$	Al_2O_3, CuO, TiO_2, Cu-EG or water	10 – 150 nm	0.2 - 9	21 - 51
Khanafer *et al.* (2011)	$\frac{k_{eff}}{k_f} = 0.9843 + 0.398\phi^{0.7383} + \left(\frac{1}{d_p(nm)}\right)^{0.02246}\left(\frac{\mu_{eff}(T)}{\mu_f(T)}\right)^{0.0235} - 3.9517\left(\frac{\phi}{T}\right) + 34.034\frac{\phi^2}{T^3} + 32.509\frac{\phi}{T^2}$ with $\mu_{eff} = -0.4491 + \frac{28.837}{T} + 0.574\phi - 0.1634\phi^2 + 23.053\frac{\phi^2}{T^2} + 0.0132\phi^3 - 2354.735\frac{\phi}{T^3} + 23.498\frac{\phi^2}{d_p^2} - 3.0185\frac{\phi^3}{d_p^2}[m.Pa.s]$ and $\mu_f(T) = 2.414x10^{-5}x10^{\frac{247.8}{T-40}}$	Al_2O_3-water (Das *et al.*, 2003)	38.4 nm	1 - 4	21 - 51
		Al_2O_3-water(Chon *et al.*, 2005)	47 nm	1 & 4	21 - 70
		Al_2O_3-water (Chon *et al.*, 2005)	150 nm	1	21 - 62
		Al_2O_3-water (Minsta *et al.*, 2009)	36 nm	3.1 & 9	21 - 39
		Al_2O_3-water (Minsta *et al.*, 2009)	47 nm	3.3 - 9	22 - 47
		Al_2O_3-water (Chon *et al.*, 2005)	11	1	21 - 70

Akbari *et al.* (2011)	$\frac{k_{eff}}{k_f} = \frac{[k_p(1+2\alpha)+2k_f]-2\phi[k_f-k_p(1-\alpha)]}{[k_p(1+2\alpha)+2k_f]+\phi[k_f-k_p(1-\alpha)]} + \frac{552*10^5*2^{(Q/2)}\phi d_p^E}{Q-1.4}Re^Q$ with $\alpha = \frac{2R_k k_f}{d_p}$, $Re = \frac{1}{\nu}\sqrt{\frac{18\kappa T}{\pi\rho_p d_p}}$ and Q = 2 for water, Q = 1.6 for EG, E=0.525 for Al_2O_3-water, E=0.52 for CuO-water, E=0.44 for Cu-water, E=0.493 for Al_2O_3-EG, E=0.442 for CuO-EG	Al_2O_3-water (Wen & Ding, 2004)	42 nm	0.29 - 1.6	22
		Al_2O_3-water (Masuda *et al.*, 1993)	13 nm	1.3 - 4.3	32
		Al_2O_3-water (Eastman *et al.*, 1997)	33 nm	1 - 5	-
		Al_2O_3-EG (Xie *et al.* 2002)	26 nm	1.8 - 5	Room
		CuO-water (Wang & Choi, 1999)	23 nm	4.6 - 9.6	24
		CuO-water (Hwang *et al.*, 2006)	33 nm	1	-
		CuO-EG (Eastman *et al.*, 2001)	35 nm	1 - 4	17 - 37
		Cu-water (Xuan *et al.*, 2003)	100 nm	1 - 4	23

Yiamsawasd et Wongwises (2012)	$\frac{k_{eff}}{k_f} = A\phi^B T^C \left(\frac{k_p}{k_f}\right)^D$ Where: A, B, C, and D are coefficients for different nanofluids	Al_2O_3-water	120 nm	1-8	15 – 65
		Al_2O_3-EG-water (20/80 wt. %)	120 nm	1-8	15 – 65
		TiO_2-water	21 nm	1-8	15 – 65
		TiO_2-EG/water (20/80 wt. %)	21 nm	1-8	15 -65
Shaker *et al.* (2014)	$\frac{k_{eff}}{k_f} = \frac{1 + 2\xi\phi\hbar^{-3}}{1 - \xi\phi\hbar^{-3}}$ with $\xi = \frac{k_p - k_f}{3(\Im 1 k_p - \Im 2 k_f)}$, $\Im 1 = \frac{1}{\hbar} + \arctan(\hbar) - \frac{\pi}{2}$ $\Im 2 = \arctan(\hbar) + \frac{\hbar}{1+\hbar^2} + \frac{8\hbar}{(1+\hbar^2)^2} + \frac{8\hbar^3}{(1+\hbar^2)^3} - \frac{\pi}{2}$, $\hbar = \frac{r}{h}$	Al_2O_3-water	11- 150	0.5 – 5.5	-
		Al_2O_3-EG	20 - 150	0.5 – 5.5	-

2.5 Conclusion

Literature shows that there is an enhancement of the effective thermal conductivity of nanofluids compared with base fluids. Several empirical and theoretical correlations are available to model the thermal conductivity of nanofluids. Experimental investigations show either an agreement or disagreement with the theoretical studies and whether the predictions by the existing mathematical models of the effective thermal conductivity of nanofluids are valid or not.

The effective thermal conductivity of nanofluids takes into consideration various major mechanisms and parameters. The major mechanisms are the nanolayer, Brownian motion and clustering. The recognised important parameters can be the volume fraction of the nanoparticles, temperature, particle size, thermal conductivity of the nanolayer, thermal conductivity of nanoparticle, thermal conductivity of the base fluid and pH of the nanofluid.

Overall, each mathematical model or correlation predicts its value of the thermal conductivity ratio of the nanofluids for the same value of the given parameters. However, each mathematical model or correlation gives a good prediction of the thermal conductivity of specific nanofluids in certain given conditions. In addition, the precision of each thermal conductivity model depends on the involved mechanisms and/or parameters.

None of the previous experimental correlations and models was based on the glycerol-based nanofluids data. The literature review pointed on the lack of reported data on the thermal conductivity of both MgO-glycerol and Al_2O_3-glycerol nanofluids to date.

CHAPTER 3: EXPERIMENTAL SET-UP AND THERMAL CONDUCTIVITY MEASUREMENT

3.1 Introduction

This chapter describes the investigated materials, their physical characterisation and the nanofluid preparation. It also presents the thermal conductivity measurements, the uncertainties and validation of the experimental data. Appendix A: presents the uncertainty analysis of the thermal conductivity ratio of glycerol-based nanofluid.

3.2 Material

This study investigated two types of nanoparticles (MgO and Al_2O_3). Three α-Al_2O_3 nanoparticles of different diameters were analysed, i.e. 40 nm (S1), 80 nm (S2) and 100 nm (S3). The Al_2O_3 nanopowder of 80 nm was purchased from US Research Nanomaterials, Inc. (Houston, TX, USA). The 40 nm and 100 nm nanoparticles were procured from MK Nano, Inc. (Mississauga, ON, Canada).

Three MgO nanoparticles of different diameters with factory specification of 20 nm (S4), 40 nm (S5) and 100 nm (S6) were provided for analysing. The MgO nanopowder of 100 nm was purchased from Nanostructured and Amorphous Materials, Inc. (Houston, TX, USA). The two other MgO nanoparticles were procured from US Research Nanomaterials, Inc. (Houston, TX, USA) for the average particle sizes of 20 nm and 40 nm. The physicochemical properties of the nanoparticles [35, 43] are listed in Table 3.1. Merck Millipore (Darmstadt, Germany) supplied the glycerol (base fluid).

Table 3.1: Properties of the nanoparticles

Chemical formula	Diameter (nm)	Purity (%)	True density at 20 °C (g/cm^3)	Thermal conductivity (W/mK)
Al_2O_3	40	99.5	3.7	40.0
Al_2O_3	80	99+	3.5 – 3.9	40.0
Al_2O_3	100	99.9	3.7	40.0
MgO	20	99+	3.58	48.4
MgO	40	99+	3.58	48.4
MgO	< 100	99+	3.58	48.4

3.3 Physical characterisation

3.3.1 Characterisation methods

The physical characterisation of the nanoparticles was evaluated by using the X-ray Fluorescence Spectroscopy (XRF), an X-ray powder diffraction and the combined XRD and XRF respectively. The XRF analysis was conducted using an ARL 9400XP spectrometer. The XRD analysis of the prepared samples of nanoparticles was carried out on a PANanalytical X'Pert Pro powder diffractometer with Co-Kα radiation source (λ = 1.78901 Å) at 50 kV and current of 50 mA. The results were recorded over a 2θ range of 10 ° to 90 ° with a scanning rate of 0.02°/s.

Transmission electron microscopy (TEM) analysis of the samples was conducted using JEM 2100F (JEOL, USA) to evaluate the shape and the size of particles. The JEM 2100F works with an accelerating voltage of 200 kV in the range of 50 V/min at variable steps of 2 ppm/min. The JEM 2100F achieves the highest TEM image quality with a point image resolution at 0.23 nm accuracy [66]. The TEM samples were prepared by dispersing the α-Al_2O_3 or MgO nanopowder in acetone,

followed by ultrasonication of five minutes. TEM image files were analysed using ImageJ software (NIH, Bethesda, MD, USA).

The crystallite size of various nanoparticle patterns was estimated using the Scherrer equation (3.1) [67]:

$$d_{cryst} = \frac{K\lambda}{\beta \cos\theta} \tag{3.1}$$

where K is the shape factor, λ is the wavelength of X-ray source, β is the full-width at half maximum in radian and θ is the diffraction angle in radian.

The equation (3.1) predicts the crystallite size with 10% accuracy when the shape factor K of 1 is considered [68]. The shape factor (K) is a numeric value describing the form of the nanoparticle, type of approach calculation and the size distribution. K is equal to 0.89 and 0.94 for a spheric particle with cubic symmetry crystallites determined by integral breadth and FWHM respectively [69, 70]. In both cases, an approximate value of 1 can also be used [71]. In TEM image analysis, equation (3.2) defines the circularity parameter. The circularity value ($circ$) of 1 and approaching 0 refer to the perfect circle and increasingly elongated shaped object respectively [72].

$$circ = 4\pi\left(\frac{A_p}{P}\right)^2 \tag{3.2}$$

where A_p and P are the projected area and outside perimeter of the outline of the nanoparticle respectively.

3.3.2 Sample characterisation

The particle sizes of the samples of α-Al_2O_3 and MgO nanoparticles revealed by TEM images are shown in Figure 3.1 and Figure 3.2 respectively. As observed in these figures, the shape of α-Al_2O_3 and MgO nanoparticles is nearly spherical. Figure 3.3 and Figure 3.4 show the particle size distribution of the α-Al_2O_3 and MgO nanoparticles, determined using ImageJ software. The particle size distribution is based on the TEM image analysis of more than 500 particles, which were individually counted.

Both samples S1 (40 nm) and S2 (80 nm) show two prominent peaks bimodal data, each of its own with a separate central tendency, while the 100 nm nanoparticle reveals a unimodal data (Figure 3.4). In Sample S1, one group of the population has a mean particle size of 34 ± 18 nm and the other group has a mean particle size of 136 ± 43 nm. The sample S2, on the other hand, has one group of population with a mean particle size of 20 ± 11 nm, whereas the second population has an average particle size of 113 ± 30 nm. The difference between two means for both samples is statistically significant at approximate 5% level of significance [73].

The three α-Al_2O_3 nanoparticles also show a positive skewed size distribution, in the range of 19 nm (d_{10}), 54 nm (d_{50}) and 155 nm (d_{90}) for the 40 nm, 12 nm (d_{10}), 21 nm (d_{50}) and 127 nm (d_{90}) for the 80 nm and 97 nm (d_{10}), 134 nm (d_{50}) and 187 nm (d_{90}) for the 100 nm respectively [74, 75]. However, the three α-Al_2O_3 nanoparticles respect the lognormal distribution with the mean particle size and standard deviation of 55 ± 2 nm for 40 nm α-Al_2O_3 nanoparticle, 31 ± 3 nm for 80 nm α-Al_2O_3 nanoparticle and for 134 ± 1 nm for 100 nm α-Al_2O_3 nanoparticle respectively [14]. The accuracy of

the TEM images of JEL 2100F is 0.23 nm [66]. There are significant differences in nanoparticle sizes between the obtained values and manufacturer's values.

The three MgO nanoparticles show a positive skewed size distribution, in the range of 16 nm (d_{10}), 21 nm (d_{50}) and 27 nm (d_{90}) for the 20 nm, 71 nm (d_{10}), 125 nm (d_{50}) and 166 nm (d_{90}) for the 40 nm and 71 nm (d_{10}), 106 nm (d_{50}) and 126 nm (d_{90}) for the 100 nm respectively.

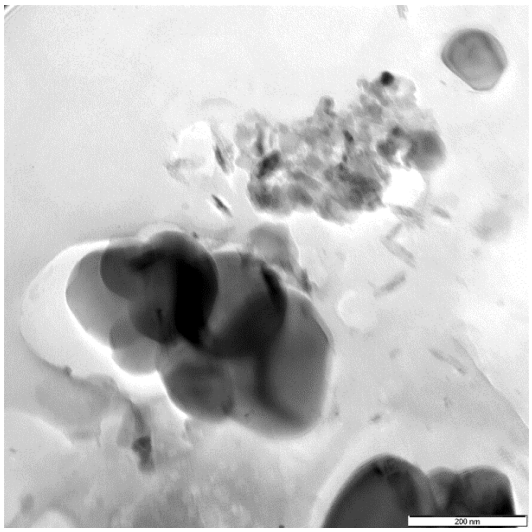

(a)

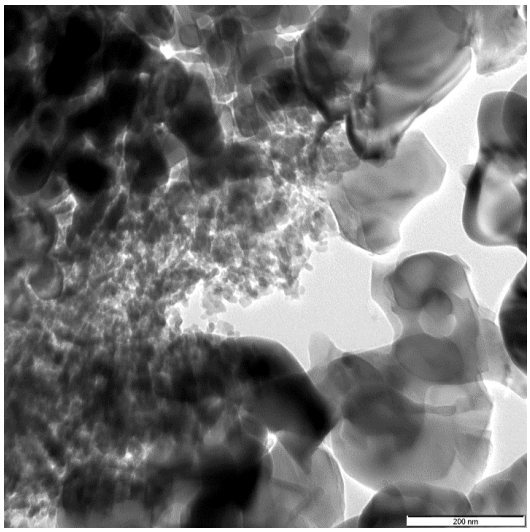

(b)

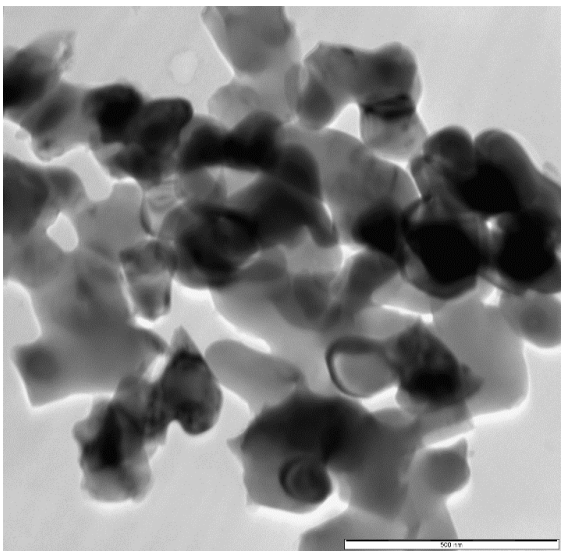

(c)

Figure 3.1: TEM image of Al_2O_3 nanoparticles (a) 40 nm, (b) 80 nm and (c) 100 nm

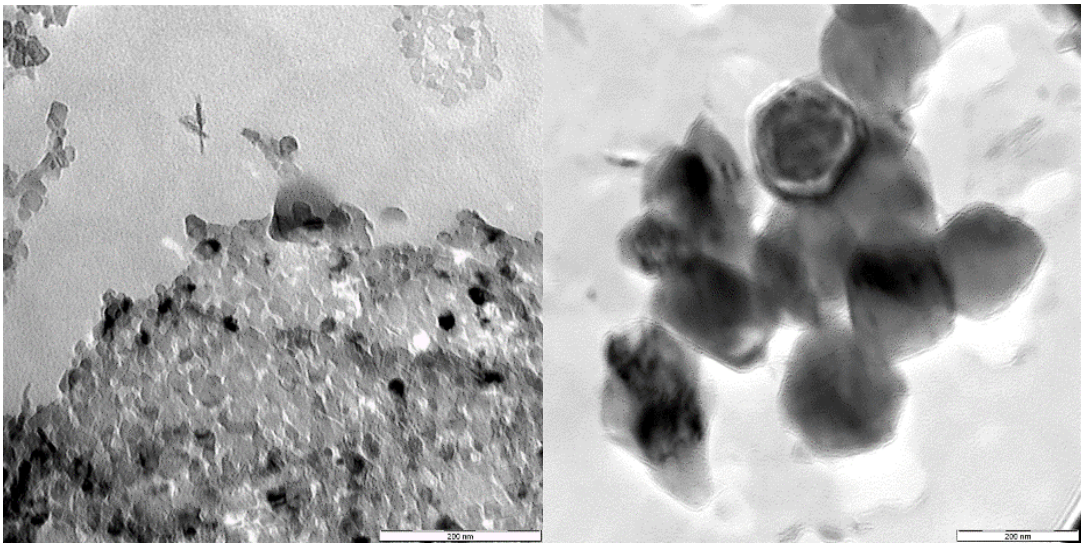

(a) (b)

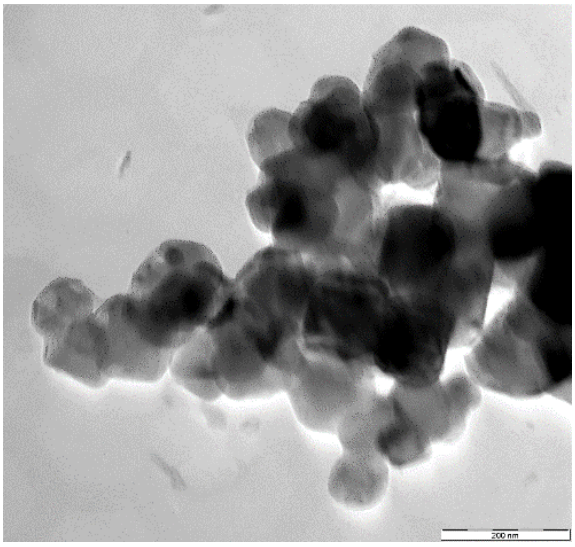

(c)

Figure 3.2: TEM image of MgO nanoparticles (a) 20 nm, (b) 40 nm and (c) 100 nm

However, the MgO nanoparticles respect the lognormal distribution. The mean of the lognormal distribution is 21 ± 1 nm for 20 nm MgO nanoparticle, 119 ± 2 nm for 40 nm MgO nanoparticle and 104 ± 1 nm for 100 nm MgO nanoparticle respectively. The circularity values of 21 nm, 104 nm and 119 nm MgO nanoparticles are 0.8, 0.9 and 0.9 respectively, whereas it is equal to 0.9, 0.9 and 0.9 for 31 nm, 55 nm and 134 nm α-Al_2O_3 nanoparticles respectively. The circularity values of the three sizes of two nanoparticles indicate that the studied nanoparticles have a shape closer to a sphere than that of an elongated object.

The obtained particle sizes of the three α-Al_2O_3 nanoparticles and the 40 nm MgO nanoparticle are far removed from the manufacturer's values. Because the manufacturer does not analyse nanoparticle TEM batch by batch, this unforeseen event can occur in the nanoparticle manufacturing process. Therefore, this report is based on TEM analysis and not on the manufacturer's values.

Figure 3.5 shows XRD patterns of α-Al_2O_3 nanoparticles. The patterns (see Figure 3.5) are in good agreement with the standard diffraction data of two types of Al_2O_3, one is rhombohedral system of corundum (Al_2O_3) of PDF file No. 01-089-7717 and the second monoclinic Al_2O_3 (PDF file No. 01-086-1410) for 55 nm, a rhombohedral system of corundum (Al_2O_3) of PDF file No. 98-008-8029 for 31 nm and both rhombohedral corundum (PDF file No. 01-081-2267) and rhombohedral Millosevichite (Al_2 $[SO_4]$)$_3$ of PDF file No. 01-077-0066 for 134 nm.

Figure 3.6 shows the typical XRD patterns of the MgO nanoparticle samples. While the diffraction peaks of 111, 200, 220 and 311 of 21 nm and 119 nm can be indexed as the cubic structure periclase [MgO] (PDF file No. 01-087-0651), the other small peaks displayed XRD patterns of brucite [$Mg(OH)_2$] (PDF file No. 01-083-0114). The main peaks of the 104 nm MgO can be indexed to the cubic structure of periclase [MgO] (PDF file No. 01-078-0430).

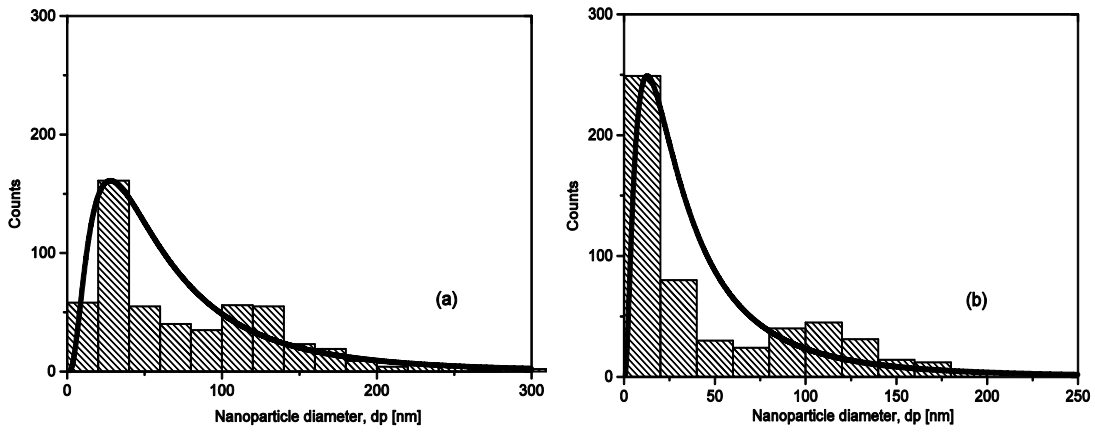

(a) (b)

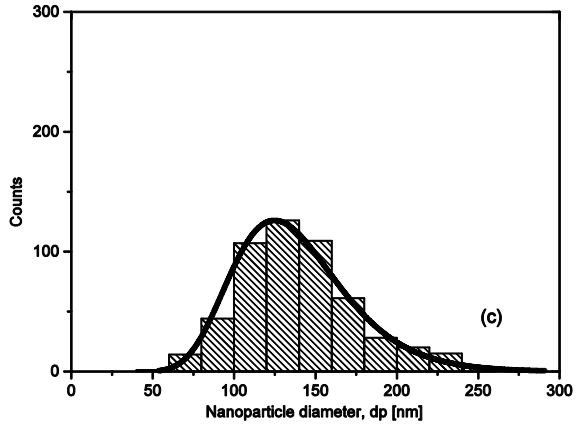

(c)

Figure 3.3: Particle size distribution of α-Al_2O_3 nanoparticles (a) 40 nm, (b) 80 nm and (c) 100 nm

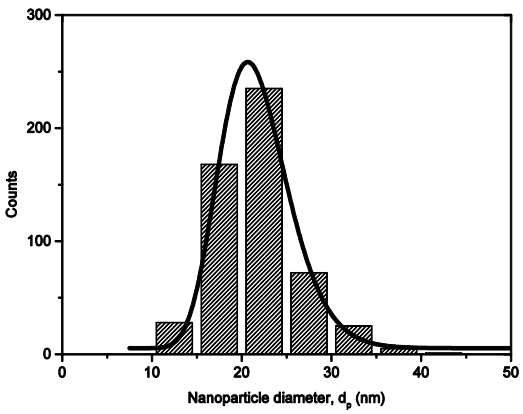

(a)

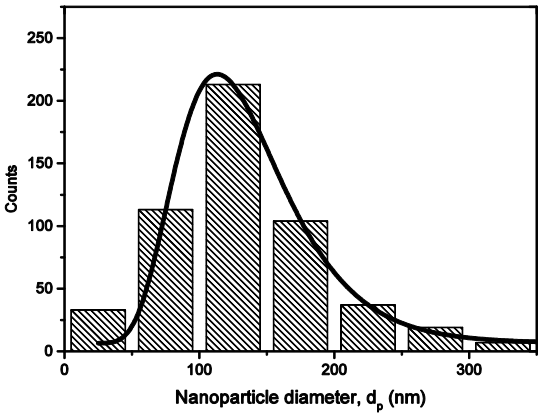

(b)

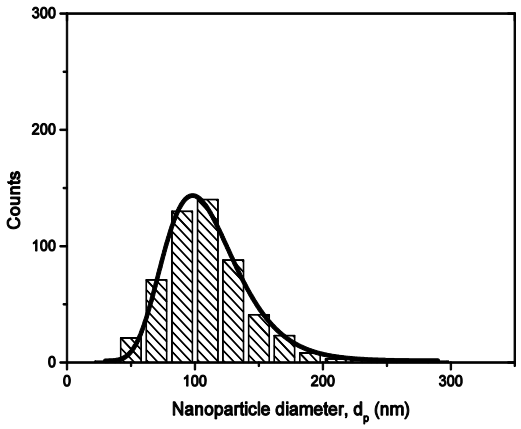

(c)

Figure 3.4: Particle size distribution of MgO nanoparticles: (a) 20 nm, (b) 40 nm and (c) 100 nm

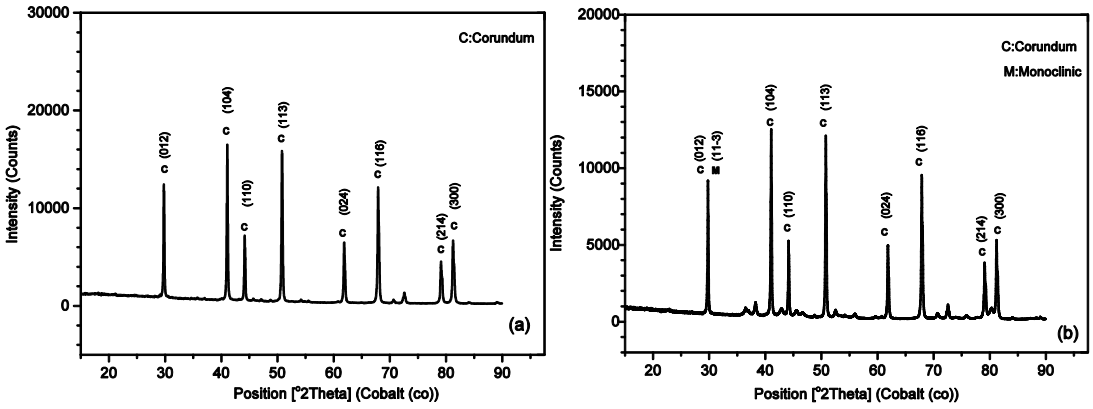

(a) (b)

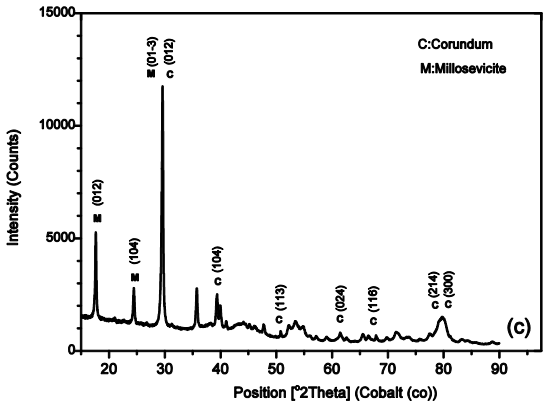

(c)

Figure 3.5: X-ray diffraction pattern of α-Al_2O_3 nanoparticles: (a) 31 nm, (b) 55 nm and (c) 134 nm powder

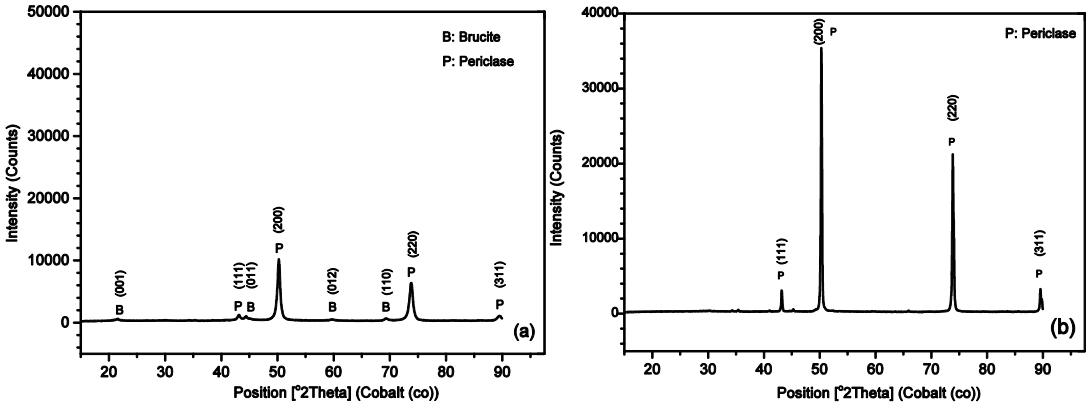

(a) (b)

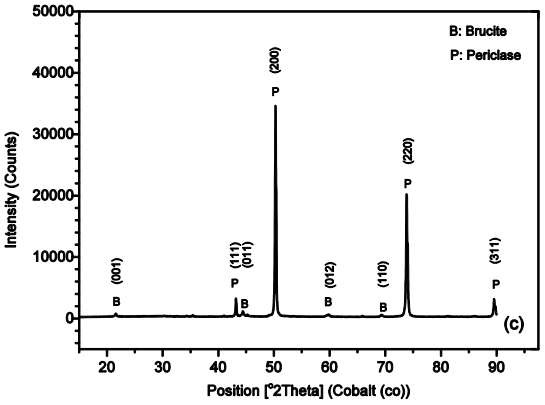

(c)

Figure 3.6: X-ray diffraction pattern of MgO nanoparticles: (a) 21 nm, (b) 104 nm and (c) 119 nm powder

The mineralogical analysis of α-Al_2O_3 samples confirms that both 55 nm and 134 nm consist of a mixture of corundum and Millosevichite while 31 nm is composed of corundum (see Table 3.2). The same analysis reveals that both 21 nm and 119 nm consist of a mixture of periclase (MgO) and (brucite), but with a high concentration of periclase, while 104 nm is essentially composed of periclase (Table 3.3).

Table 3.2: Mineralogical composition of α-Al_2O_3 nanoparticles

Mineral	**Nanoparticles**					
	40 nm α-Al_2O_3		80 nm α-Al_2O_3		100 nm α-Al_2O_3	
	Weight (%)	3 *SD*	Weight (%)	3 *SD*	Weight (%)	3 *SD*
Millosevichite (Al_2SO_4)	19.5		0	0	-	
Corundum (Al_2O_3)	80.5		100	0	-	

Table 3.3: Mineralogical composition of MgO nanoparticles

Mineral	**Nanoparticles**					
	20 nm MgO		40 nm MgO		100 nm MgO	
	Weight (%)	3 *SD*	Weight (%)	3 *SD*	Weight (%)	3 *SD*
Brucite [$Mg(OH)_2$]	14.28	0.81	6.53	0.33	0.00	0
Periclase [MgO]	85.72	0.81	93.47	0.33	100.00	0

The average crystalline sizes from α-Al_2O_3 patterns are 34 nm for the 31 nm, 43 nm for 55 nm and 32 nm for 134 nm Al_2O_3 nanoparticles respectively. For the MgO nanoparticles, the estimated crystalline sizes are 17 nm for the 21 nm MgO, 40 nm for 119 nm MgO and 40 nm for 104 nm MgO nanoparticles respectively. One can see that they are up to three times smaller than their corresponding average particle sizes. However, the calculation was done without correction for instrumental, stress broadening and any other possible sources of line broadening.

3.4 Preparation of nanofluids

3.4.1 Preparation of glycerol-based nanofluids

Two-step techniques were applied to prepare nanofluids in this work. Both nanoparticles used in this method are first produced as dry powders by chemical or physical methods by manufacturers. The nanosized powder was then dispersed into a glycerol (base fluid) in the second processing step with the help of intensive ultrasonic agitation, high-shear mixing and homogenising.

The various samples of α-Al_2O_3-glycerol or MgO-glycerol nanofluids were prepared in a 100 ml beaker with no surfactant for the volume fractions ranging from 0.5% to 4%. The nanofluid was ultrasonicated with S14 sonotrod (UP200S Hielscher of 200 Watts operated at 24 kHz) [76] for two hours to ensure uniform dispersion of the nanoparticles. The UP200S regulated to transfer an acoustic irradiation of 75% amplitude for the period of 0.9 sec/sec to nanofluid. A thermal bath (LAUDA ECO RE1225 Silver) was used to obtain and maintain different temperatures of nanofluids during the measurement process. After that, the nanofluids were kept still for 30 minutes to minimise the forced convection produced by both ultrasonicator probe and the thermal bath. Figure 3.7 shows the sample preparation set-up.

Figure 3.7: Nanofluid preparation set-up

The volume fraction of nanoparticles ϕ was determined using equation (3.3):

$$\phi = \frac{\frac{W_p}{\rho_p}}{\frac{W_p}{\rho_p} + \frac{W_{gly}}{\rho_{gly}}} x100\% \qquad (3.3)$$

where W_p, W_{gly}, ρ_p and ρ_{gly} are respectively the weight of nanoparticles, weight of glycerol, density of nanoparticles and the density of glycerol.

3.4.2 Effect of sonication time

Figure 3.8 (a) and (b) show the effect of sonication time on the effective thermal conductivity of MgO-glycerol nanofluids with variable nanoparticle sizes at 1% and 4% volume fraction of MgO nanoparticles. In figure 3.8 (a) and (b), each experimental data represents an average value of at least five measurements for each sonication time. Error bars represent the standard deviation of the experimental data.

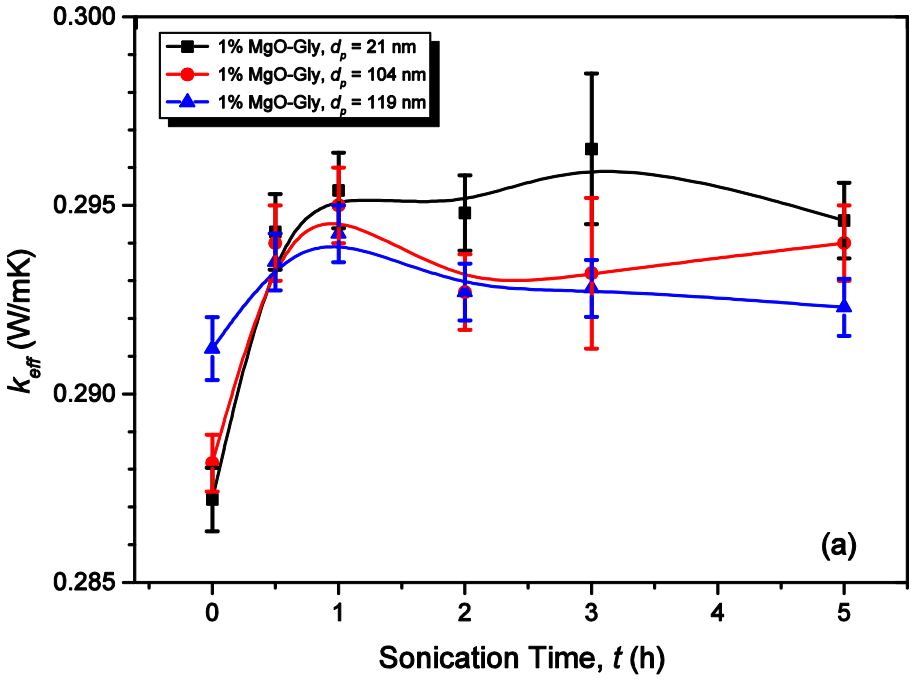

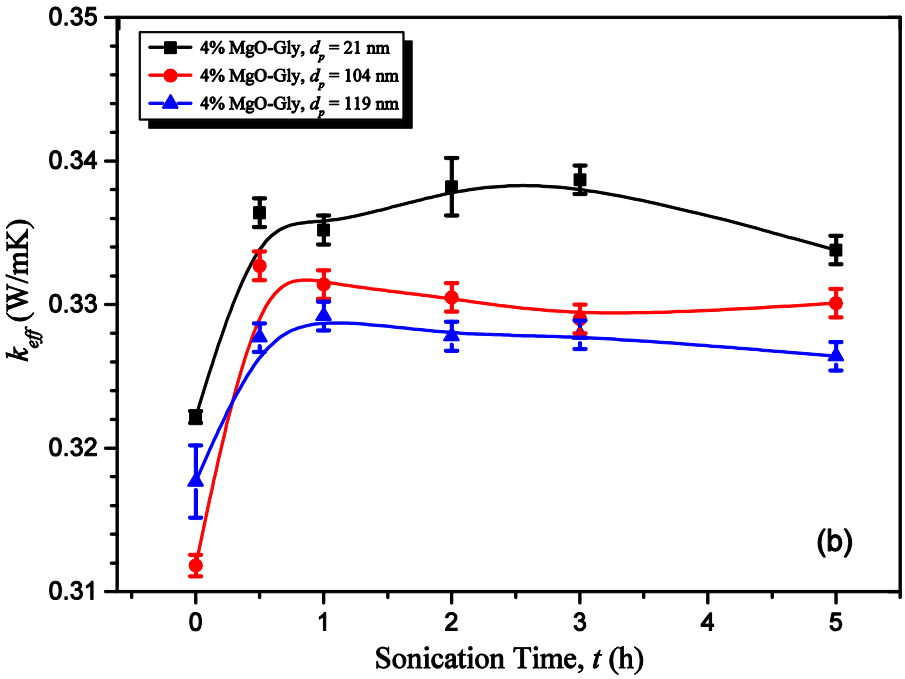

Figure 3.8: Effect of sonication time on the effective thermal conductivity of MgO-glycerol nanofluids with variable nanoparticle sizes at different volume fractions: (a) 1% MgO-glycerol and (b) 4% MgO-glycerol

An increase in k_{eff} of MgO-glycerol nanofluids is observed as the sonication time increases up to one hour for all three MgO nanofluids. After that, it is almost constant. Each nanoparticle size shows almost the same trend at both 1% and 4% volume fraction MgO-glycerol nanofluids.

One can also notice that the k_{eff} of MgO-glycerol increases with a decrease in nanoparticle size. The average increase in k_{eff} of MgO-glycerol nanofluids is 2% and 5% for 1% and 4% respectively. All the sonication investigations were acquired with oscillation amplitude of 75% and pulse-pulse mode factor of 90% per second. The sonication possibly decreases the average MgO cluster size in the nanofluids and

improves the dispersion of nanoparticles into the glycerol in the initial time up to the optimum time (1 hour). Afterwards, it can produce stable nanofluids.

The observation is not supported by the recent observations of Kole and Dey (ZnO-EG), Shima *et al.* (CuO-EG and Fe_3O_4-Kerozene) and Hong *et al.* (ZnO-Water) [77]. However, they did not mention the oscillation amplitude and pulse-pulse mode factor of the prepared nanofluids.

3.5 Thermal conductivity measurement device

The thermal conductivity of both glycerol and nanofluid was measured with the KD2 Pro Thermal Properties Analyser (Decagon Device, USA). The handled device measures the thermal conductivity values ranging from 0.02 to 2 W/mK over the temperature range of 0 ˚C to 50 ˚C with 5% accuracy. It is based on the transient hot-wire source method.

The apparatus consists of handled controller and sensors that operate in the temperature ranges of 0 ˚C to 50 ˚C and -50 ˚C to 150 ˚C. The device uses a stainless steel needle (KS-1) having a length and diameter of 60 mm and 1.3 mm. The needle sensor is constituted with heater and temperature sensor. The probe is inserted vertically into the fluid sample. A small amount of heat is applied to the sample for half the time, and the measurements are taken over the full time. The probe's temperature is monitored over time while a current is passed through the heater [78]. The KD2 Pro thermal analyser complies with both ASTM D5334 standard and IEEE 442-1981 regulations.

3.6 Validation of experimental data

Figure 3.9 shows thermal conductivity values of glycerol measured with the KD2 Pro and the reference data for temperatures ranging from 20 ˚C to 45 ˚C [79, 80]. The reference values show a deviation of less than 1% between them. Each experimental data set represents an average of nine measurements at various temperatures. Error bars denote the standard deviation of each piece of experimental data. The results show that the measured data are in excellent agreement with available reference data, within ± 2% accuracy. The KD2 Pro has been successively used by several researchers [11, 81, 82].

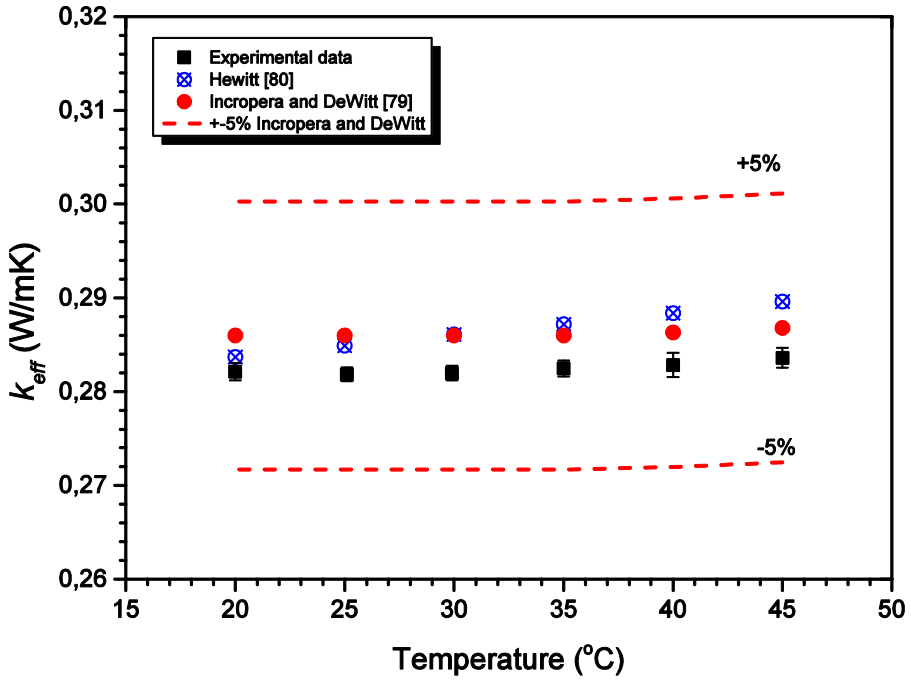

Figure 3.9: Validation of KD2 Pro instrument with glycerol

3.7 Uncertainty

The uncertainty of experimental results (u) was determined from both the bias error (instrument) and precision error arising from the deviation in the experimental data set. The bias error in measurement of thermal conductivity by KD2 Pro is 5%. The accuracy of the weighing scale is 0.01g. The uncertainty of the experiment is obtained by the following [83]:

$$u = \pm\sqrt{(u_B)^2 + (u_P)^2} \tag{3.4}$$

with

$$u_p = \pm t_{v,p} * SD \tag{3.5}$$

where u_B, u_p, $t_{v,p}$ and SD are bias error, precision or random error in measurement with P% probability, weighing function for v degree of freedom and P% probability and sample standard deviation respectively.

The uncertainty in TCR (u_{TCR}) is computed with equation (3.6). The uncertainty analysis of the TCR is presented in Appendix A:

$$u_{TCR} = \left[\left(\frac{\delta k_{eff}}{k_f}\right)^2 + \left(\frac{-k_{eff}}{[k_f]^2}\delta k_f\right)^2\right]^{0.5} \tag{3.6}$$

where $u_{k_{eff}}$ and u_{k_f} are uncertainty at P% probability including both bias and precision errors associated with the measured effective thermal conductivity of nanofluids and thermal conductivity of the base fluid respectively. However, the uncertainty in the effective thermal conductivity and TCR is between 5% and 8.5%.

3.8 Conclusions

Chapter 3 discussed the physical characterisation of nanoparticles, the nanofluid preparation and the validation of the experimental data. The study investigated two types of nanoparticles, namely MgO and α-Al_2O_3. TEM image files of MgO and α-Al_2O_3 nanoparticles were analysed using ImageJ software (NIH, Bethesda, MD, USA) to ascertain the nanoparticle size of investigated materials. The particle size distribution of various nanoparticle sizes was based on the TEM image analysis of more than 500 particles, which were individually counted.

The results showed significant differences in nanoparticle sizes between the obtained values and manufacturer's values. The three MgO nanoparticles respected the lognormal distribution with the mean particle size respectively of 21 ± 1 nm for 20 nm MgO nanoparticle, 119 ± 2 nm for 40 nm MgO nanoparticle and for 104 ± 1 nm for 100 nm MgO nanoparticle. The three α-Al_2O_3 nanoparticles respected the lognormal distribution with the mean particle size respectively of 55 ± 2 nm for 40 nm α-Al_2O_3 nanoparticle, 31 ± 3 nm for 80 nm α-Al_2O_3 nanoparticle and for 134 ± 1 nm for 100 nm α-Al_2O_3 nanoparticle.

The results of sonication time presented in this chapter were obtained on the MgO-glycerol nanofluids sonicated with oscillation amplitude of 75% and pulse-pulse mode factor of 90% per second. The effective thermal conductivity of MgO-glycerol nanofluids increased with sonication time up to an optimum (stable) value of one hour, then became almost constant up to five hours for the three sizes of MgO nanoparticles. The 21 nm MgO-glycerol gave the highest values of k_{eff}, followed by 104 nm MgO

and 119 nm at almost all various sonication times. The effective thermal conductivity increased with the increase in nanoparticle volume fractions for all three nanoparticle sizes.

The sonication time of two hours for nanofluid preparation was used in this investigation due to the previous experimental results and the published research results from literature.

For validation of the measurement, the thermal conductivity of glycerol was compared with the published data by Incropera and DeWitt [79] for temperatures ranging from 20 ˚C to 45 ˚C. The measured data were within 2% accuracy with available reference data.

3.9 Recommendation

The physical characterisation of nanoparticles must be determined before the thermal conductivity measurement to ascertain the nanoparticle composition and size distribution because they are crucial for the nanofluid behaviour.

CHAPTER 4: EXPERIMENTAL INVESTIGATION AND MODEL DEVELOPMENT FOR THE THERMAL CONDUCTIVITY OF α-Al_2O_3-GLYCEROL NANOFLUIDS

4.1 Introduction

This chapter discusses the thermal conductivity of stable α-Al_2O_3-glycerol-based nanofluid results. The results are presented for each measurable parameter influencing the thermal conductivity of nanofluids such as particle volume fraction, temperature and nanoparticle particle size. Each experimental data represents an average value of five measurements at a given conditions. Error bars represent the standard deviation of each experimental data. A linear regression analysis is conducted to evaluate the individual impact of each parameter on the TCR, assuming the other variables are held constant, while a regression analysis is conducted to determine how the measurable variables jointly influence the TCR of α-Al_2O_3-glycerol-based nanofluids. Appendix B: discusses the regression analysis models and significance tests.

4.2 Particle volume fraction studies

Figure 4.1 shows the effect of the particle volume fraction (at dosages of 0.5%, 1%, 2% and 4%) on the effective thermal conductivity ratio of α-Al_2O_3-glycerol nanofluids; α-Al_2O_3 nanoparticles dispersed in glycerol yielded higher thermal conductivity than the base fluid (glycerol).

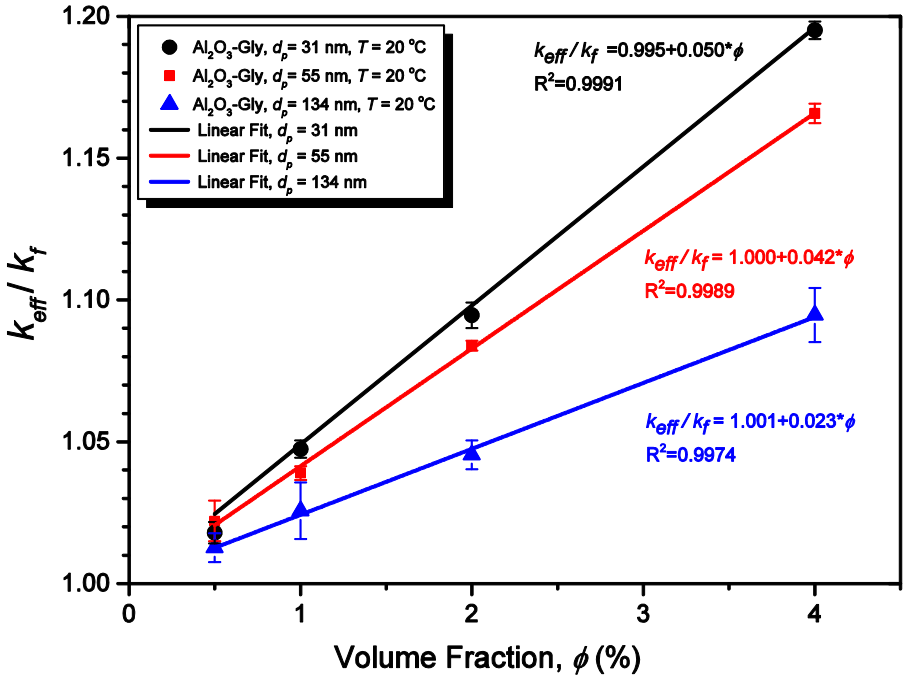

Figure 4.1: Influence of nanoparticle volume fraction on the thermal conductivity ratio of the three sets of α-Al_2O_3-glycerol nanofluids at 20 °C

The best fitting line equation and corresponding R-square values are relative to the given nanoparticle diameter and temperature. It is apparent in Figure 4.1 that the thermal conductivity ratio increases linearly with an increase in volume fraction for each particle size for α-Al_2O_3-glycerol nanofluids where $\boldsymbol{\phi}$ is the α-Al_2O_3 nanoparticle volume fraction expressed per unit.

Table 4.1 gives the results of the linear regression analysis conducted to determine the effect of volume fraction on the TCR of α-Al_2O_3-glycerol nanofluid. The significant p of F-statistic of the α-Al_2O_3-glycerol nanofluids model is less than 0.001. It suggests that the null hypothesis should not be rejected. There is a linear relationship between the volume fraction and the TCR of α-Al_2O_3-glycerol nanofluids, given by equation (4.1). R-square of 0.822 for α-Al_2O_3-glycerol linear equations expresses that the

volume fraction explains 82.2% of the variability in the TCR values. The residual and other variables can explain the remaining 17.8% for α-Al_2O_3-glycerol of variation in TCR.

$$\frac{k_{eff}}{k_f} = 0.997 + 3.824 * \phi \quad (4.1)$$

where $\boldsymbol{\phi}$ is the α-Al_2O_3 nanoparticle volume fraction expressed per unit.

Table 4.1 Results of linear regression analysis of TCR of α-Al_2O_3-glycerol vs. volume fraction

Model	R	R Square	Std. Error of the Estimate	Statistics	
				F	P
α-Al_2O_3	0.907	0.822	0.024	322.8	0.000

Altogether, there is a linear increase in TCR with an increase in α-Al_2O_3 nanoparticle volume fraction. This outcome is in agreement with other studies of various types of nanofluids [1, 21, 49, 59, 77, 84]. The thermal conductivity ratio improved up to 19.5%, 16.6% and 9.5% of the α-Al_2O_3 nanoparticle volume fraction of 4% for 31 nm, 55 nm and 134 nm size nanoparticles respectively at 20 ˚C.

Figure 4.1 clearly depicts the impact of particle size on the TCR. Small particle size leads to higher thermal conductivity of nanofluids than that of the big sizes. The same situation was perceived at various ranges of temperature.

The improvement of the thermal conductivity ratio for the α-Al_2O_3-glycerol nanofluids with respect to the volume fraction could possibly be explained by one or more

mechanisms including Brownian motion, nanoparticle clustering or layering at the solid-liquid interface. The suspended α-Al_2O_3 nanoparticles in the glycerol increase the surface area and the heat capacity of the glycerol, and both interaction and collision among α-Al_2O_3 nanoparticles are strengthened [37, 85]. The Brownian diffusion coefficient (see Section 2.3.2) is directly proportional to temperature and reciprocal to both nanoparticle diameter and viscosity of the liquid. Nanofluids prepared with the smaller size of nanoparticles will result in more severe collisions among nanoparticles and fluid molecules than one made with the big size. The particle-to-particle interaction increases as the distances between nanoparticles decrease by increasing the volume fraction of the nanoparticle. The increase in nanoparticle volume fraction intensifies the collision and interaction among nanoparticles, diffusion into nanofluid and the heat capacity of the glycerol leading to the enhancement of the thermal conductivity of α-Al_2O_3-glycerol nanofluids.

4.3 Temperature studies

Figure 4.2 shows the effect of temperature on the effective thermal conductivity of α-Al_2O_3-glycerol nanofluids for three different sizes of nanoparticles (31 nm, 55 nm and 134 nm). As can be observed in Figure 4.2, the temperature dependence of the effective thermal conductivity of the α-Al_2O_3 nanofluids with different particle sizes has a similar pattern to the base fluid (glycerol). Similar findings were reported for the Al_2O_3-water nanofluids [49], and ethylene glycol-based nanofluids containing Al_2O_3, MgO, ZnO, SiO_2, and graphene nanoparticles [15, 33, 36, 49].

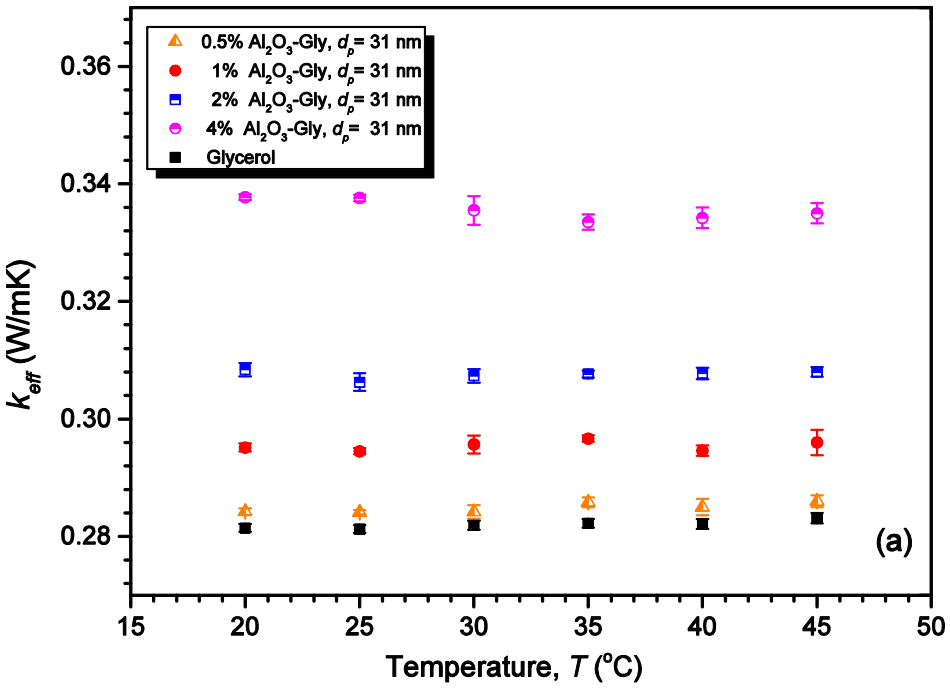

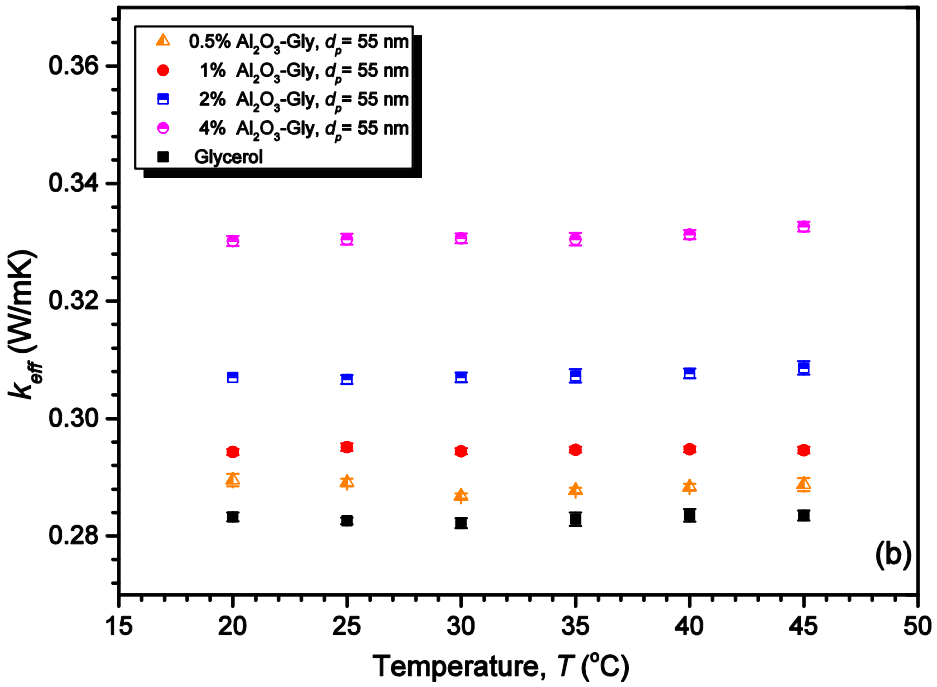

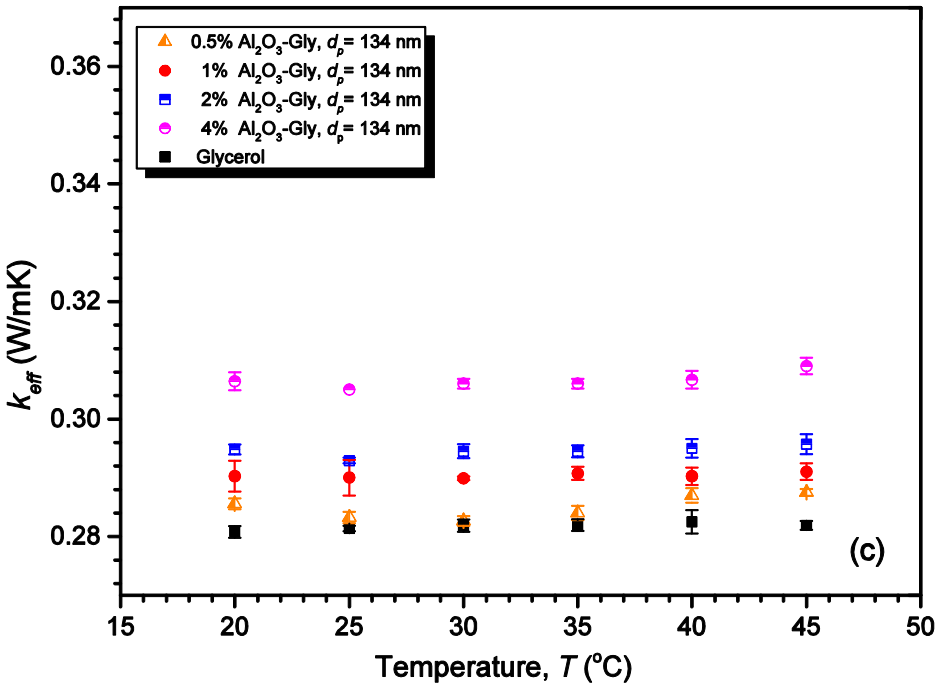

Figure 4.2: Temperature dependence of the effective thermal conductivity of α-Al_2O_3-glycerol nanofluids at different volume fractions: (a) 31 nm, (b) 55 nm and (c) 134 nm

Figure 4.3 shows the thermal conductivity ratio of α-Al_2O_3-glycerol nanofluids at different volume fractions as a function of temperature. The estimated linear relationships between the temperature and the TCR of α-Al_2O_3-glycerol nanofluid are given by equation (4.2):

$$\frac{k_{eff}}{k_f} = 1.071 - 7.02 * 10^{-5} * T \qquad (4.2)$$

where T is temperature expressed in ˚C.

Equation (4.2) can be simplified in equation (4.3) as its slope value will contribute insignificantly to improve the TCR for the range of tested temperature.

$$\frac{k_{eff}}{k_f} = 1.071 \tag{4.3}$$

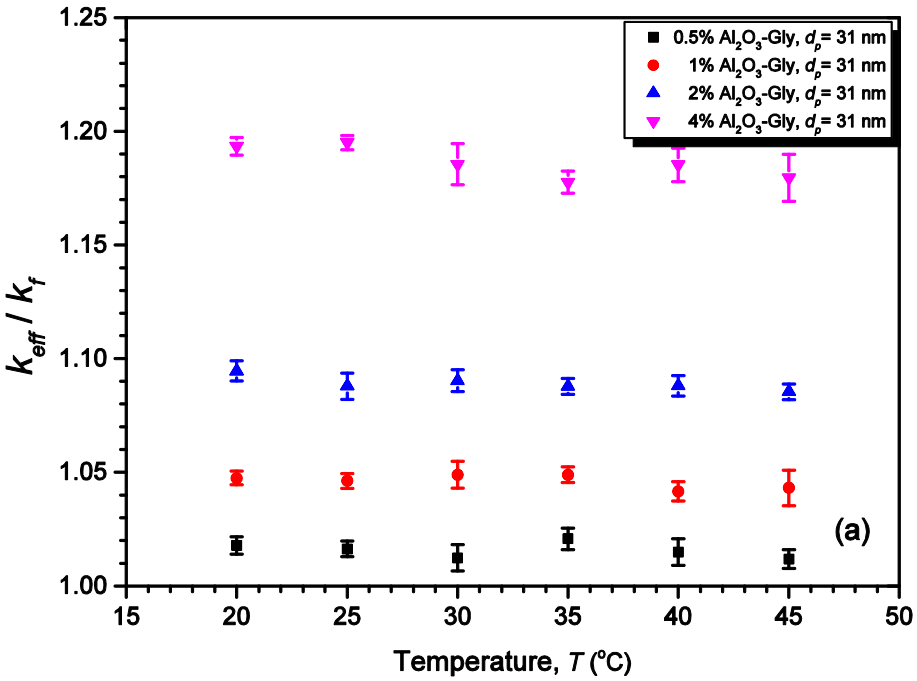

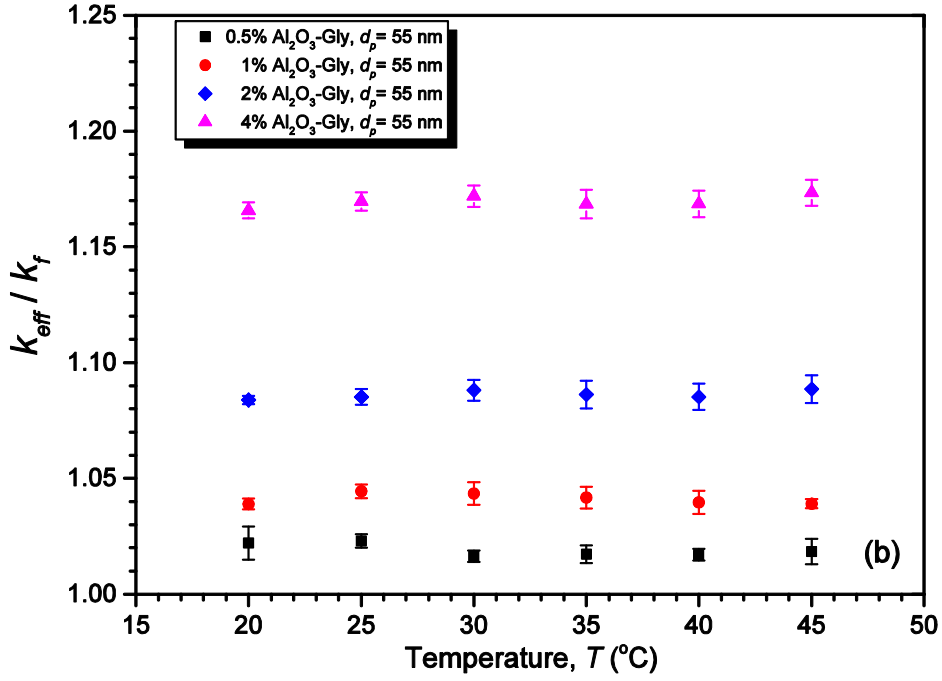

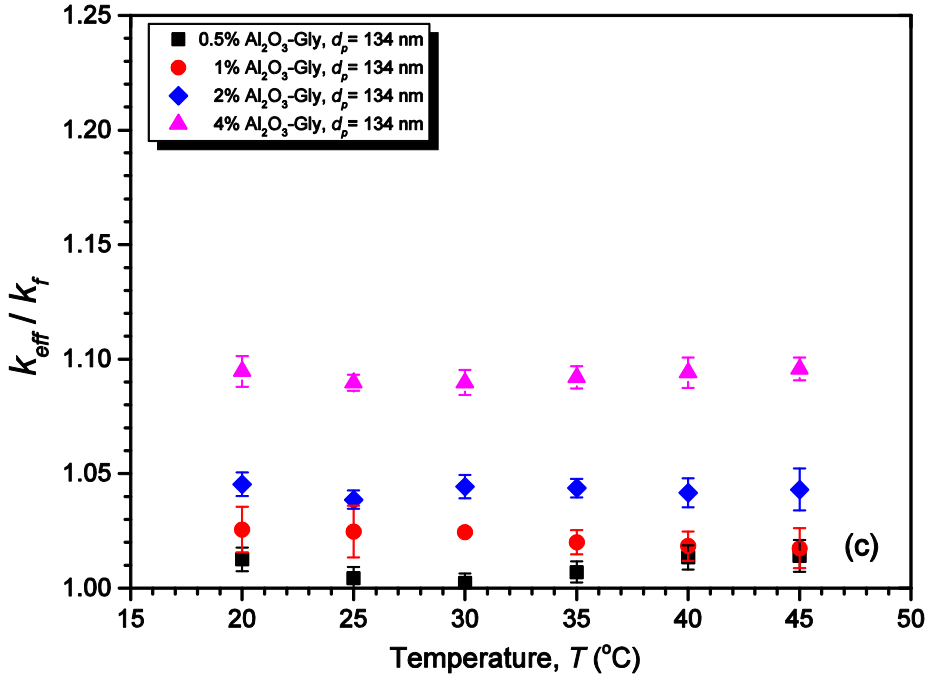

Figure 4.3: Temperature dependence of the thermal conductivity ratio of α-Al_2O_3-glycerol nanofluids at different volume fractions: (a) 31 nm, (b) 55 nm and (c) 134 nm

As observed in Table 4.2, the obtained equations have unadjusted R-square = 0.0001 and significant p of F-statistic > 0.05 (acceptable level). The t-ratios of intercept and slope (temperature) are 39.87 and -0.09 for α-Al_2O_3-glycerol nanofluids. Their corresponding significant p-values are 0.000 ($p < 0.05$) and 0.930 ($p > 0.05$). The significant p-values of both F-statistic of the model and t-ratio of the slope of the model are not significant. Thus, there is no dependence of TCR with temperature for glycerol-based α-Al_2O_3-glycerol nanofluids. The simplification of equation (4.3) is statistically justified.

Table 4.2: Results of linear regression analysis of TCR of α-Al_2O_3-glycerol vs. volume fraction

Model	R	R Square	Std. Error of the Estimate	Statistics	
				F	p
α-Al_2O_3	0.01	0.0001	0.057	0.01	0.930

Xie *et al.* also state that there is no dependence of TCR with temperature for both 5% Fe_3O_4-kerosene and 1% MgO-EG nanofluids over the temperature range of 10 ºC to 60 ºC [35, 86]. They explain that the effective thermal conductivity of both nanofluids varies with temperature rise while the (k_{eff} / k_f)almost constant. However, Saleh *et al.* [81] and also some others [21, 33, 81, 87, 88] state that the effective thermal conductivity ratio of nanofluids varies with an increase in temperature. For this reason, it can be said that the effect of temperature on thermal conductivity ratio depends on the nanofluid characteristics.

Figure 4.3 also shows that the thermal conductivity of α-Al_2O_3-glycerol nanofluids varies significantly with increase in ϕ, as depicted in Section 4.2.

4.4 Nanoparticle size studies

Figure 4.4 provides the effect of particle size on the α-Al_2O_3-glycerol nanofluid thermal conductivity ratio at room temperature. Equation (4.4) gives the estimated straight-line regression of TCR on diameter computed:

$$\frac{k_{eff}}{k_f} = 1.0997 - 4.29 * 10^{-4} * d_p \qquad (4.4)$$

where $\boldsymbol{d_p}$ is the diameter of α-Al_2O_3 expressed in nm.

Table 4.3: Results of linear regression analysis of TCR of α-Al_2O_3-glycerol vs. particle size

Model	R	R Square	Std. Error of the Estimate	Statistics	
				F	p
α-Al_2O_3	0.334	0.111	0.054	8.78	0.004

The linear equation of α-Al_2O_3-glycerol nanofluids has R^2 of 0.111. It means that the the diameter of α-Al_2O_3 nanoparticles explains 11.1% of the variability in the TCR values. The residual and other variables can explain the remaining 88.9% of the variation in TCR. The F-statistic of the model is 8.78 with corresponding significant p of 0.004 ($p < 0.05$). The p-value suggests rejecting the null hypothesis. Thus, there is a linear relationship between the diameter and the TCR for α-Al_2O_3-glycerol nanofluids. The t-ratios of intercept and slope (diameter) are 88.82 and -2.96 respectively. Their corresponding significant p-values are 0.000 and 0.004 ($p < 0.05$). The model is highly significant. The thermal conductivity ratio of α-Al_2O_3-glycerol nanofluids increases with decreasing particle size for a given volume fraction and temperature.

The Brownian diffusion coefficient (see Section 2.3.2) could explain the variation of TCR of α-Al_2O_3-glycerol nanofluids vs. diameter. The Stokes-Einstein equation (2.1) shows that nanofluids prepared with a small size nanoparticle will result in a higher *D* coefficient than the one made with the bigger size. Consequently, more severe collisions among nanoparticles and fluid molecules will be present in nanofluids, which will lead to better thermal conduction [87, 88]. In addition, smaller particles exhibit a larger surface area to volume ratio than the bigger particles, which can result in a

noticeable enhancement of the effective thermal conductivity [15]. This theory could not explain any enhancement of TCR of MgO-glycerol nanofluid with increase in diameter.

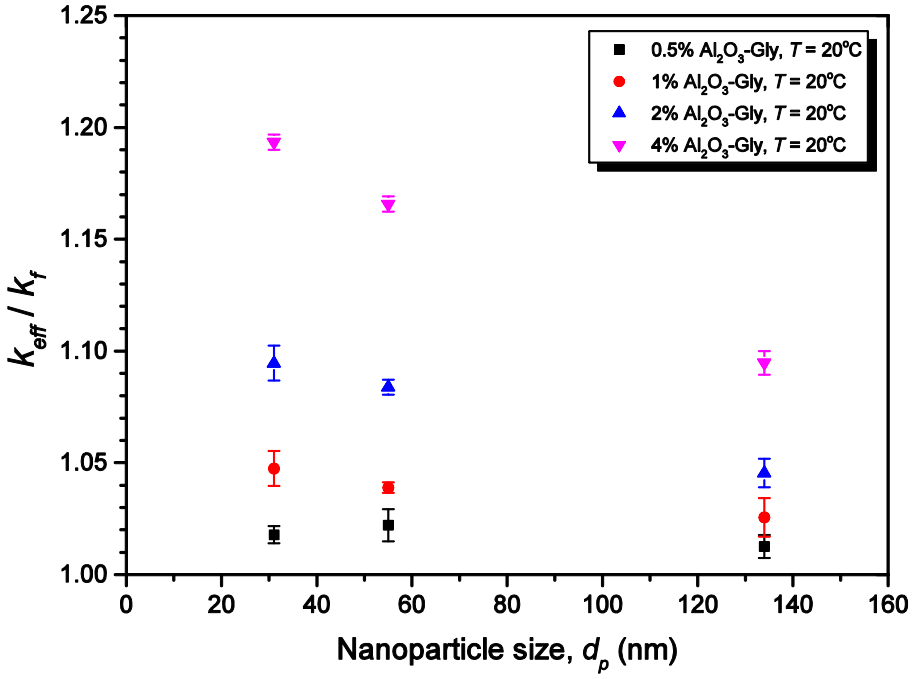

Figure 4.4: Influence of nanoparticle size on the effective thermal conductivity ratio at three different volume fractions of α-Al_2O_3-glycerol nanofluid at 20 °C

4.5 Stability of α-Al_2O_3-glycerol-based nanofluids

The stability of α-Al_2O_3-glycerol samples was evaluated for 4% volume fraction. No surfactant was used in the preparation of nanofluids. Thirty minutes after sonication, the effective thermal conductivity was acquired for each particle size at one-hour step, up to 50 hours. The results observed in Figure 4.5 show no change in the effective thermal conductivity of α-Al_2O_3-glycerol with time after nanofluid preparation. For clarity, the data were plotted at four-hour intervals. The regression analysis approach

analyses the strength of the relationship between the elapsed time and the effective thermal conductivity of α-Al_2O_3-glycerol.

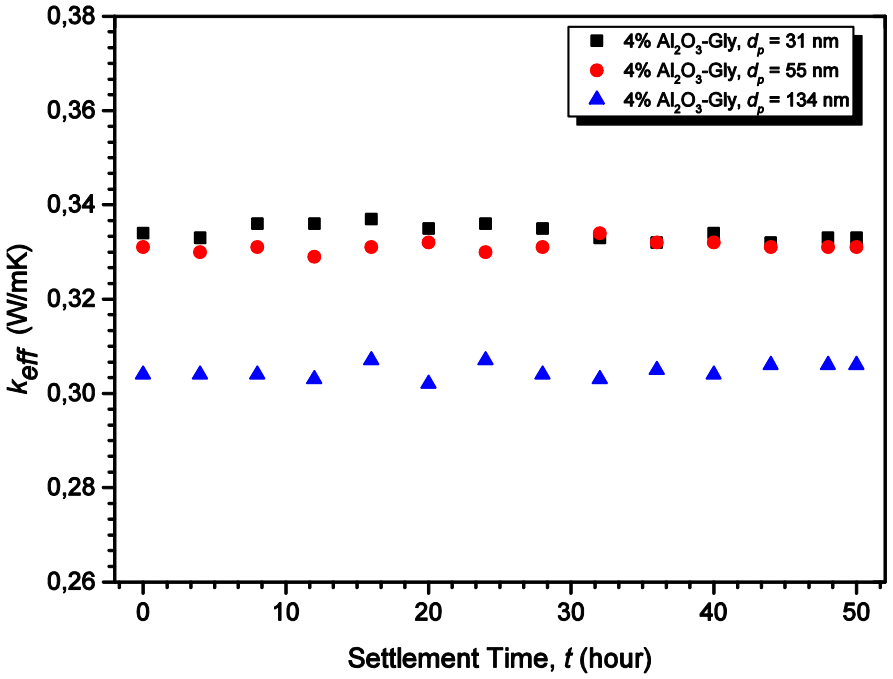

Figure 4.5: Influence of settlement time on the effective thermal conductivity of 4% α-Al_2O_3-glycerol nanofluids

The estimated linear equation of α-Al_2O_3-glycerol nanofluids between the elapsed time after preparation and the effective thermal conductivity computed of α-Al_2O_3-glycerol nanofluids is given by equation (4.5). Table 4.4 gives the results of a linear regression analysis of the effective thermal conductivity of the models vs. elapsed time after preparation. The t-statistic of the slope of the model is 0.175. Its corresponding significant p-values is 0.861, which is greater than 0.05.

The R-square and p-value of both the F- and t-statistics are 0.000 and greater than 0.05 respectively. The F-statistic values cannot reject the null hypothesis. The variation of

effective thermal conductivity of both models vs. elapsed time after preparation is not statistically justified. There is no dependence of the effective thermal conductivity of both models with elapsed time up to 50 hours. As a result, equation 4.5 can be simplified in equation (4.6).

$$k_{eff} = 0.323 - 3.66 * 10^{-9} * t \quad (4.5)$$

where t is elapsed time in seconds.

$$k_{eff} = 0.323 \quad (4.6)$$

The best model is the naive model, which is the mean value of thermal conductivity for each given diameter. The mean values and standard deviation of the effective thermal conductivity of α-Al_2O_3-glycerol are 0.335 ± 0.002 W/mK, 0.331 ± 0.001 W/mK and 0.304 ± 0.001 W/mK for 31 nm, 55 nm and 134 nm respectively.

Table 4.4: Results of linear regression analysis of the effective thermal conductivity of α-Al_2O_3-glycerol vs. elapsed time after preparation

Model	**R**	**R Square**	**Std. Error of the Estimate**	**Statistics**	
				F	**p**
α-Al_2O_3	0.014	0.000	-0.006	0.031	0.861

The thermal conductivity constancy of α-Al_2O_3-glycerol nanofluids in the early hours after sonication could possibly be explained by the absence of clustering and settling of nanoparticles as commonly found in the literature [35, 37, 89, 90]. The effective thermal conductivity measurement indicates the stability of α-Al_2O_3-glycerol-based nanofluids

at room temperature for at least 50 hours after preparation. This outcome disagrees with the results of Xie *et al.* and Khaddar *et al.* described in Section 2.2.8.

4.6 Comparison of the thermal conductivity models with α-Al_2O_3 glycerol experimental data

4.6.1 Introduction

This section describes the comparison of predicted results obtained from some existing theoretical models and experimental correlation with the obtained experimental data of α-Al_2O_3-glycerol nanofluids. In this work, seven of the existing models will be used to predict the present experimental data, namely the Maxwell, Bruggeman, effective medium, Corcione, Peterson, Shake and Vajjha models.

4.6.2 Effect of volume fraction

Figure 4.6 provides comparisons at room temperature of the predicted effective thermal conductivity versus volume fraction relationship for various models (Maxwell, Bruggeman, Corcione, effective medium theory, Peterson, Vajjha and Shaker) with the experimental data set of three sizes of α-Al_2O_3-glycerol nanofluids. As shown in Figure 4.6 (a) and (b), Peterson underpredicts the experimental data of the nanofluids prepared with 31 nm and 55 nm α-Al_2O_3-glycerol nanofluids, whereas Vajjha overpredicts for $\phi < 4\%$. The Corcione model shows a very light increase of TCR with ϕ compared with the experimental data, increasing ϕ results in the diversion from experimental data. The other models give a good match to experimental data of $\phi < 2\%$, even if their predicted values are slightly lesser than the experimental results.

Figure 4.6 (c) discloses almost similar outcomes as for 31 nm and 55 nm α-Al_2O_3-glycerol nanofluids, except that the results of the Shaker, Maxwell, Peterson, Bruggeman and effective medium models are slightly higher than the experimental data for $\phi > 2\%$.

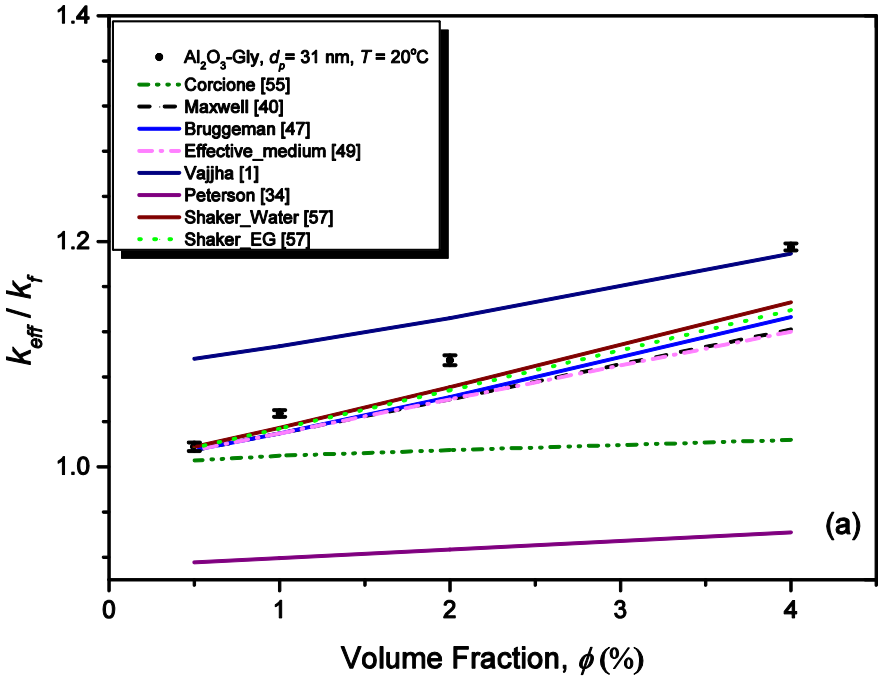

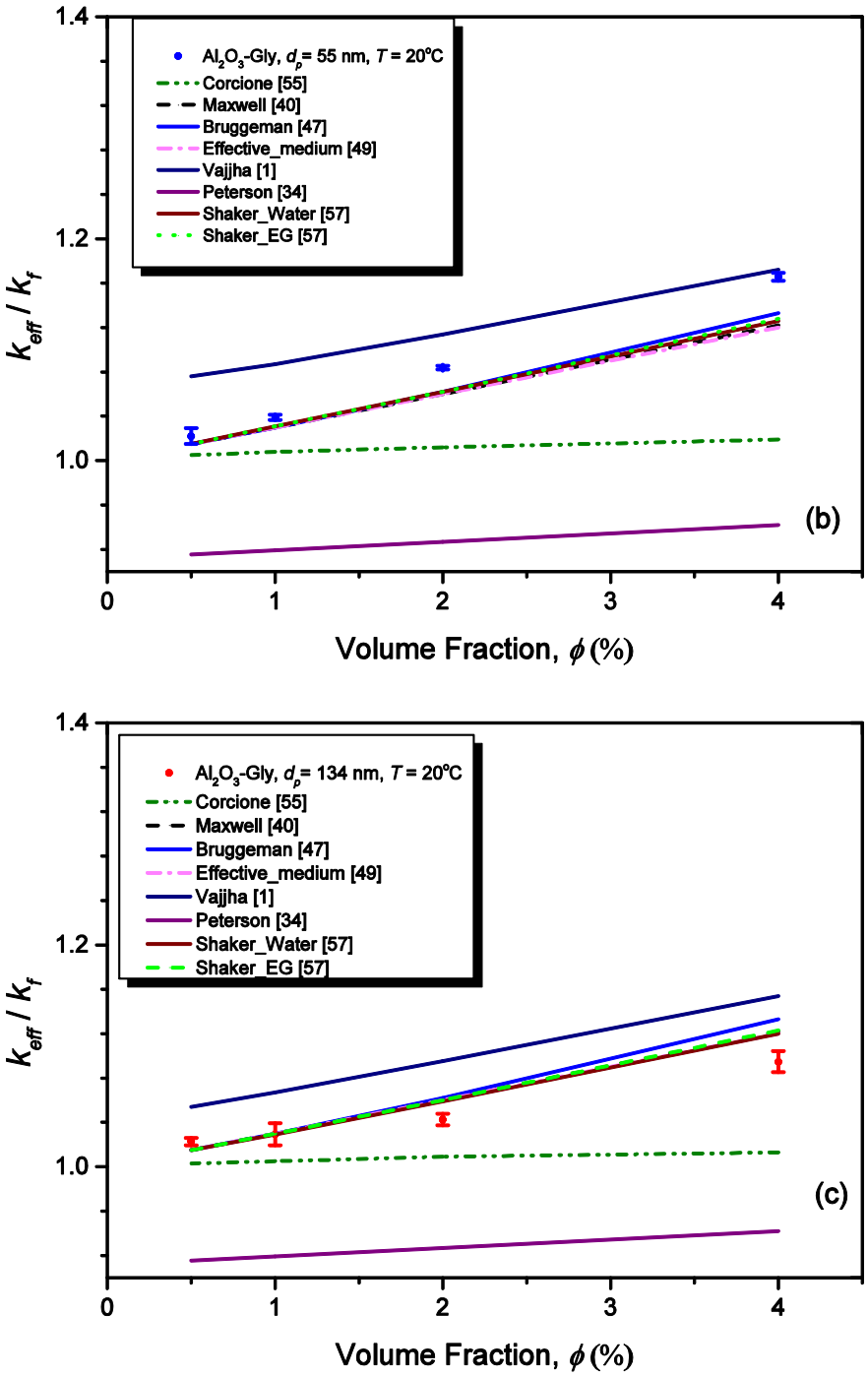

Figure 4.6: Comparison of the thermal conductivity ratio variation with volume fraction of experimental data and existing equations for α-Al_2O_3-glycerol nanofluid at 20 ˚C: (a) 31 nm, (b) 55 nm and (c) 134 nm

The Maxwell, Bruggeman, effective medium theory and Shaker models show a good match with the experimental data at 20 ˚C when $\phi < 2\%$ for all three α-Al_2O_3-glycerol nanofluids, whereas the models of Corcione and Peterson mostly underpredict the TCR. Similar patterns are observed for the other temperatures.

4.6.3 Effect of temperature

Figure 4.7 presents a comparison of the predicted thermal conductivity ratio versus temperature relationship for selected models with experimental data of 4% α-Al_2O_3-glycerol nanofluids for the three different sizes. The Corcione model underpredicts the experimental data of 31 nm, 55 nm and 134 nm α-Al_2O_3-glycerol nanofluids. The Vajjha model gives good predictions of temperature < 30˚C for both 31 nm and 55 nm α-Al_2O_3-glycerol nanofluids. The Corcione, Peterson and Vajjha models increase with a rise in temperature contrary to the expected trend, which is the TCR remaining unaffected with the temperature increase. The other models follow the expected trend and predict values that are lower than the experimental data for both 31 nm and 55 nm (see Figure 4.7 (a) and(b)), and greater than the experimental data for 134 nm α-Al_2O_3-glycerol nanofluids (see Figure 4.7 (c)).

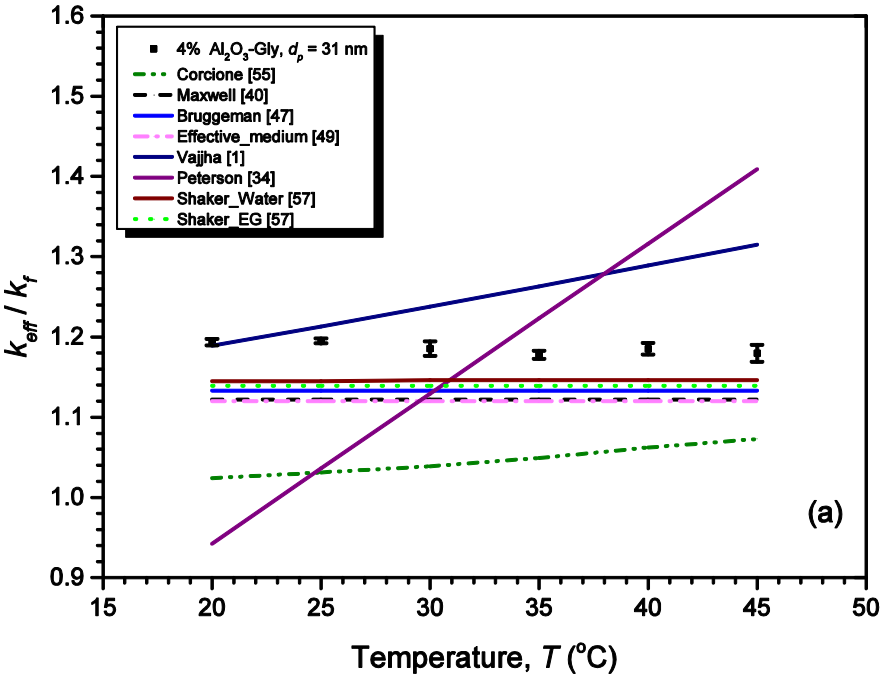

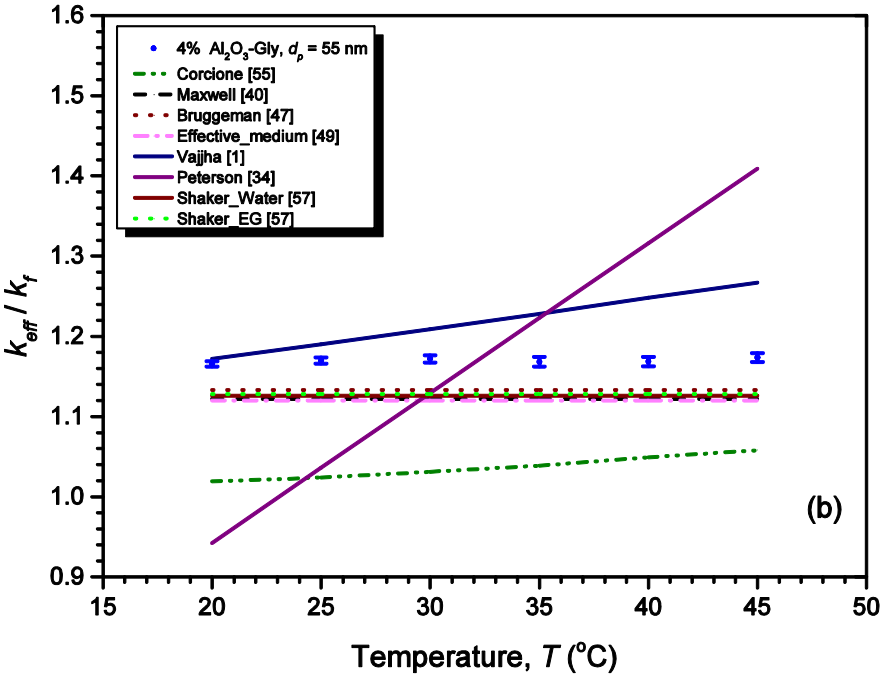

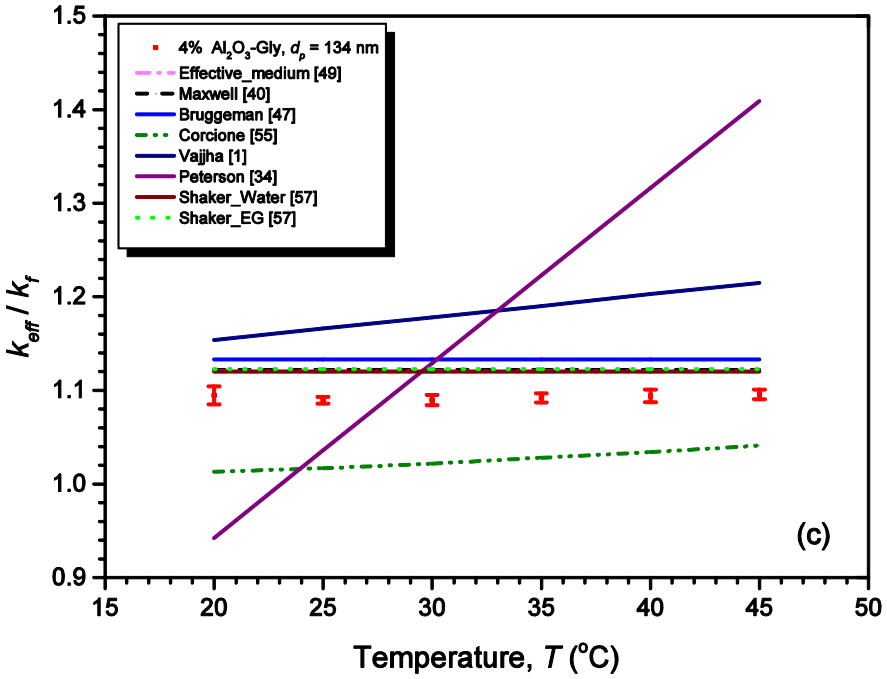

Figure 4.7: Comparison of the thermal conductivity ratio variation with temperature between experimental data and existing equations for 4% α-Al_2O_3-glycerol nanofluids: (a) 31 nm, (b) 55 nm and (c) 134 nm

4.6.4 Effect of particle diameter

Figure 4.8 provides comparisons of the TCR variation with nanoparticle diameter between experimental data set and selected models for 4% α-Al_2O_3-glycerol nanofluids. The Vajjha models overestimate the experimental data set, whereas the Corcione models underestimate. Both Shaker models give a good fit and a quite similar trend with experimental data. The TCR of α-Al_2O_3-glycerol nanofluids agrees quite well with the prediction of Maxwell, Bruggeman and effective medium, but their trend is contrary to the expected one. Peterson overestimates the TCR for the diameter of the three sizes of α-Al_2O_3-glycerol nanofluids. The Peterson prediction model does not follow the experimental data trend.

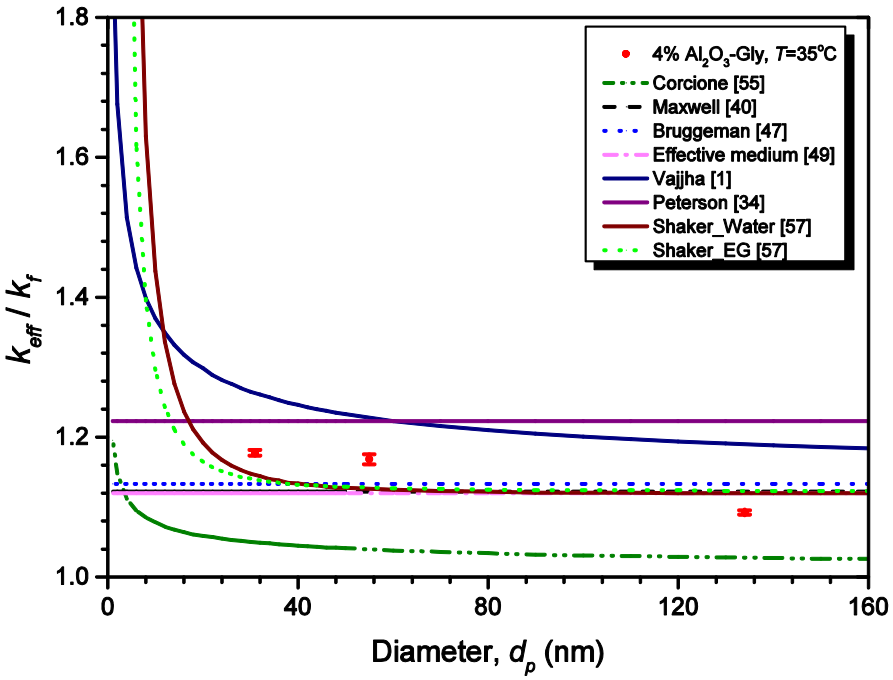

Figure 4.8: Comparison of the thermal conductivity ratio variation with nanoparticle diameter between experimental data set and existing equations for 4% α-Al_2O_3-glycerol nanofluids at 35 ˚C

4.7 New empirical correlation for the thermal conductivity ratio of α-Al_2O_3-glycerol

A new empirical correlation for the thermal conductivity α-Al_2O_3-glycerol nanofluids is determined. The novel equation is a modified version of a non-dimensional model proposed by Corcione [55] (see section 2.4). The regression analysis is used to determine the relationship between the studied parameters. Thus, F-statistic and associated p-value are used to verify whether the relationship between $\left(k_{eff} \,/\, k_f\right)$ and Xj predictor variables is not a random ($p < 0.05$). The t-statistic and related p-value assess the reliability of the partial regression coefficients ($p < 0.0\ 5$) in the equation [91]. Appendix B: condenses the regression analysis concepts. In the proposed correlation for the thermal conductivity of α-Al_2O_3-glycerol nanofluid, the nanoparticle

thermal conductivity is normalised with the thermal conductivity of base fluid (k_f). The nanoparticle diameter (d_p), the nanofluid temperature and the viscosity of the base fluids are normalised to the nanoparticle Reynolds number defined by Corcione in equation (4.7). Corcione used in the equation another important dimenssionless number which representes certain physical properties of the base fluid, named the Prandtl number (Pr_f) expressed by equation (4.8).

$$Re_p = \frac{2\rho_f \kappa T}{\pi {\mu_f}^2 d_p} \tag{4.7}$$

$$Pr_f = \frac{\mu_f C_{pf}}{k_f} \tag{4.8}$$

The developed empirical correlation that is expressed by equation (4.9) is the result of the regression analysis with 95% confidence level:

$$\frac{k_{eff}}{k_f} = 1 + Re_p^{0.4377} Pr_f^{0.9400} \phi^{1.0475} \left(\frac{40}{k_f}\right)^{0.6661} \tag{4.9}$$

where Re_p is the nanoparticle Reynolds number, Pr_f the Prandtl number of the base fluid (glycerol), ϕ the nanoparticle volume fraction, C_{pf} the specific heat of the base fluid, k_p the thermal conductivity of the α-Al_2O_3 nanoparticles (equal to 40 W/mK) and k_f the thermal conductivity of the glycerol (W/mK). The new correlation for the thermal conductivity of α-Al_2O_3-glycerol nanofluid is satisfactory for 20 ˚C < T < 45 ˚C, 0% < ϕ < 4% and 31 nm < d_p < 134 nm.

Equation (4.9) converging at 10^{-15} has an adjusted R-square = 0.980, F = $3.7*10^5$ and significant p = 0.0000. The t-statistic of the exponents of Re_p, Pr_f, ϕ and k_p / k_f is

19.4, 20.3, 38.5 and 16.1 respectively. The p-values associated with the t-ratio of all their exponents and slope of the equation are equal to 0.0000 ($p < 0.001$). The statistical significance of all the exponents of the equation is high. However, the p-value of the slope of the equation and the exponents of both Prandtl number and temperature are not statistically significant in the general Corcione model. There was a high linear correlation (R = 0.9992) between the terms $k_p \ / \ k_f$ and the slope of the equation, after removal of the temperature term ($T \ / \ T_{fr}$). Thus, the slope term was also removed to deal with the multicollinearity in the model. The temperature is still present in the new model, as the Reynolds number is directly proportional to temperature. There is no autocorrelation in the residuals and the residual sum is zero. The comparison between the predicted thermal conductivity ratio from the present model and the experimental results shows an excellent agreement with maximum relative error of +1.57%, -2.37% and the average relative error of -0.03% (see Figure 4.9). The present analysis provides evidence that the novel model is statistically significant.

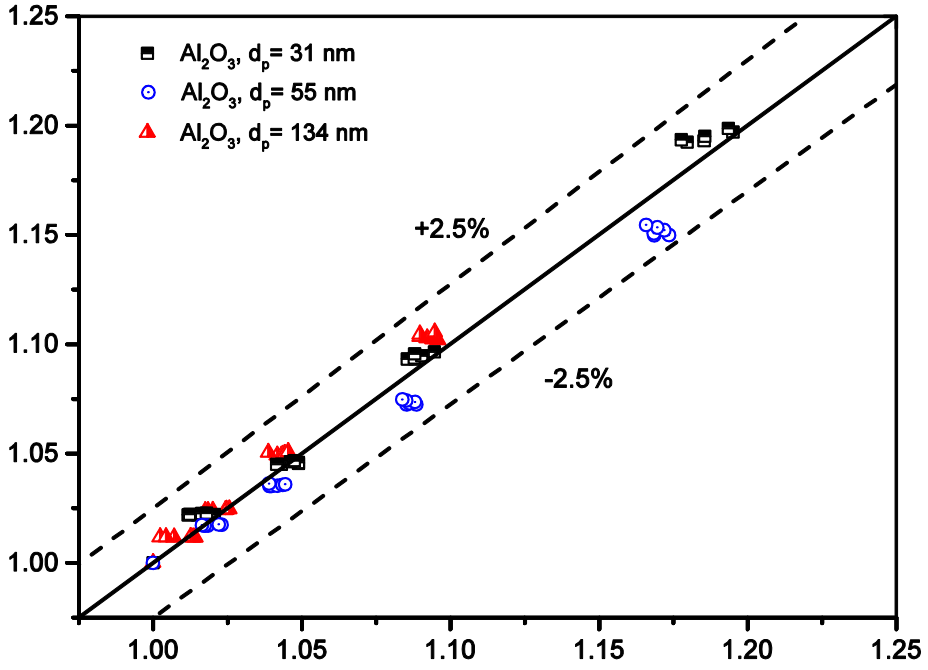

Figure 4.9: Comparison of the thermal conductivity ratio between the predicted values from the present correlation and the experimental data on α-Al_2O_3-glycerol nanofluids

Figure 4.10 shows a temperature dependence of Reynolds number for 31 nm, 55 and 134 nm size α-Al_2O_3-glycerol nanofluids. The Reynolds number increases with an increase in temperature and a decrease in nanoparticle sizes, as the Brownian velocity effect is much stronger for the smallest particles than for the bigger particles (Figure 4.11). For a given temperature and volume fraction, the TCR decreases with the rise in nanoparticle size.

Figure 4.12 depicts the impact of temperature on the three standardised parameters of the novel equation for α-Al_2O_3-glycerol nanofluid.

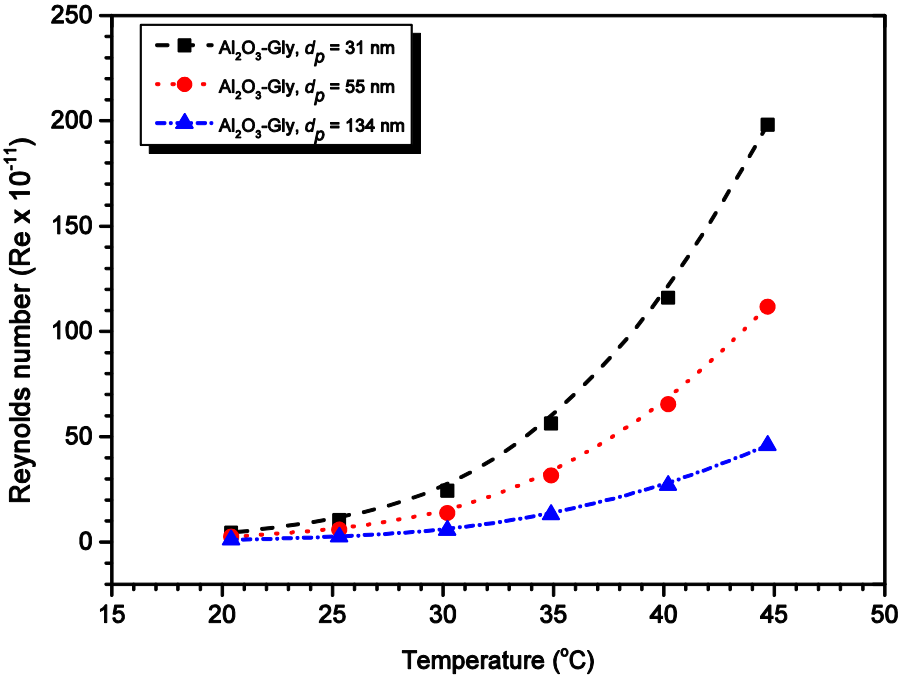

Figure 4.10: Reynolds number of different particle sizes of α-Al_2O_3-glycerol nanofluids

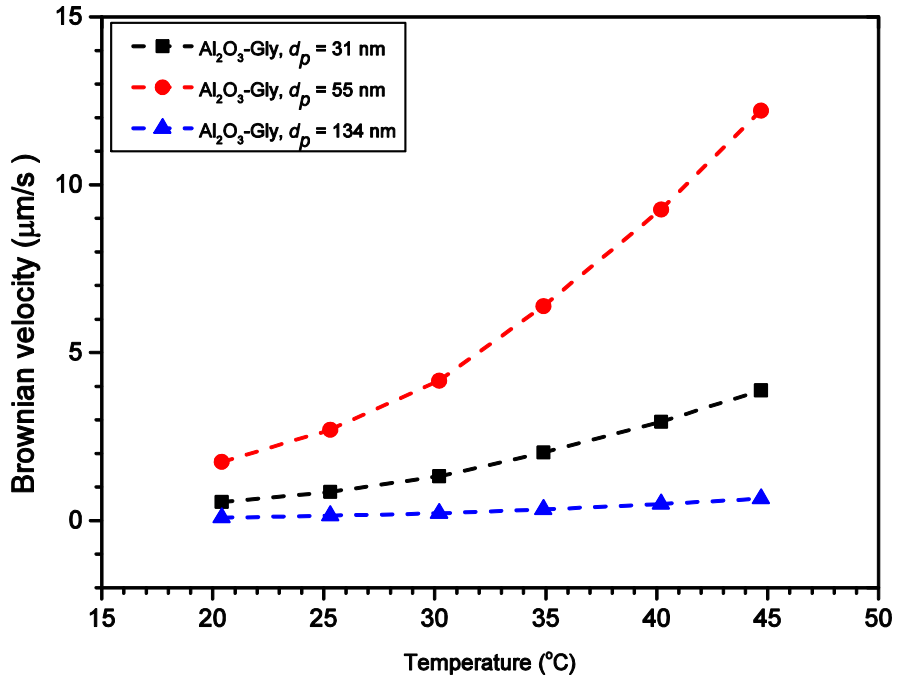

Figure 4.11: Brownian velocity of different particle sizes of α-Al_2O_3-glycerol nanofluids

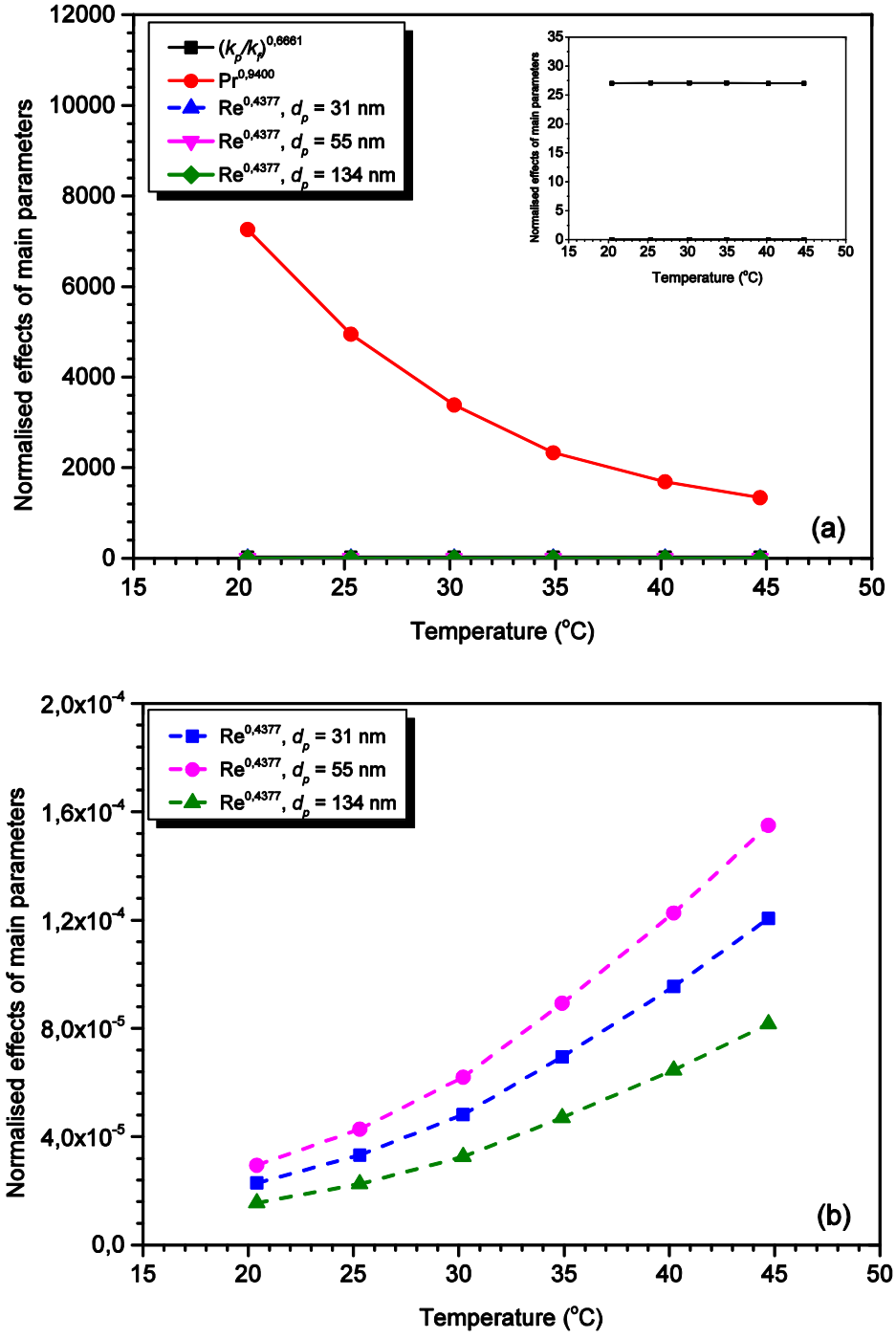

Figure 4.12: Temperature dependence effect on the three standardised parameters of the novel equation at 1% volume fraction α-Al_2O_3-glycerol nanofluids of (a) the three parameters and (b) $\boldsymbol{Re_p}$ parameters

The three standardised parameters are the Reynolds number term $\left(Re_p\right)^{0.4377}$, Prandtl number term $\left(Pr_f\right)^{0.9400}$ and thermal conductivity of nanoparticle normalised to the thermal conductivity of glycerol term $\left[\left(k_p \,/\, k_f\right)\right]^{0.6661}$.

Figure 4.12 reveals that the normalised Pr_p decreases with a rise in temperature whereas the standardised Re_p increases and $\left(k_p \,/\, k_f\right)$ is almost constant. The magnitude of the Pr_f term is much bigger compared with both the Re term and standardised $\left(k_p \,/\, k_f\right)$. The normalised Pr_f is the major parameter describing the enhancement of TCR of α-Al_2O_3-glycerol nanofluids, as opposed to the Reynolds number for the case of Al_2O_3-deionized water nanofluid [92]. The impact of the Pr_f term is about 920 000 times bigger than the effect of the standardised Re_p for the 31 nm size α-Al_2O_3-glycerol nanofluids at 20 ˚C. The described phenomenon strengthens with the increase in concentration of suspended α-Al_2O_3 nanoparticle in the glycerol. The high exponent value of the Prandtl number and the high value of glycerol Prandtl number compared with water, which is about 1 800 times bigger, can explain the main effect of the Prandtl number on the effective thermal conductivity of α-Al_2O_3-glycerol nanofluid at 20 ˚C [93].

Altogether, the model depicts that the thermal conductivity ratio increases with an increase in volume fraction, decreases with an increase in nanoparticle size and slightly decreases with a temperature rise.

4.8 Conclusion

The α-Al_2O_3 nanoparticles dispersed in glycerol yielded a higher thermal conductivity than the base fluid (glycerol). There was a linear increase in TCR with an increase in α-Al_2O_3 nanoparticle volume fraction.

R-square of 0.822 for α-Al_2O_3-glycerol linear equations expressed that 82.2% of the variability in the TCR values vs. volume fraction was explained by the obtained model. Residual and other variables could explain the remaining 17.8% for α-Al_2O_3-glycerol of variation in TCR.

There was no statistical evidence of enhancement of TCR with increasing temperature for the α-Al_2O_3-glycerol nanofluids. The temperature dependence of the effective thermal conductivity of both nanofluids with different particle sizes tracked the base fluid (glycerol), but at a high level of magnitude.

The TCR of α-Al_2O_3-glycerol increased with decreasing particle size. There was no dependence of the effective thermal conductivity of the α-Al_2O_3-glycerol nanofluid model with elapsed time up to 50 hours.

Although the prediction by particular models was within the acceptable range of experimental data of α-Al_2O_3-glycerol nanofluids for the various involved parameters, the models' trend either did not follow the expected pattern for each analysed parameter or was not consistent in all conditions. The Maxwell, Bruggeman, effective medium, Corcione, Peterson, Shake and Vajjha models could not explain the enhancement of the thermal conductivity of α-Al_2O_3-glycerol nanofluids consistently.

Equation (4.9) is the new empirical correlation for the thermal conductivity of α-Al_2O_3-glycerol nanofluids:

$$\frac{k_{eff}}{k_f} = 1 + Re_p^{0.4377} Pr_f^{0.9400} \phi^{1.0475} \left(\frac{40}{k_f}\right)^{0.6661} \tag{4.9}$$

The novel equation is a modified version of a non-dimensional model proposed by Corcione. The regression analysis provides evidence that the novel model is statistically significant, with the maximum relative error of +1.57%, -2.37% and the average of -0.03%. The new model has an adjusted R^2 = 0.980 and very significant p-value (p=0.0000) of the F-statistic of the model. The new model illustrates that the thermal conductivity ratio increases with an increase in volume fraction, decreases with a rise in nanoparticle size and slightly decreases with a temperature rise.

The normalised Pr_f is the major parameter describing the enhancement of TCR of α-Al_2O_3-glycerol nanofluids, as opposed to the Reynolds number for the case of α-Al_2O_3-glycerol nanofluid.

4.9 Recommendation

The thermal conductivity investigation could be extended to hydrodynamic size distribution and zeta potential of the glycerol-based nanofluids. This approach could provide a more comprehensive understanding of both the stability of nanofluid and thermal conductivity behaviour of glycerol-based nanofluids.

Further research could examine the viscosity of glycerol-metal oxide nanofluids to understand its impact on the thermal conductivity of glycerol-based nanofluids.

CHAPTER 5: EXPERIMENTAL INVESTIGATION AND MODEL DEVELOPMENT FOR THE THERMAL CONDUCTIVITY OF GLYCEROL-MgO-BASED NANOFLUIDS

5.1 Introduction

This chapter presents the experimental and theoretical determination of the effective thermal conductivity of three different sizes of magnesium oxide (MgO) nanoparticles dispersed in glycerol. The study procedure is similar to the one presented in Section 4.1 for α-Al_2O_3-glycerol nanofluid.

5.2 Influence of volume fraction on the thermal conductivity of MgO-glycerol-based nanofluids

Figure 5.1 shows the effect of particle volume fraction on the effective thermal conductivity ratio of MgO nanofluids prepared at different volume fractions, 0.5%, 1%, 2% and 4% respectively. For clarity, the standard deviation of data was omitted. The MgO-glycerol nanofluid yielded higher thermal conductivity than the glycerol (base fluid).

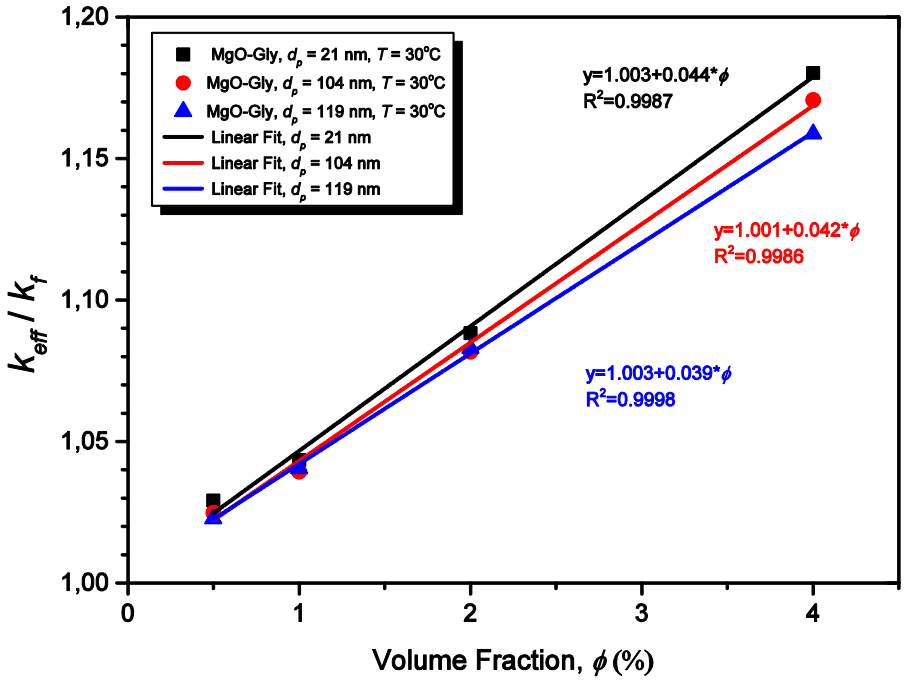

Figure 5.1: Influence of nanoparticle volume fraction on the thermal conductivity ratio of the three sets of MgO-glycerol nanofluids at 30 °C

The fitting line equation and corresponding R-square are relative to the given nanoparticle diameter and temperature. For each given particle size and temperature, the thermal conductivity ratio increases linearly with an increase in MgO volume fraction. The significant p of the F-statistic of the MgO model is less than 0.001. Therefore, the null hypothesis can be rejected. As a result, there is a linear relationship between the volume fraction and the TCR of MgO nanofluids.

Equation (5.1) is a result of linear regression analysis conducted to determine the effect of volume fraction on the TCR of MgO-glycerol nanofluids. R-square of 0.986 for MgO-glycerol linear equations expresses that 98.6% of the variability in the TCR values is explained by the obtained model. Residual and other variables can explain the remaining 1.4% of variation in TCR for MgO-glycerol.

$$\frac{k_{eff}}{k_f} = 1.001 + 4.213 * \phi \quad (5.1)$$

where $\boldsymbol{\phi}$ is the MgO nanoparticle volume fraction expressed per unit.

Table 5.1: Results of linear regression analysis of TCR of MgO-glycerol vs. volume fraction

Model	R	R Square	Std. Error of the Estimate	Statistics	
				F	p
MgO	0.993	0.986	0.007	5062.2	0.0000

Altogether, there is a linear increase in TCR with an increase of MgO nanoparticle volume fraction. This outcome is in agreement with the α-Al_2O_3-glycerol nanofluid studies developed in Section 4.2 and other studies of various types of nanofluids [1, 21, 49, 59, 77, 84]. The thermal conductivity ratio reaches the maximum of 18%, 17% and 16% for 21 nm, 104 nm and 119 nm MgO-glycerol nanofluids respectively at 30 ˚C. Figure 5.1 clearly depicts the impact of particle size on the TCR. A small particle size leads to a higher thermal conductivity of nanofluids than a bigger size. The same situation was perceived at various ranges of temperatures.

The improvement of the thermal conductivity ratio for the MgO nanofluids with respect to the volume fraction could possibly be explained by one or more mechanisms as described in Section 4.2.

5.3 Influence of temperature on the thermal conductivity of MgO-glycerol-based nanofluids

Figure 5.2 shows the effect of temperature on the effective thermal conductivity of MgO-glycerol nanofluids for three different sizes of nanoparticles (21 nm, 104 nm and 119 nm). The temperature dependence of the effective thermal conductivity of the nanofluids with different particle sizes tracks the base fluid (glycerol) but at another level of magnitude. Similar findings were reported for the Al_2O_3-water nanofluids [49], and ethylene glycol-based nanofluids containing Al_2O_3, MgO, ZnO, SiO_2, and graphene nanoparticles [15, 33, 36, 49].

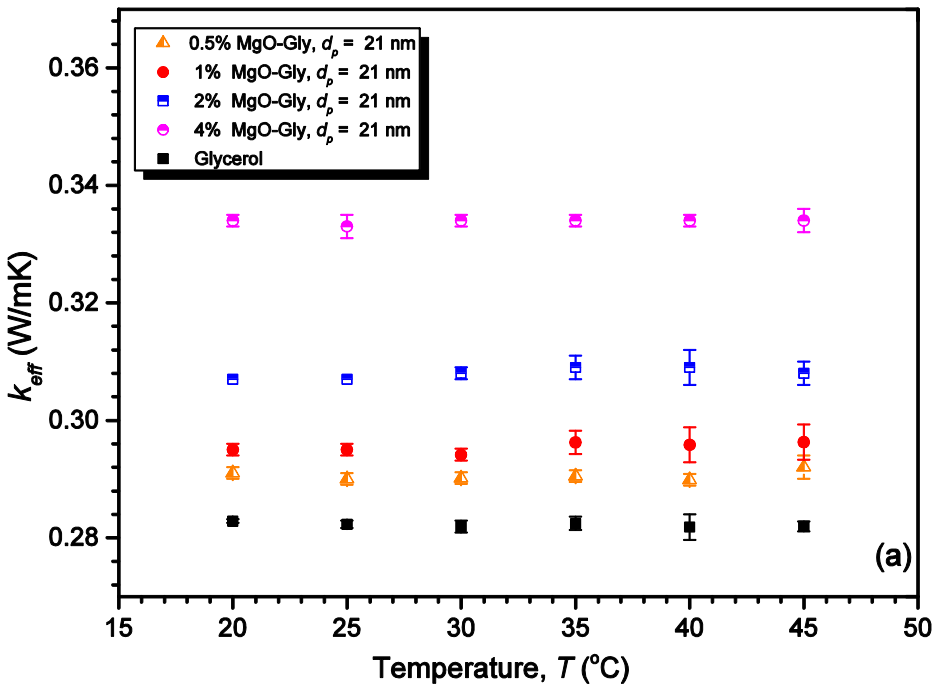

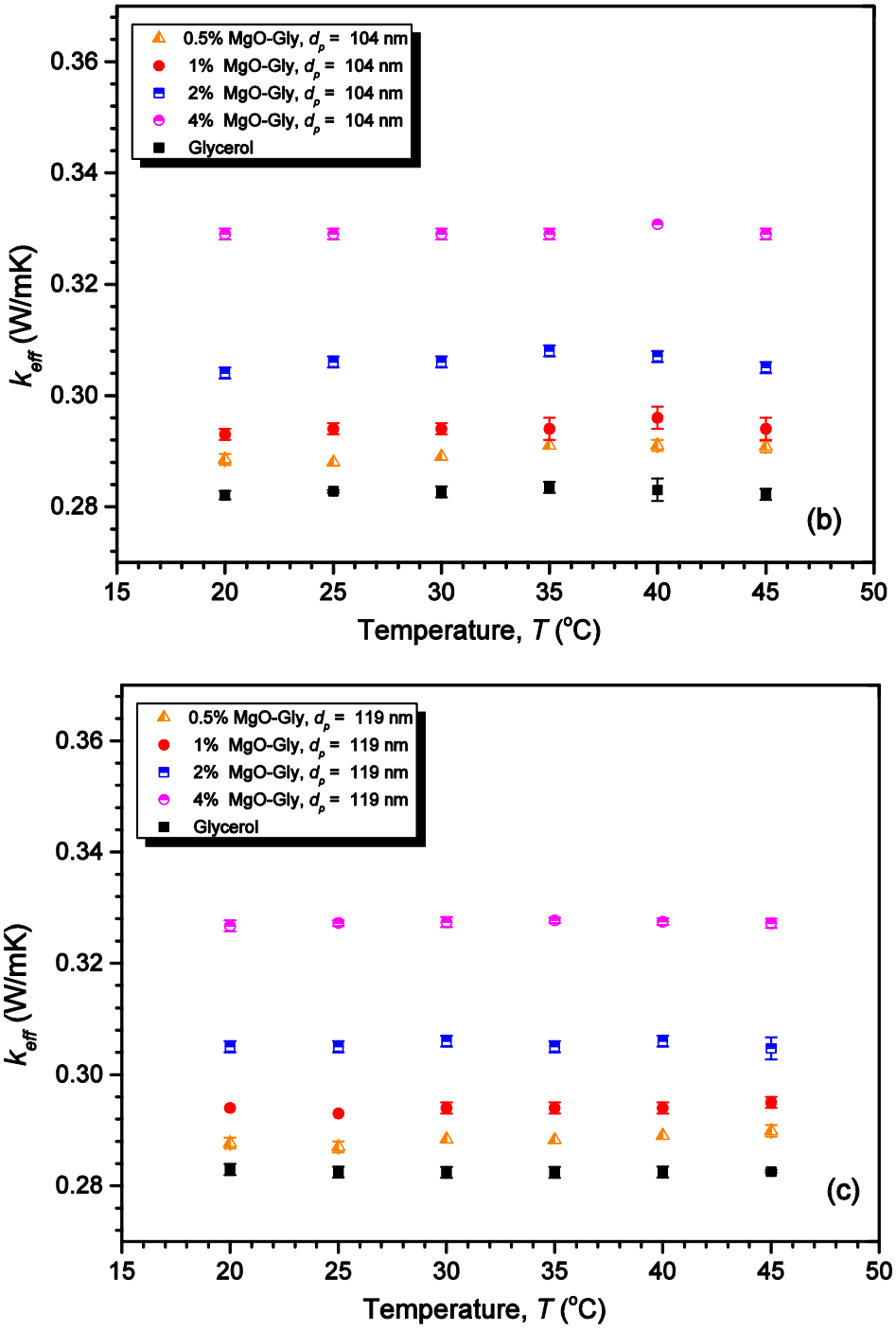

Figure 5.2: Temperature dependence of the effective thermal conductivity of MgO-glycerol nanofluids at different MgO volume concentrations: (a) 21 nm, (b) 104 nm and (c) 119 nm

Figure 5.3 shows the thermal conductivity ratio of MgO-glycerol nanofluids at different volume fractions as a function of temperature. The estimated linear relationships between the temperature and the TCR computed of MgO-glycerol nanofluid are given by equation (5.2):

$$\frac{k_{eff}}{k_f} = 1.075 - 1.73 * 10^{-4} * T \tag{5.2}$$

where T is temperature expressed in ˚C.

Equation (5.2) can be simplified in equation (5.3) as its slope is insignificant.

$$\frac{k_{eff}}{k_f} = 1.075 \tag{5.3}$$

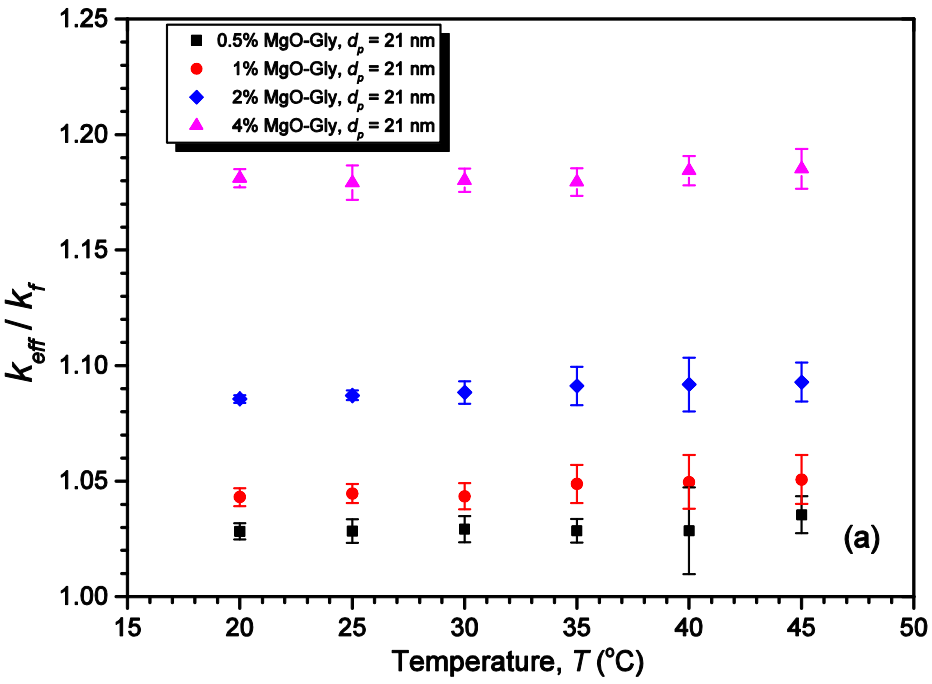

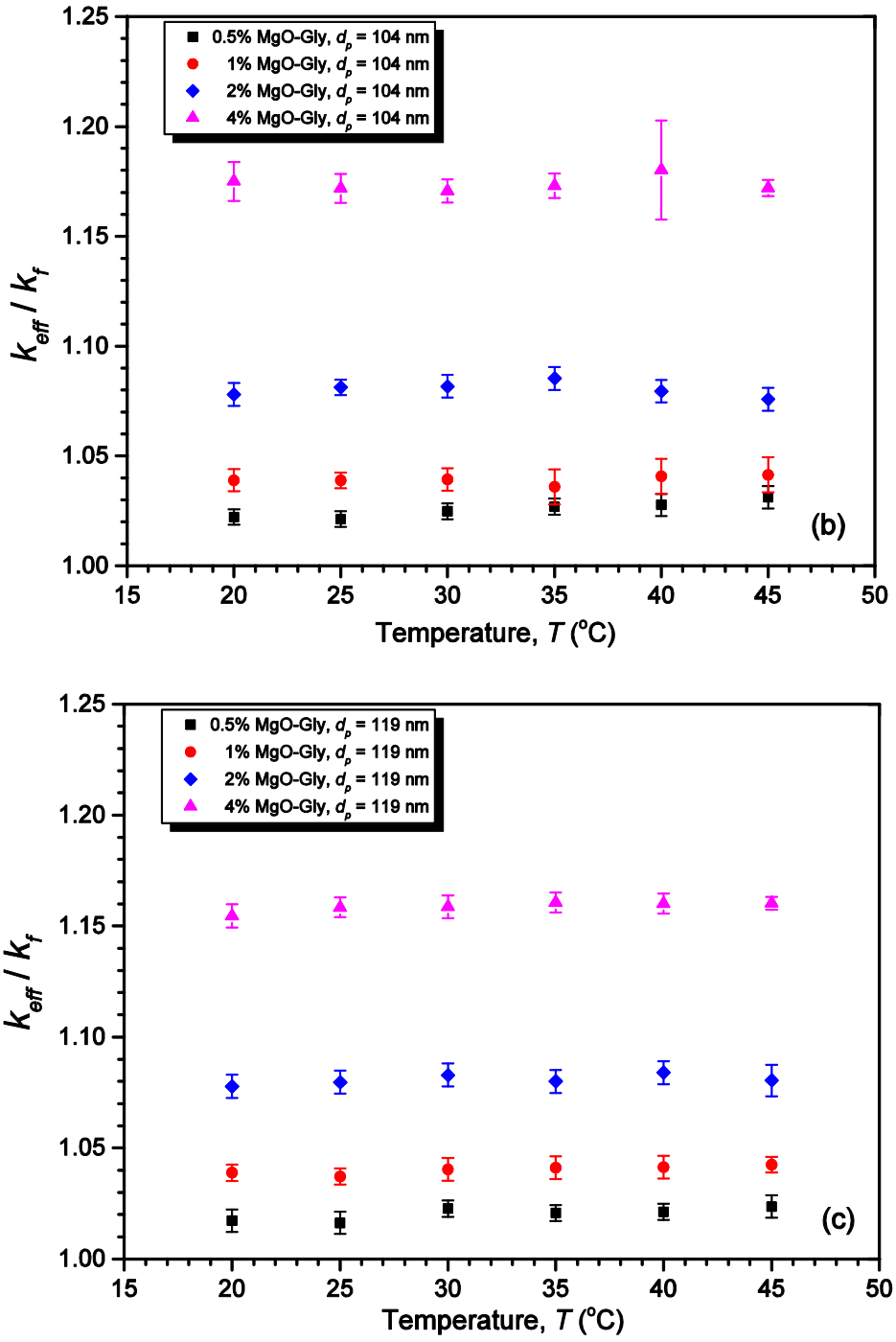

Figure 5.3: Temperature dependence of the effective thermal conductivity ratio of MgO-glycerol nanofluids at different MgO volume concentrations: (a) 21 nm, (b) 104 nm and (c) 119 nm

As can be seen in Table 5.2, the obtained equation has unadjusted R-square = 0.001 and significant p of F-statistic > 0.05 (acceptable level). The t-ratios of intercept and slope (temperature) are 39.76 and 0.22 for the MgO-glycerol nanofluids. Their corresponding significant p-values are 0.000 and 0.830 for MgO (p > 0.05). The significant p-values of both the F-statistic of the model and t-ratio of the slope of the model are not significant. The null hypothesis cannot be rejected. Thus, there is no evidence of a linear relationship between the TCR and temperature for glycerol-based MgO nanofluids. The best model to describe the TCR vs. ratio is the naive model, which is the mean value of TCR at each given volume fraction and nanoparticle diameter.

The outcome has also been commonly confirmed in the literature by certain authors and unconfirmned by others, as highlighted in Section 4.3. Figure 5.3 also shows that the thermal conductivity of MgO-glycerol nanofluids varies significantly with increase in ϕ, as depicted in Section 4.2.

Table 5.2: Results of linear regression analysis of TCR of MgO-glycerol vs. temperature

Model	R	R Square	Std. Error of the Estimate	Statistics	
				F	p
MgO	0.026	0.001	0.058	0.05	0.830

5.4 Influence of nanoparticle size on the thermal conductivity of MgO-glycerol-based nanofluids

In order to assess the influence of the nanoparticle size on the effective thermal conductivity ratio of MgO-glycerol nanofluid, experimental data sets were conducted

for different nanoparticle volume fractions (0.5%, 1%, 2% and 4%) at various temperatures (20 °C, 25 °C, 35 °C and 45 °C). Figure 5.4 provides the effect of particle size on the MgO-glycerol nanofluid thermal conductivity ratio at room temperature. For the given volume fraction and temperature, the thermal conductivity ratio decreases with increasing particle size. The thermal conductivity ratio of MgO-glycerol nanofluid in the case of the same volume fraction is higher for smaller particle sizes. The 104 nm MgO-glycerol has $\left(k_{eff} \,/\, k_f\right)$ values close to 119 nm MgO-glycerol nanofluids at almost all temperatures. Equation (5.4) gives the estimated straight-line regression of TCR on the diameter computed:

$$\frac{k_{eff}}{k_f} = 1.089 - 1.08 * 10^{-4} * d_p \tag{5.4}$$

Can the equation (5.4) be simplified in equation (5.5) as its slope is insignificant? The answer is presented in the next paragraph.

$$\frac{k_{eff}}{k_f} = 1.089 \tag{5.5}$$

The R-square of MgO-glycerol nanofluid is 0.007 with the significant p of the F-statistic of 0.495 (see Table 5.3), which is > 0.05 suggesting that the null hypothesis cannot be rejected. There is no linear relationship between the diameter and the TCR.

Table 5.3: Results of linear regression analysis of TCR of MgO-glycerol vs. particle size

Model	R	R Square	Std. Error of the Estimate	Statistics	
				F	p
MgO	0.067	0.007	0.057	0.471	0.495

The t-ratios of intercept and slope (diameter) are 75.3 and -6.69 respectively. The corresponding p-values of t-ratio are 0.000 and 0.495 ($p > 0.05$). Thus, only 0.7% of the variability in the TCR values is explained by the model, and there is no evidence that the variation in diameter could explain the TCR enhancement. The naive model fits better than the model (5.4).

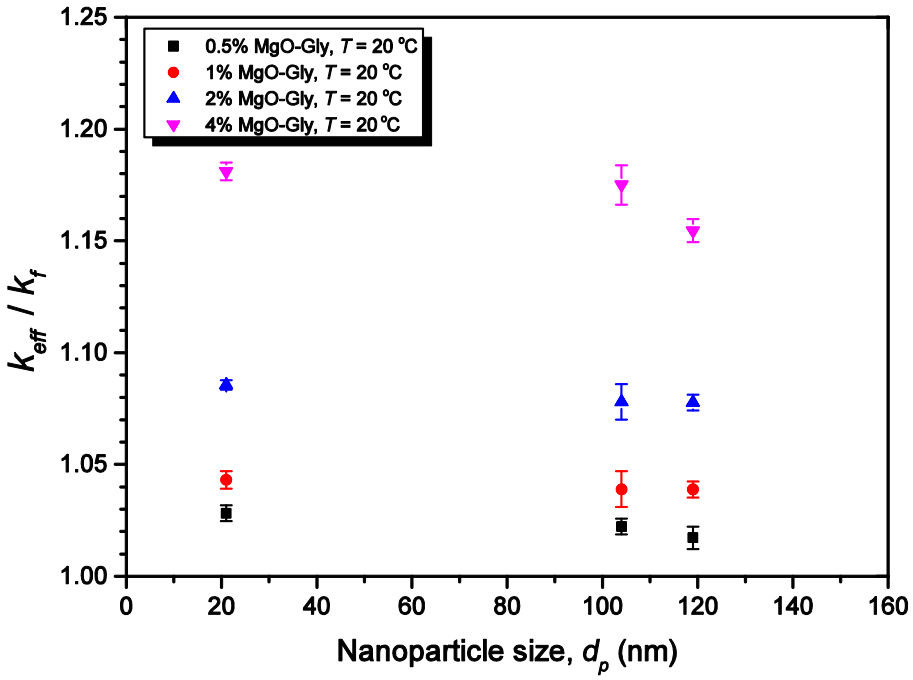

Figure 5.4: Influence of nanoparticle size on the effective thermal conductivity ratio at three different volume fractions of MgO-glycerol nanofluid at 20 °C

5.5 Stability of MgO-glycerol-based nanofluids

The stability of MgO nanofluid samples was evaluated at a maximum volume fraction (4%). No surfactant was used in the preparation of nanofluids. Thirty minutes after sonication, the effective thermal conductivity was acquired for each particle size at one-hour step, up to 50 hours. The results observed in Figure 5.5 show no apparent change in effective thermal conductivity of MgO-glycerol with time after nanofluid preparation.

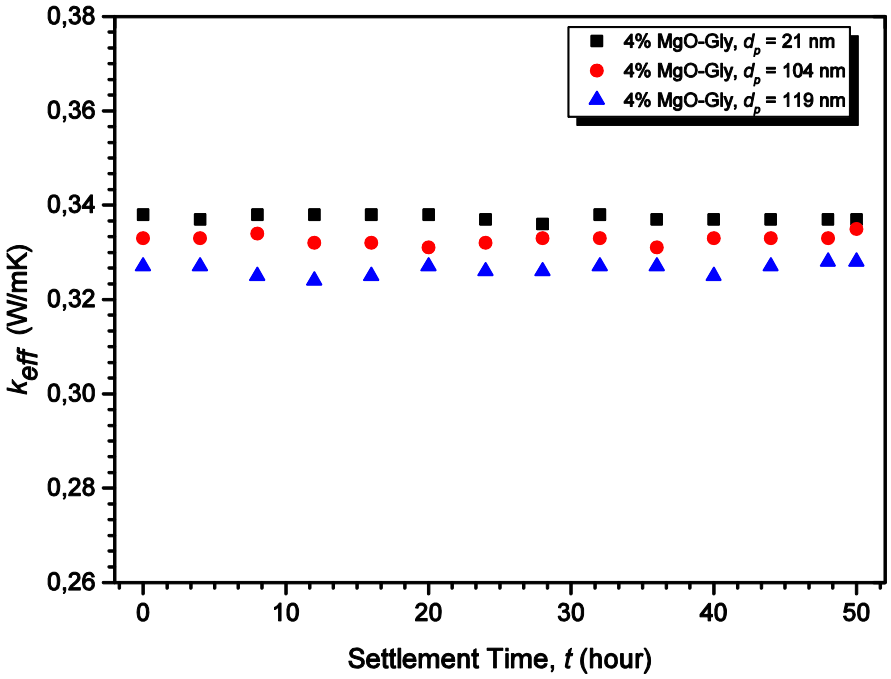

Figure 5.5: Influence of settlement time on the effective thermal conductivity of MgO-glycerol nanofluids at 4% volume fraction

The estimated linear equation of 4% MgO-glycerol nanofluids between the elapsed time after preparation and the effective thermal conductivity computed of the MgO nanofluid is provided by equation (5.5). Table 5.4 gives the results of the linear regression analysis of the effective thermal conductivity of the model vs. elapsed time after preparation.

The t-statistic of the slope of the model is 0.007. The corresponding significant p-value is 0.995, which is greater than 0.05.

$$k_{eff} = 0.332 - 4.82 * 10^{-11} * t \quad (5.6)$$

where t is elapsed time in seconds.

Equation (5.6) can be simplified in equation (5.7) as its slope is insignificant.

$$k_{eff} = 0.332 \quad (5.7)$$

As observed in Table 5.4, the R-square and significant p of both the F- and t-statistics are 0 and greater than 0.05 respectively. The F-statistic values cannot reject the null hypothesis. The variation of effective thermal conductivity of the model vs. elapsed time after preparation is not statistically justified. There is no linear dependence of effective thermal conductivity of the model with elapsed time up to 50 hours. The best model is the naive model, which is the mean value of thermal conductivity for each given diameter. The mean values of effective thermal conductivity of 4% MgO-glycerol are 0.337 ± 0.001 W/mK, 0.332 ± 0.001 W/mK and 0.326 ± 0.001 W/mK for 1 nm, 104 nm and 119 nm respectively.

Table 5.4: Results of linear regression analysis of the effective thermal conductivity of MgO-glycerol vs. elapsed time after preparation

Model	**R**	**R Square**	**Std. Error of the Estimate**	**Statistics**	
				F	**p**
4% MgO	0.000	0.000	0.058	0.000	0.995

The outcome agrees with the α-Al_2O_3-glycerol nanofluid studies in Section 4.5. The study of effective thermal conductivity with elapsed time indicates the stability of MgO-glycerol nanofluids with high volume fraction at room temperature, consequently at low volume fraction as well.

5.6 Comparison of the thermal conductivity models with MgO-glycerol experimental data

5.6.1 Introduction

This section provides the comparison of predicted results obtained from the existing theoretical models (presented in Section 4.6.1) and experimental correlation with the obtained experimental data of MgO-glycerol nanofluids.

5.6.2 Effect of volume fraction

Figure 5.6 provides comparisons of the predicted effective thermal conductivity versus volume fraction relationship for various models (Bruggeman, Corcione, effective medium theory, Maxwell and Shaker) with experimental data sets of three sizes of MgO-glycerol nanofluids at room temperature. The Vajjha and Peterson models were set aside since they were not based on the MgO nanoparticles.

As shown in Figure 5.6 (a), (b) and (c), the Corcione model underpredicts the experimental data set of MgO-glycerol nanofluids for the volume fraction range. Besides, its slope depicts a slight increase with an increase in volume fraction, which is far removed from the experimental data trend. The other models are within the acceptable range and have a similar trend to the experimental data set. They display an excellent fit when the volume fraction is less than 4%.

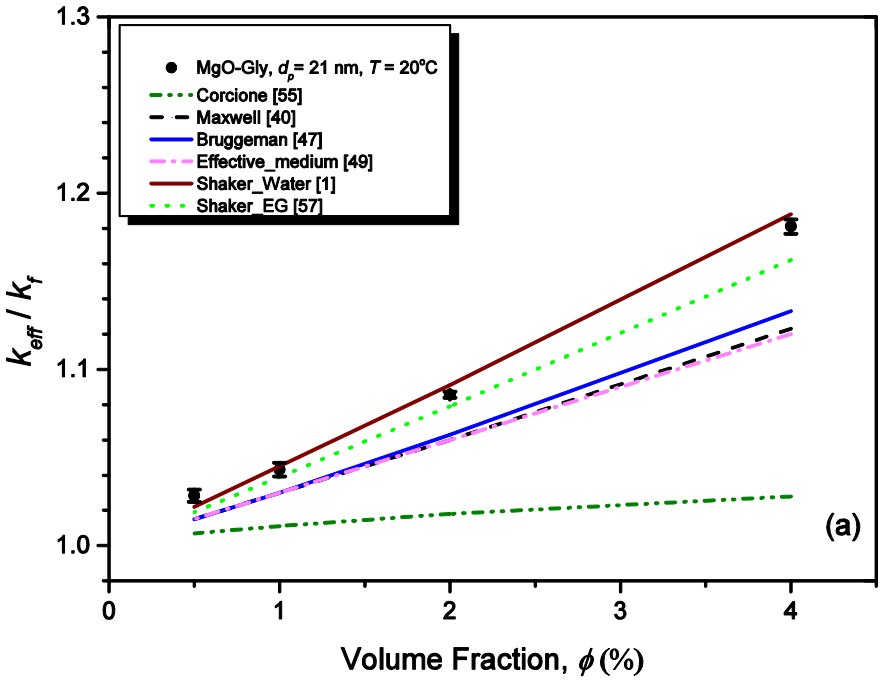

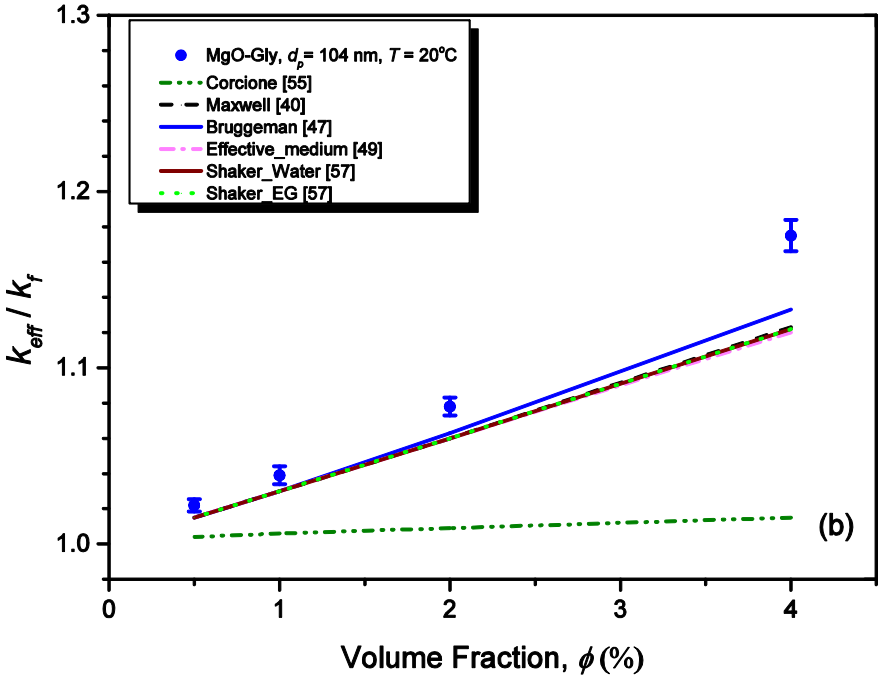

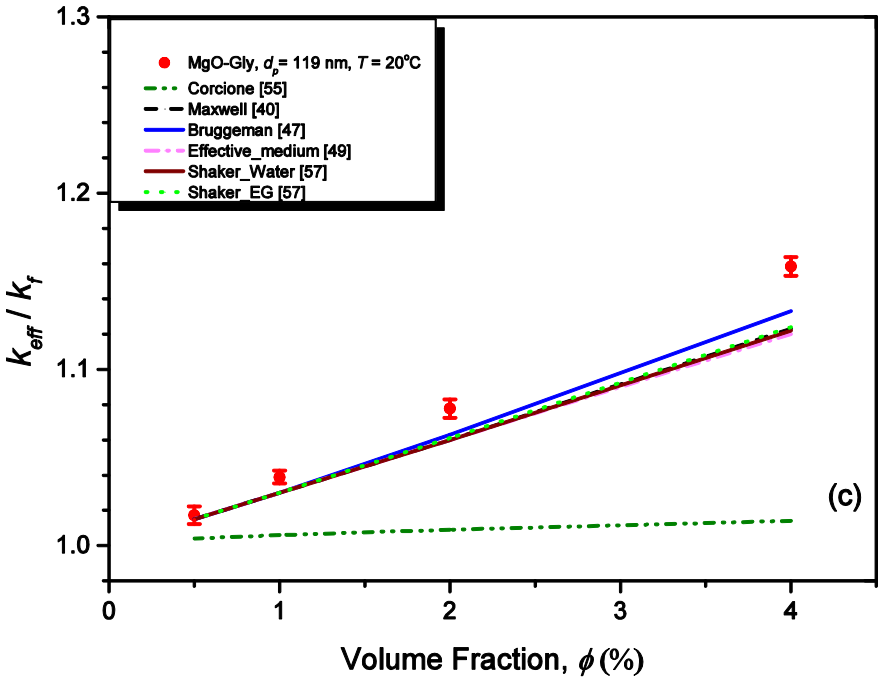

Figure 5.6: Comparison of the thermal conductivity ratio variation with volume fraction of experimental data and existing equations for MgO-glycerol nanofluids at 20 ˚C: (a) 21 nm, (b) 104 nm and (c) 119 nm

5.6.3 Effect of temperature

Figure 5.7 presents a comparison of the predicted thermal conductivity ratio versus temperature relationship for selected models with experimental data of 4% MgO-glycerol nanofluids. The Corcione model underpredicts the experimental data of all the sizes of MgO nanofluids. All the models are unchanged with increasing temperature, opposed to the Corcione, which shows an increasing trend for all the three sizes of MgO nanofluids. The Shaker model will give good predictions if the 21 nm MgO-glycerol nanofluid h parameter is between 8 and 11, or slightly bigger than 11 (see Figure 5.7). Figure 5.7 (b) and (c) show that all the models underpredict the experimental data of both 104 nm and 119 nm MgO-glycerol nanofluids.

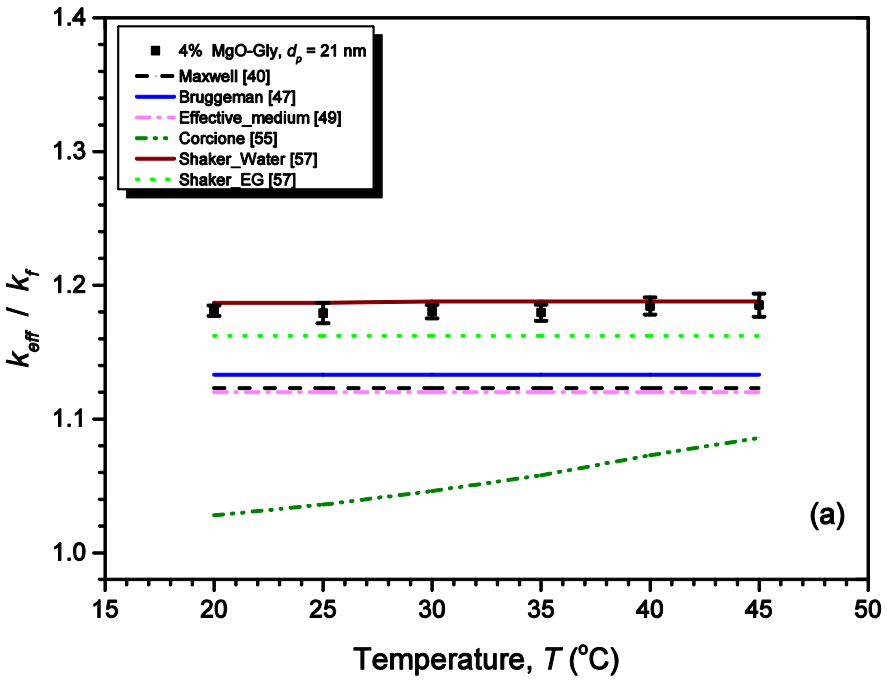

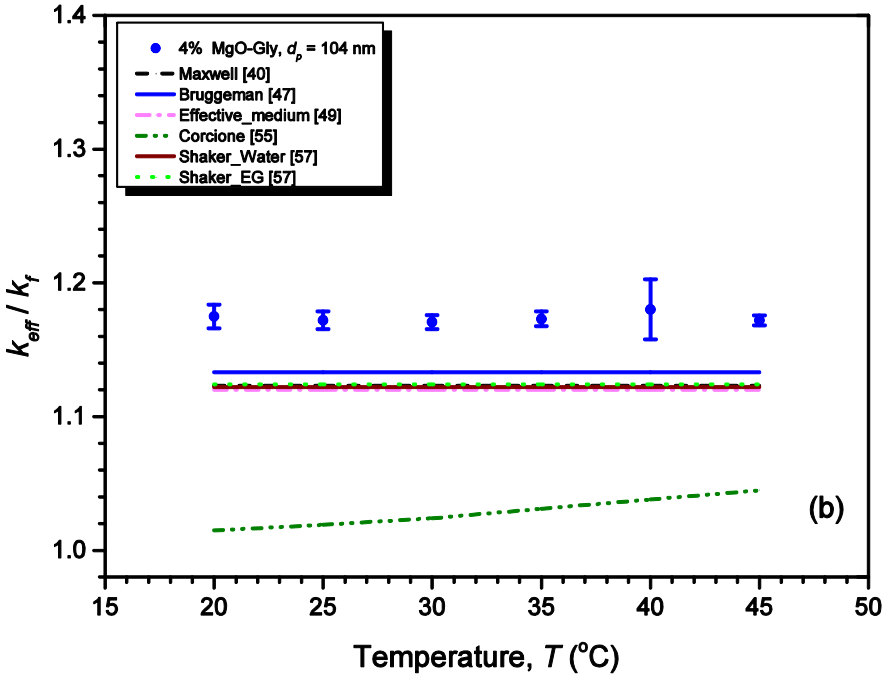

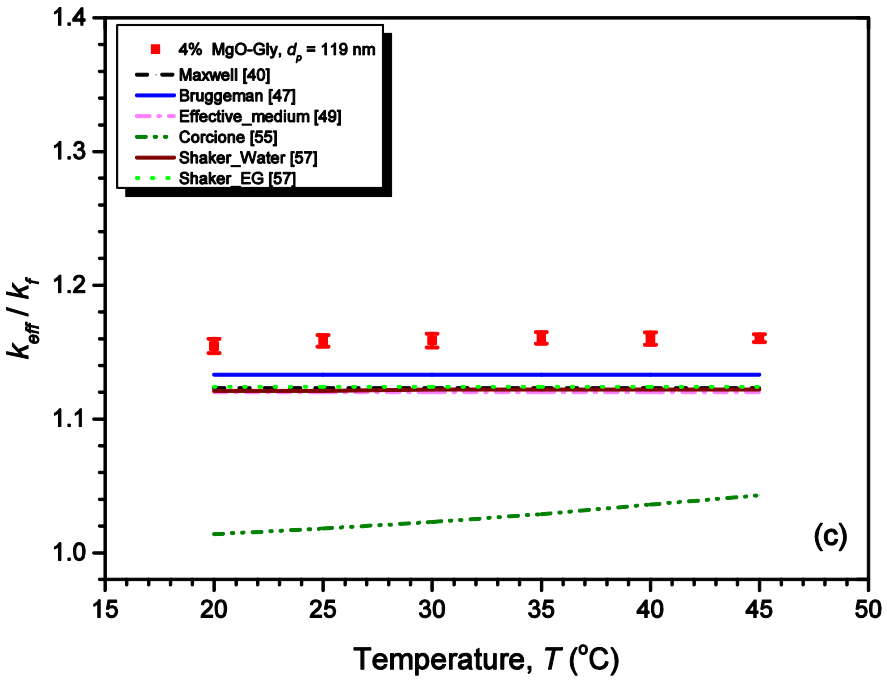

Figure 5.7: Comparison of the thermal conductivity ratio variation with temperature between experimental data and existing equations for 4% MgO-glycerol nanofluids: (a) 21 nm, (b) 104 nm and (c) 119 nm

5.6.4 Effect of particle diameter

Figure 5.8 plots the comparisons of the predicted TCR versus diameter relationship for the models above with experimental data sets of MgO-glycerol nanofluids prepared with 4% volume fraction at 35 ˚C. The TCR of MgO-glycerol nanofluids agrees quite well with the prediction by the Shaker models of a diameter less than 104 nm. The Corcione model underestimates the experimental data sets of MgO-glycerol. The other models are unaffected by the diameter variation.

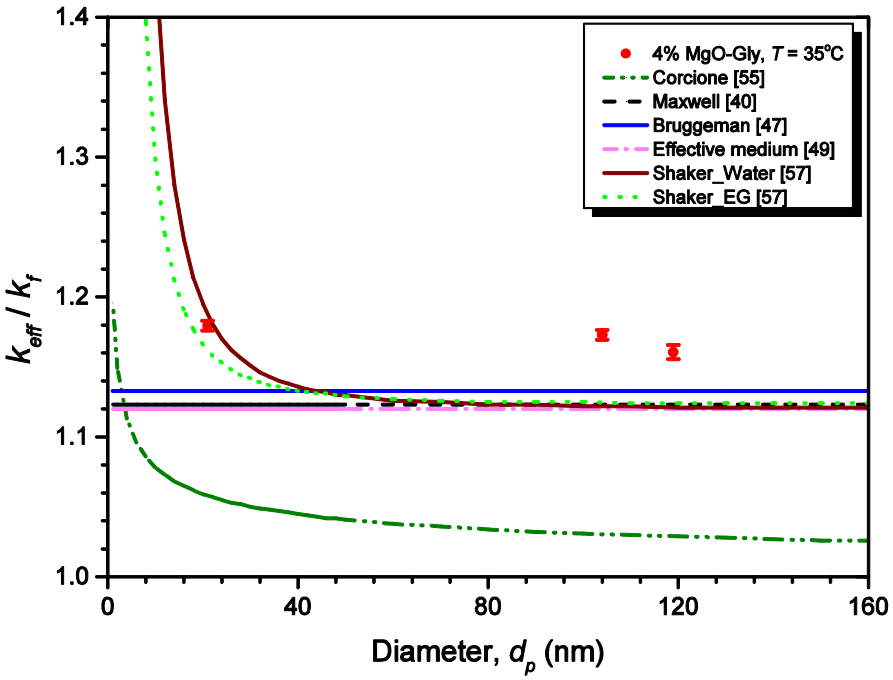

Figure 5.8: Comparison of the thermal conductivity ratio variation with nanoparticle diameter between experimental data and existing equations for 4% MgO-glycerol nanofluids at 35 ˚C

In summary, the selected models fail to predict consistently in all conditions the thermal conductivity ratio for MgO nanofluids of volume fractions ranging from 0.5% to 4%, measured in the temperature range of 20 ˚C to 45 ˚C. The classical models and Corcione equation could not consistently explain the enhancement of the thermal conductivity of MgO-glycerol nanofluids in all conditions. Each existing correlation model works for the particular nanofluid and condition.

5.7 New empirical correlation for the thermal conductivity ratio of MgO-glycerol

This section presents the development of a new empirical correlation for the thermal conductivity of the MgO-glycerol nanofluid. The development procedure and

assumptions are similar to the Al_2O_3-glycerol nanofluid case presented in Section 4.7. The developed empirical correlation for the thermal conductivity of the MgO-glycerol nanofluid is expressed by equation (5.8). No collinearity exists between the exploratory parameters as the VIF of exploratory parameters < 10.

$$\frac{k_{eff}}{k_f} = 1 + Re_p^{0.0603} Pr_f^{0.1066} \phi^{0.9918} \left(\frac{48.4}{k_f}\right)^{0.3646} \tag{5.8}$$

where Re_p is the nanoparticle Reynolds number expressed by equation (4.7), Pr_f the Prandtl number of the base fluid (glycerol), ϕ the nanoparticle volume fraction, C_{pf} the specific heat of the base fluid, k_p the thermal conductivity of the MgO nanoparticles (equal to 48.4 W/mK) and k_f the thermal conductivity of the glycerol (W/mK). The new correlation for the thermal conductivity of MgO-glycerol nanofluid is satisfactory for 20 ˚C < T < 45 ˚C, 0% < ϕ < 4% and 21 nm < d_p < 119 nm.

Equation (5.5), converging at 10^{-15}, has an adjusted R^2 = 0.995, F = $1.50*10^6$ and significant p = 0.0000. The t-statistic of the exponents of Re_p, Pr_f, ϕ and k_p / k_f are 9.8, 7.1, 85.1 and 22.8 respectively. The p-values associated with the t-ratio of all the exponents and slope of the equation are equal to 0.0000 (p < 0.001). The statistical significance of all the exponents of the equation is high. In the general Corcione model, the p-value of the slope of the equation and the exponents of both Prandtl number and temperature are not statistically significant. There is a high linear correlation (R = 0.9992) between the terms k_p / k_f and the slope of the equation, after removal of the temperature term (T / T_{fr}). Thus, the slope term was also removed to deal with the multicollinearity in the model. However, the temperature is still present in the new

model, as the Reynolds number is directly proportional to temperature. There is no autocorrelation in the residuals, and the residual sum is zero. The comparison between the predicted thermal conductivity ratio from the present model and the experimental results shows an excellent agreement with maximum relative error of -1.24%, +0.68% and the average relative error of -0.03% (see Figure 5.9). The present analysis provides evidence that the novel model is statistically significant.

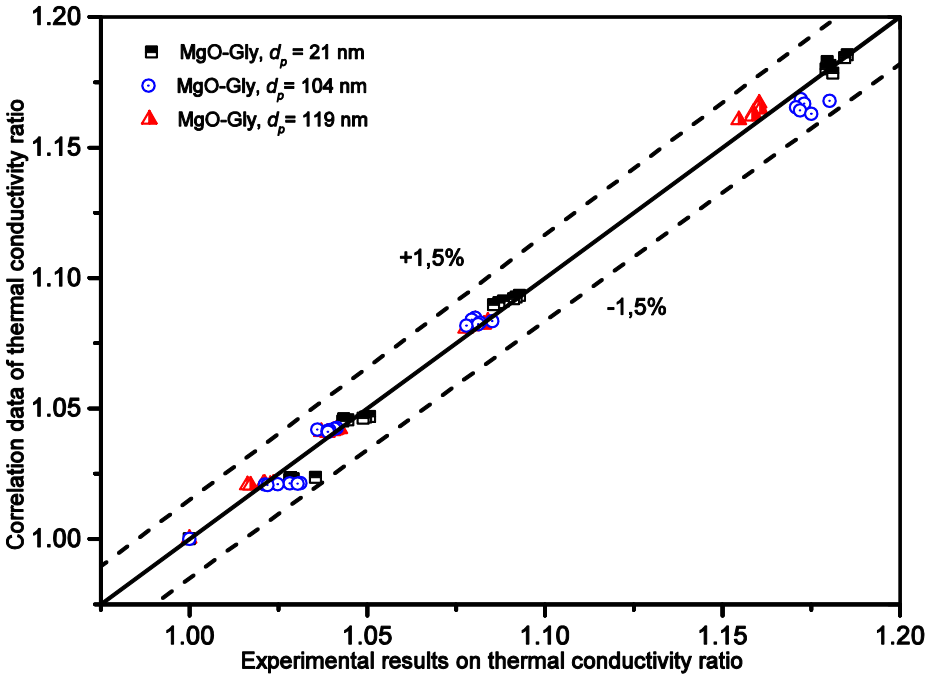

Figure 5.9: Comparison of the thermal conductivity ratio between the predicted values from the present correlation and the experimental data on MgO-glycerol nanofluids

Figure 5.10 shows an intense temperature dependence of the Reynolds number for 21 nm in comparison with both 104 nm and 119 nm MgO-glycerol nanofluids. The Reynolds number increases as nanoparticle size decreases, because the Brownian velocity effect is much stronger for smaller particles than for bigger particles (Figure

5.11). For a given temperature and volume fraction, the TCR decreases as the nanoparticle size increases.

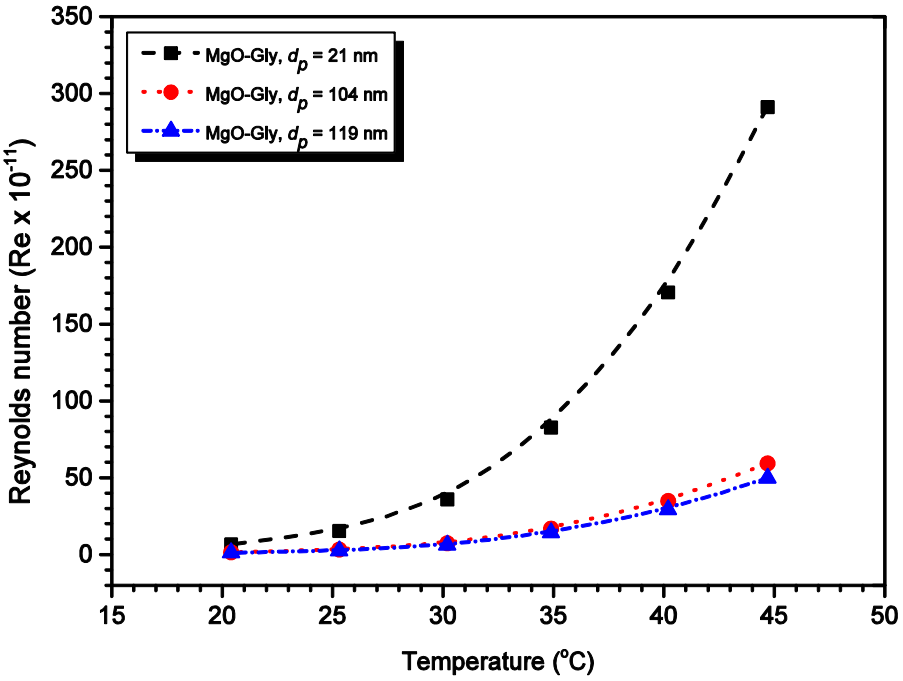

Figure 5.10: Reynolds number of different particle sizes of MgO-glycerol nanofluids

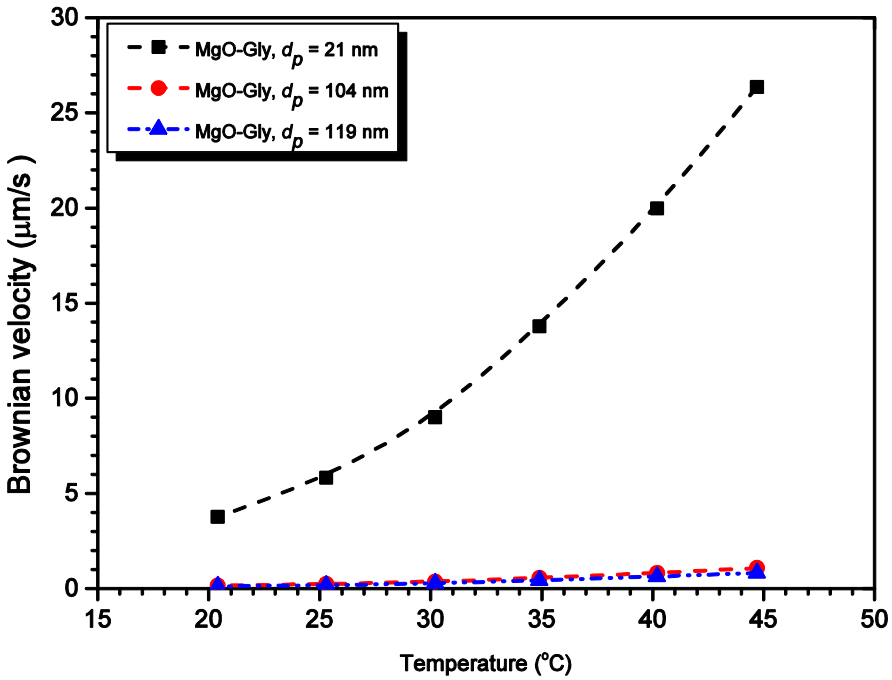

Figure 5.11: Brownian velocity of different particle sizes of MgO-glycerol nanofluids

Figure 5.12 depicts the impact of temperature on the three parameters of the novel equation for 21.1 nm MgO-glycerol nanofluid at 1% volume fraction. The three standardised parameters are the Reynolds number term $\left(Re_p\right)^{0.0603}$, Prandtl number term $\left(Pr_f^{0.1066}\right)$ and thermal conductivity of nanoparticle normalised to the thermal conductivity of the glycerol term $\left[\left(k_p \,/\, k_f\right)\right]^{0.3646}$. Figure 5.12 shows that the normalised Re_p increases with a rise in temperature, whereas the parameter Pr_f decreases. The magnitude of variation, in absolute value, of standardised Re_p is bigger than standardised Pr_f. The combined effect of normalised Re_p and Pr_f slightly increases with a temperature rise. However, the impact of both standardised Re and Pr_f numbers on the $\left(k_{eff} \,/\, k_f\right)$ is small compared with the standardised $\left(k_p \,/\, k_f\right)$.

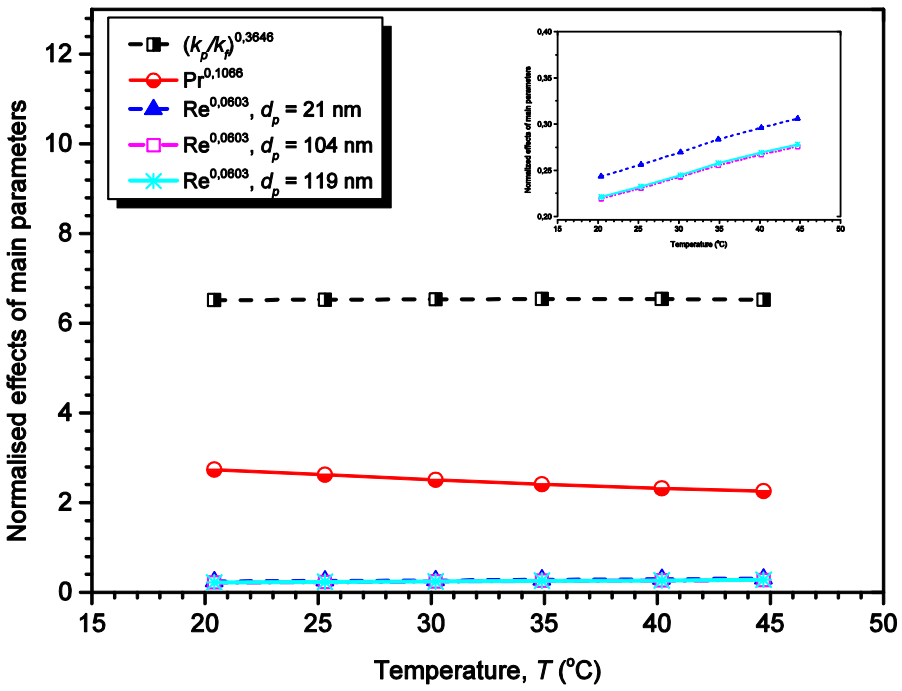

Figure 5.12: Temperature dependence effect on the three parameters of the novel correlation of the MgO-glycerol nanofluids

The normalised term (k_p / k_f)at 20 ˚C is 27 and 30 times bigger than the effect of the standardised (Re_p) term for the 21 nm and both 104 nm and 119 nm MgO-glycerol nanofluids respectively (see Figure 5.12). The normalised $(k_p / k_f)$is the major parameter describing the enhancement of the TCR of MgO-glycerol nanofluids, as opposed to the Reynolds number for the case of Al_2O_3-deionized water nanofluids [92]. This can be explained by the very low Brownian velocity occurring in the glycerol-based fluid due to its very high viscosity (about 1 530 times bigger than water at 20 ˚C) and capacity to diffuse heat, which is very low compared with its momentum, as opposed to water [93]. The described phenomenon strengthens with the increased concentration of suspended MgO nanoparticles in the glycerol. Altogether, the model depicts that the thermal conductivity ratio increases with an increase in volume fraction,

slightly decreases with an increase in nanoparticle size and is unaffected by temperature rise.

5.8 Conclusion

The MgO nanoparticles dispersed in glycerol yielded a higher thermal conductivity than the base fluid (glycerol). There was a linear increase in TCR with an increase in MgO nanoparticle volume fraction.

The R-square of 0.986 for MgO-glycerol linear equations expressed that 98.6% of the variability in the TCR values vs. volume fraction was explained by the obtained model. Residual and other variables could explain the remaining 1.4% for MgO-glycerol of variation in TCR.

The temperature dependence of the effective thermal conductivity of the MgO-glycerol nanofluids with different particle sizes tracked the base fluid (glycerol). There was no statistical evidence of enhancement of TCR with increasing temperature for MgO-glycerol nanofluids at the given temperature and volume fraction.

The TCR of MgO-glycerol remained constant with decreasing particle size. The linear regression analysis showed that there was no dependence of effective thermal conductivity of MgO-glycerol nanofluid models with elapsed time up to 50 hours.

The selected models (Maxwell, Bruggeman, effective medium, Corcione, Peterson, Shaker and Vajjha) failed to predict consistently the thermal conductivity ratio for MgO-glycerol nanofluids of volume fractions ranging from 0.5% to 4%, measured in

the temperature range of 20 ˚C to 45 ˚C in all the conditions. Each existing correlation model worked for the particular nanofluid and condition.

The novel correlation for the thermal conductivity of MgO-glycerol nanofluid was derived by modifying the Corcione model. The developed empirical correlation for the thermal conductivity of the MgO-glycerol nanofluid, obtained by regression analysis, is expressed by equation (5.8):

$$\frac{k_{eff}}{k_f} = 1 + Re_p^{0.0603} Pr_f^{0.1066} \phi^{0.9918} \left(\frac{48.4}{k_f}\right)^{0.3646} \quad (5.8)$$

where $k_p = 48.4$. The new correlation has an adjusted R^2 = 0.995 and p-value associated with F-statistic less than 0.001. No collinearity exists between the exploratory parameters as the VIF of exploratory parameters < 10. The comparison between the predicted thermal conductivity ratio from the present model and the experimental results shows an excellent agreement with the maximum relative error of -1.24%, +0.68% and the average relative error of -0.03%.

The normalised $(k_p \,/\, k_f)$ is the major parameter describing the enhancement of the TCR of MgO-glycerol nanofluids, not the Reynolds number for the case of Al_2O_3-water nanofluids. This can be explained by the very low Brownian velocity occurring in the glycerol-based fluid due to its very high viscosity (about 1 530 times bigger than water at 20 ˚C) and capacity to diffuse heat, which is very low compared with its momentum, as opposed to water.

5.9 Recommendation

In addition to the recommendation in Chapter 4 (4.9), the investigation of the thermal conductivity of more glycerol-based metal oxide nanofluids can be done to understand better their impact because the MgO-glycerol and α-Al_2O_3-glycerol nanofluids behave differently. Consequently, a hybrid thermal conductivity correlation for glycerol-based metal oxide nanofluid will be determined.

Another interesting extension of this work would be the investigation of both thermal conductivity and viscosity of 40:60, 60:40 and 80:20 (by mass) glycerol-and-water-mixture-based nanofluids. This research will enable a comparative study of the heat transfer capability between the glycerol-water-based nanofluids and ethylene glycol-water-based nanofluids.

CHAPTER 6: CONCLUSIONS AND RECOMMENDATIONS

6.1 Summary

The study researched the experimental investigation and model development for the effective thermal conductivity of glycerol-based nanofluids prepared with MgO and α-Al_2O_3 nanoparticles. The work analysed the impact of measurable predictors, namely volume fraction, temperature and nanoparticle sizes on the thermal conductivity of glycerol-based nanofluids. The experimental data were compared with the prediction by selected models that might work for glycerol-based nanofluids. The regression analysis evaluated individually and jointly the impact of predictors on the thermal conductivity of glycerol-based nanofluids. As a result, a new model of thermal conductivity of glycerol-based nanofluids was developed.

6.2 Conclusions

The literature review presented in Chapter 2 showed that there was an enhancement in the effective thermal conductivity of nanofluids compared with the base fluids. Several empirical and theoretical correlations were available to model the thermal conductivity of nanofluids. Experimental investigations showed either an agreement or disagreement with the theoretical studies and whether the predictions by the existing mathematical models of the effective thermal conductivity of nanofluids were valid or not.

None of the experimental correlations and available models was based on the glycerol-based nanofluid data. To the best of my knowledge, there were no reported data on the

thermal conductivity of both MgO-glycerol and α-Al_2O_3-glycerol nanofluids at the time of writing.

Chapter 3 discussed the physical characterisation of two different nanoparticles (MgO and Al_2O_3) and the glycerol-based nanofluid preparation. TEM image files of MgO and Al_2O_3 nanoparticles were analysed using ImageJ software (NIH, Bethesda, MD, USA) to ascertain the nanoparticle sizes of the materials. The three MgO nanoparticles respected the lognormal distribution with the mean particle size of 21 ± 1 nm for 20 nm MgO nanoparticle, 119 ± 2 nm for 40 nm MgO nanoparticle and for 104 ± 1 nm for 100 nm MgO nanoparticle respectively, whereas the three α-Al_2O_3 nanoparticles also respected the lognormal distribution with the mean particle size of 55 ± 2 nm for 40 nm α-Al_2O_3 nanoparticle, 31 ± 3 nm for 80 nm α-Al_2O_3 nanoparticle and for 134 ± 1 nm for 100 nm α-Al_2O_3 nanoparticle respectively.

The effective thermal conductivity of the three MgO-glycerol nanofluids increased with sonication time up to an optimum (stable) value of one hour, then became almost constant time. The sonication time of two hours for nanofluid preparation was used in this investigation due to previous experimental results and published research from literature.

Chapter 4 referred to the thermal conductivity of glycerol-based nanofluid results. Experimental results showed that α-Al_2O_3 nanoparticles dispersed in glycerol produced higher thermal conductivity than the base fluid (glycerol). There was a linear increase in TCR with an increase in α-Al_2O_3 nanoparticle volume fraction, with R-square and p-value of 0.822 and 0.000 respectively. Therefore, the volume fraction explained 82.2%

of the variability in the TCR values. The residual and other variables could explain the remaining 17.8% for α-Al_2O_3-glycerol of variation in TCR.

There was no statistical evidence of enhancement of TCR with increasing temperature for α-Al_2O_3-glycerol nanofluid. The TCR of α-Al_2O_3-glycerol increased with decreasing particle size. There was no dependence of effective thermal conductivity of α-Al_2O_3-glycerol nanofluid models with elapsed time up to 50 hours.

The Maxwell, Bruggeman, effective medium, Corcione, Peterson, Shaker, Vajjha models could not explain the enhancement of the thermal conductivity of α-Al_2O_3-glycerol nanofluids consistently.

Equation (4.9) is the developed empirical correlation for the thermal conductivity of α-Al_2O_3-glycerol nanofluids from the Corcione model by regression analysis.

$$\frac{k_{eff}}{k_f} = 1 + Re_p^{0.4377} Pr_f^{0.9400} \phi^{1.0475} \left(\frac{40}{k_f}\right)^{0.6661} \quad (4.9)$$

The regression analysis provided evidence that the novel model was statistically significant (p-value of 0.0000 and an unadjusted R-square of 0.980), with the maximum relative error of +1.57%, -2.37% and the average of -0.03%. The new model illustrated that the thermal conductivity ratio increased with an increase in volume fraction, decreased with a rise in nanoparticle size and slightly decreased with a temperature rise.

The Pr_f was the major parameter describing the enhancement of TCR of α-Al_2O_3-glycerol nanofluids, as opposed to the nanoparticle Reynolds number for the case of α-Al_2O_3-deionized water nanofluid. The high exponent value of the Prandtl number and

the high value of glycerol Prandtl number, which was about 1 800 times bigger than water, could explain the main effect of the Prandtl number on the effective thermal conductivity of α-Al_2O_3-glycerol nanofluid at 20 ˚C.

Chapter 5 presented the experimental and theoretical investigation of the MgO-glycerol nanofluid. There was a linear increase in TCR with an increase in MgO nanoparticle volume fraction, with R-square of 0.986 and p-value of F-statistic of 0.0000. Therefore, the volume fraction explained 96.6% of the variability of the thermal conductivity. Residual and other variables could explain the remaining 1.4% for MgO-glycerol of variation in TCR.

The TCR of MgO-glycerol remained constant with decreasing particle size. The linear regression analysis of effective thermal conductivity with elapsed time revealed that the MgO-glycerol nanofluid remained stable for at least 50 hours after preparation.

The Maxwell, Bruggeman, effective medium, Corcione, Peterson, Shake and Vajjha models failed to predict consistently the thermal conductivity ratio for MgO-glycerol nanofluids of volume fractions ranging from 0.5% to 4%, measured in the temperature range of 20 ˚C to 45 ˚C in all the conditions. Each existing correlation model worked for the particular nanofluid and condition.

The developed empirical correlation for the thermal conductivity of the MgO-glycerol nanofluid, obtained by the same procedure as the α-Al_2O_3-glycerol model, is expressed by equation (5.8):

$$\frac{k_{eff}}{k_f} = 1 + Re_p^{0.0603} Pr_f^{0.1066} \phi^{0.9918} \left(\frac{48.4}{k_f}\right)^{0.3646} \qquad (5.8)$$

The new correlation, with an adjusted R-square = 0.995 and p-value associated to F-statistic less than 0.001, reveals no collinearity between the independent variables ($VIF < 10$). There is an an excellent agreement with the maximum relative error of -1.24%, +0.68% and the average relative error of -0.03% between the predicted thermal conductivity ratio from the present model and the experimental results of MgO-glycerol nanofluid.

The normalised $(k_p \,/\, k_f)$ was the major parameter describing the enhancement of the TCR of MgO-glycerol for 1% volume fraction nanofluid, not the nanoparticle Reynolds number for the case of Al_2O_3-water nanofluids. The very low Brownian velocity occurring in the glycerol-based fluid due to its very high viscosity (about 1 530 bigger than water at 20 ˚C) and capacity to diffuse heat, which was very low compared with its momentum, as opposed to water, could explain the impact of $(k_p \,/\, k_f)$.

Altogether, the variability thermal conductivity of MgO-glycerol nanofluid could be explained only by the volume fraction regardless of the particle size of nanoparticle because of its high R-square of 0.987 compared with 0.82 for α-Al_2O_3-glycerol nanofluid. The impact of particle size was more prominent for the α-Al_2O_3-glycerol than for the MgO-glycerol nanofluid. The main parameter in the thermal conductivity of MgO-glycerol nanofluid was the $(k_p \,/\, k_f)$ whereas it was the Prandtl number for the α-Al_2O_3-glycerol nanofluid. Both nanoparticles behaved differently in the base fluid, glycerol.

6.3 Recommendations

Before the thermal conductivity investigation, the nanoparticle's physical characterisation must be determined to ascertain the nanoparticle composition and size distribution, which are crucial in the nanofluid behaviour.

The study could be extended to hydrodynamic size distribution and zeta potential of the glycerol-based nanofluids. This approach could provide a more comprehensive understanding of both the stability of nanofluid and the thermal conductivity behaviour of glycerol-based nanofluids.

Other research could be the investigation of the thermal conductivity of more glycerol-based metal oxide particles to understand better the behaviour of the different metal oxide nanoparticles because the MgO-glycerol and α-Al_2O_3-glycerol nanofluids behaved differently.

Also, further research could be the investigation of viscosity of glycerol-metal oxide nanofluids to understand the impact on the thermal conductivity of glycerol-based nanofluids.

Another interesting extension of this work could be the investigation of both thermal conductivity and viscosity of 60:40 and 80:20 (by mass) glycerol-and-water-mixture-based nanofluids. This research will enable a comparative study on the heat transfer capability between the glycerol-water-based nanofluids and ethylene-glycol water-based nanofluids.

REFERENCES

[1] R. S. Vajjha and D. K. Das, "Experimental determination of thermal conductivity of three nanofluids and development of new correlations," *International Journal of Heat and Mass Transfer,* vol. 52, pp. 4675-4682, 2009.

[2] M. Dehghandokht, M. G. Khan, A. Fartaj, and S. Sanaye, "Flow and heat transfer characteristics of water and ethylene glycol-water in a multi-port serpentine meso-channel heat exchanger," *International Journal of Thermal Sciences,* vol. 50, pp. 1615-1627, 2011.

[3] S. Senthilraja, M. Karthikeyan, and R.Gangadevi, "Nanofluid applications in future automobiles: comprehensive review of existing data," *Nano-Micro Letters,* vol. 2, pp. 306-310, 2011.

[4] ASTM International. *Proposed ASTM Engine Coolant Standards Focus on Glycerin*. ASTM International new releases, April, 2010. Available: http://www.astmnewsroom.org/default.aspx?pageid=2115 . [Online; accessed 14 April 2014].

[5] F. Yang, M. A. Hanna, and R. Sun, "Value-added uses for crude glycerol-a byproduct of biodiesel production," *Biotechnology for Biofuels,* vol. 5, pp. 1-10, 2012.

[6] R. Ciriminna, C. D. Pina, M. Rossi, and M. Pagliaro, "Understanding the glycerol market," *European Journal of Lipid Science and Technology,* vol. 116, pp. 1432-1439, 2014.

[7] M. J. Kao and C. R. Lin, "Evaluating the role of spherical titanium oxide nanoparticles in reducing friction between two pieces of cast iron," *Journal of Alloys and Compounds*, vol. 483, pp. 456-459, 2009.

[8] Z. Huang, W. Kan, Y. Lu, T. Cheng, L. Yu, and X. Hu, "Effect of nanoparticle suspensions on liquid fuel hot-plate ignition," *Journal of Nanotechnology in Engineering and Medicine*, vol. 5, no. 031004, pp. 1-5, 2014.

[9] H. Liu, M. Bai, J. Lv, L. Zhang, P. Wang, and C. Hu, "Experimental study and analysis of lubricants dispersed with nanodiamond particles on diesel engine," *Journal of Nanotechnology in Engineering and Medicine*, vol. 5, no. 041001, pp. 1-7, 2014.

[10] SDA. Glycerine: An Overview. The soap and detergent association. New York, 1990. Available: http://www.google.co.za/url?sa=t&rct=j&q=&esrc=s&source=web&cd=1&ved=0CCEQFjAA&url=http%3A%2F%2Fwww.aciscience.org%2Fdocs%2Fglycerine_-_an_overview.pdf&ei=Rp2MVKvmGsTlUorZgPgD&usg=AFQjCNFTcuFrrwHDwlJ9QytlekbmxFN_ow . [Online; accessed 14 April 2014].

[11] R. M. Mostafizur, M. H. U. Bhuiyan, R. Saidur, and A. R. Abdul Aziz, "Thermal conductivity variation for methanol based nanofluids," *International Journal of Heat and Mass Transfer*, vol. 76, pp. 350-356, 2014.

[12] K. S. Suganthi and K. S. Rajan, "A formulation strategy for preparation of ZnO-propylene glycol-water nanofluids with improved transport properties," *International Journal of Heat and Mass Transfer*, vol. 71, pp. 653-663, 2014.

[13] A. N. Al-Shamani, M. H. Yazdi, M. Alghoul, A. M. Abed, M. H. Ruslan, S. Mat and K. Sopian, "Nanofluids for improved efficiency in cooling solar collectors-a review," *Renewable and Sustainable Energy Reviews*, vol. 38, pp. 348-367, 2014.

[14] M. J. Pastoriza-Gallego, L. Lugo, D. Cabaleiro, J. L. Legido, and M. M. Piñeiro, "Thermophysical profile of ethylene glycol-based ZnO nanofluids," *The Journal of Chemical Thermodynamics*, vol. 73, pp. 23-30, 2014.

[15] H. Xie, W. Yu, Y. Li, and L. Chen, "Discussion on the thermal conductivity enhancement of nanofluids," *Nanoscale Resource Letters*, no. 124, pp. 1-12, 2011.

[16] H. Ş. Aybar, M. Sharifpur, M. R. Azizian, M. Mehrabi, and J. P. Meyer, "A review of thermal conductivity models for nanofluids," *Heat Transfer Engineering*, vol. 36, pp. 1085-1110, 2014.

[17] N. Sohrabi, N. Masoumi, A. Behzadmehr, and S. M. H. Sarvari, "A simple analytical model for calculating the effective thermal conductivity of nanofluids," *Heat Transfer - Asian Research*, vol. 39, pp. 141-150, 2010.

[18] S. U. S. Choi, Z. G. Zhang, W. Yu, F. E. Lockwood, and E. A. Grulke, "Anomalous thermal conductivity enhancement in nanotube suspensions," *Applied Physics Letters*, vol. 79, pp. 2252-2254, 2001.

[19] P. Mukesh Kumar, J. Kumar, R. Tamilarasan, S. Sendhilnathan, and S. Suresh, "Review on nanofluids theoretical thermal conductivity models," *Engineering Journal*, vol. 19, pp. 67-83, 2015.

[20] Z. Mingzheng, X. Guodong, L. Jian, C. Lei, and Z. Lijun, "Analysis of factors influencing thermal conductivity and viscosity in different kinds of surfactant solutions," *Experimental Thermal and Fluid Science*, vol. 36, pp. 22-29, 2012.

[21] S. Halelfadl, T. Maré, and P. Estellé, "Efficiency of carbon nanotubes water based nanofluids as coolants," *Experimental Thermal and Fluid Science*, vol. 53, pp. 104-110, 2014.

[22] S. M. S. Murshed, "Simultaneous measurement of thermal conductivity, thermal diffusivity, and specific heat of nanofluids," *Heat Transfer Engineering*, vol. 33, pp. 722-731, 2012.

[23] W. Yu, H. Xie, L. Chen, and Y. Li, "Investigation of thermal conductivity and viscosity of ethylene glycol based ZnO nanofluid," *Thermochimica Acta*, vol. 491, pp. 92-96, 2009.

[24] D.-H. Yoo, K. S. Hong, and H.-S. Yang, "Study of thermal conductivity of nanofluids for the application of heat transfer fluids," *Thermochimica Acta*, vol. 455, pp. 66-69, 2007.

[25] F. Duan, *Thermal Property Measurement of Al_2O_3-Water Nanofluids*. Smart Nanopaticles Technology, Dr Abbas Ashim (Ed.), INTECH, 2012.

[26] D. Kumar, H. Patel, V. Kumar, T. Sundararajan, T. Pradeep, and S. Das, "Model for heat conduction in nanofluids," *Physical Review Letters*, vol. 93, no. 14, pp. 1-4, 2004.

[27] H. Jiang, Q. Xu, C. Huang, and L. Shi, "Effect of temperature on the effective thermal conductivity of n-tetradecane-based nanofluids containing copper nanoparticles," *Particuology*., 2015.

[28] K. D. Kihm, C. H. Chon, J. S. Lee, and S. U. Choi, "A new heat propagation velocity prevails over Brownian particle velocities in determining the thermal conductivities of nanofluids," *Nanoscale Research Letters*, vol. 6, no. 361, pp. 1-9, 2011.

[29] M. J. Pastoriza-Gallego, L. Lugo, J. L. Legido and M. M. Piñeiro, "Thermal conductivity and viscosity measurements of ethylene glycol-based Al_2O_3 nanofluids," *Nanoscale Research Letters*, vol. 6, pp. 1-11, 2011.

[30] X. Wang, X. Xu and SUS. Choi, "Thermal conductivity of nanoparticle-fluid mixture," *Journal of Thermophysics and Heat Transfer*, vol. 13, pp. 474-480, 1999.

[31] C. Sitprasert, P. Dechaumphai, and V. Juntasaro, "A thermal conductivity model for nanofluids including effect of the temperature-dependent interfacial layer," *Journal of Nanoparticle Research*, vol. 11, pp. 1465-1476, 2009.

[32] S. K. Das, N. Putra, P. Thiesen, and W. Roetzel, "Temperature dependence of thermal conductivity enhancement for nanofluids," *Journal of Heat Transfer*, vol. 125, pp. 567-574, 2003.

[33] M. Ghanbarpour, E. Bitaraf Haghigi, and R. Khodabandeh, "Thermal properties and rheological behavior of water based Al_2O_3 nanofluid as a heat transfer fluid," *Experimental Thermal and Fluid Science,* vol. 53, pp. 227-235, 2014.

[34] C. H. Li and G. P. Peterson, "Experimental investigation of temperature and volume fraction variations on the effective thermal conductivity of nanoparticle suspensions (nanofluids)," *Journal of Applied Physics,* vol. 99, no. 084314, pp. 1-8, 2006.

[35] H. Xie, W. Yu, and W. Chen, "MgO nanofluids: higher thermal conductivity and lower viscosity among ethylene glycol-based nanofluids containing oxide nanoparticles," *Journal of Experimental Nanoscience,* vol. 5, pp. 463-472, 2010.

[36] M. Kole and T. K. Dey, "Thermophysical and pool boiling characteristics of ZnO-ethylene glycol nanofluids," *International Journal of Thermal Sciences,* vol. 62, pp. 61-70, 2012.

[37] R. S. Khedkar, S. S. Sonawane, and K. L. Wasewar, "Influence of CuO nanoparticles in enhancing the thermal conductivity of water and monoethylene glycol based nanofluids," *International Communications in Heat and Mass Transfer,* vol. 39, pp. 665-669, 2012.

[38] L. Syam Sundar, E. Venkata Ramana, M. K. Singh, and A. C. M. Sousa, "Thermal conductivity and viscosity of stabilized ethylene glycol and water mixture Al_2O_3 nanofluids for heat transfer applications: an experimental study,"

International Communications in Heat and Mass Transfer, vol. 56, pp. 86-95, 2014.

[39] C. Pang, J. W. Lee, and Y. T. Kang, "Review on combined heat and mass transfer characteristics in nanofluids," *International Journal of Thermal Sciences*, vol. 87, pp. 49-67, 2015.

[40] X.-Q. Wang and A. S. Mujumdar, "Heat transfer characteristics of nanofluids: a review," *International Journal of Thermal Sciences*, vol. 46, pp. 1-19, 2007.

[41] P. Keblinski, S. R. Phillpot, S. U. S. Choi, and J. A. Eastman, "Mechanisms of heat flow in suspensions of nano-sized particles (nanofluids)," *International Journal of Heat and Mass Transfer*, vol. 45, pp. 855-863, 2002.

[42] Y. Feng and C. Kleinstreuer, "Nanofluid convective heat transfer in a parallel-disk system," *International Journal of Heat and Mass Transfer*, vol. 53, pp. 4619-4628, 2010.

[43] Y. Li, J. e. Zhou, S. Tung, E. Schneider, and S. Xi, "A review on development of nanofluid preparation and characterization," *Powder Technology*, vol. 196, pp. 89-101, 2009.

[44] M. Sharifpur, T. Ntumba, and J. P. Meyer, "Parametric analysis of effective thermal conductivity models for nanofluids," *ASME 2012 International Mechanical Engineering Congress and Exposition*, pp. 1-11, 2012.

[45] M. Chandrasekar, S. Suresh, and A. Chandra Bose, "Experimental investigations and theoretical determination of thermal conductivity and

viscosity of Al_2O_3/water nanofluid," *Experimental Thermal and Fluid Science,* vol. 34, pp. 210-216, 2010.

[46] Q. Xue and W. M. Xu, A model of thermal conductivity of nanofluids with interfacial shells, *Materials Chemistry and Physics*, vol. 90, no. 2–3, pp. 298-301, 2005.

[47] B. X. Wang, L. P. Zhou, and X. F. Peng, "A fractal model for predicting the effective thermal conductivity of liquid with suspension of nanoparticles," *International Journal of Heat and Mass Transfer,* vol. 46, pp. 2665-2672, 2003.

[48] R. Prasher, P. Bhattacharya, and P. E. Phelan, "Thermal conductivity of nanoscale colloidal solutions (nanofluids)," *Physical Review Letters*, vol. 94, no. 25901, pp. 1-4, 2005.

[49] E. Timofeeva, A. N. Gavrilov, J. M. McCloskey, Y. V. Tolmachev, S. Sprunt, L. M. Lopatina and J. V. Selinger, "Thermal conductivity and particle agglomeration in alumina nanofluids: experiment and theory," *Physical Review E,* vol. 76, no. 0612301, pp. 1-16, 2007.

[50] W. Yu and S. U. S. Choi, "The Role of interfacial layers in the enhanced thermal conductivity of nanofluids: a renovated Maxwell model," *Journal of Nanoparticle Research*, vol. 5, no. 1-2, pp. 167-171, 2003.

[51] R. Prasher, P. Bhattacharya, and P. E. Phelan, "Brownian-motion-based convective-conductive model for the effective thermal conductivity of nanofluids," *Journal of Heat Transfer*, vol. 128, pp. 588-595, 2006.

[52] Y. Feng, B. Yu, P. Xu, and M. Zou, "The effective thermal conductivity of nanofluids based on the nanolayer and the aggregation of nanoparticles," *Journal of Physics D: Applied Physics*, vol. 40, no. 10, pp. 3164-3171, 2007.

[53] M. Akbari, N. Galanis, and A. Behzadmehr, "A new model for nanofluid conductivity based on the effects of clustering due to Brownian motion," *Heat Transfer Asian Research*, vol. 40, no. 4, pp. 352-368, 2011.

[54] K. Khanafer and K. Vafai, "A critical synthesis of thermophysical characteristics of nanofluids," *International Journal of Heat and Mass Transfer*, vol. 54, pp. 4410-4428, 2011.

[55] M. Corcione, "Empirical correlating equations for predicting the effective thermal conductivity and dynamic viscosity of nanofluids," *Energy Conversion and Management*, vol. 52, pp. 789-793, 2011.

[56] T. Yiamsawasd and S. Wongwises, "Measurement of the thermal conductivity of titania and alumina nanofluids," *Thermochimica Acta*, vol. 545, pp. 48-56, 2012.

[57] M. Shaker, E. Birgersson, and A. Mujumdar, "Extended Maxwell model for the thermal conductivity of nanofluids that accounts for nonlocal heat transfer," *International Journal of Thermal Sciences*, vol. 84, pp. 260-266, 2014.

[58] Y. Xuan, Q. Li, and W. Hu, "Aggregation structure and thermal conductivity of nanofluids," *AIChE Journal*, vol. 49, pp. 1038-1043, 2003.

[59] W. Duangthongsuk and S. Wongwises, "Measurement of temperature-dependent thermal conductivity and viscosity of TiO_2-water nanofluids," *Experimental Thermal and Fluid Science,* vol. 33, pp. 706-714, 2009.

[60] H. Xie, M. Fujii, and X. Zhang, "Effect of interfacial nanolayer on the effective thermal conductivity of nanoparticle-fluid mixture," *International Journal of Heat and Mass Transfer,* vol. 48, pp. 2926-2932, 2005.

[61] J. A. Eastman, S. U. S. Choi, S. Li, W. Yu, and L. J. Thompson, "Anomalously increased effective thermal conductivities of ethylene glycol-based nanofluids containing copper nanoparticles," *Applied Physics Letters,* vol. 78, pp. 718-720, 2001.

[62] J. Li and C. Kleinstreuer, "Thermal performance of nanofluid flow in microchannels," *International Journal of Heat and Fluid Flow,* vol. 29, pp. 1221-1232, 2008.

[63] M. Kole and T. K. Dey, "Role of interfacial layer and clustering on the effective thermal conductivity of CuO-gear oil nanofluids," *Experimental Thermal and Fluid Science,* vol. 35, pp. 1490-1495, 2011.

[64] C. Sitprasert, P. Dechaumphai, and V. Juntasaro, "A thermal conductivity model for nanofluids including effect of the temperature-dependent interfacial layer," *Journal of Nanoparticle Research,* vol. 11, pp. 1465-1476, 2009.

[65] M. Corcione, "Rayleigh-Bénard convection heat transfer in nanoparticle suspensions," *International Journal of Heat and Fluid Flow,* vol. 32, pp. 65-77, 2011.

[66] S. I. Jeol. *JEM-2100F Transmission Electron Microscope*, 2015. Available: http://www.jeolusa.com/PRODUCTS/TransmissionElectronMicroscopes%28TEM%29/200kV/JEM-2100F/tabid/208/Default.aspx . [Online; accessed 6 March 2015].

[67] J. Ananpattarachai, P. Kajitvichyanukul, and S. Seraphin, "Visible light absorption ability and photocatalytic oxidation activity of various interstitial N-doped TiO_2 prepared from different nitrogen dopants," *Journal of Hazardous Materials*, vol. 168, pp. 253-261, 2009.

[68] C. Suryanarayana and M. G. Norton, *X-ray Diffraction: A Practical Approach.* vol. 4, New York, USA: Plenum Publishing Corporation, 1998.

[69] A. Garbout, S. Bouattour, A. B. do Rego, A. Ferraria, and A. Kolsi, "Synthesis, Raman and X-ray diffraction investigations of rubidium-doped Gd 1.8 Ti 2 O 6.7 pyrochlore oxide via a sol–gel process," *Journal of Crystal Growth*, vol. 304, pp. 374-382, 2007.

[70] C. Oprea, V. Ciupina, and G. Prodan, "Investigation of nanocrystals using TEM micrographs and electron diffraction technique," *Romanian Journal of Physics*, vol. 53, pp. 223-230, 2008.

[71] S. A. Speakman, "Estimating Crystallite Size Using XRD," MIT Center for Materials Science and Engineering, Cambridge, USA. 2012.

[72] V. Baecker, "Workshop: Image processing and analysis with ImageJ and MRI Cell Image Analyzer," Montpellier RIO Imaging, Languedoc-Roussillon, France. 30 April 2010.

[73] E. Reschenhofer, "The Bimodality Principle," *Journal of Statistics Education* vol. 9, pp. 1-14, 2001.

[74] S. Horiba. *A guidebook to particle size analysis*, November 5th, 2012. Available: https://www.horiba.com/fileadmin/uploads/.../PSA/PSA_Guidebook.pdf . [Online; accessed 3 December 2014].

[75] N. R. Dhineshbabu, G. Karunakaran, R. Suriyaprabha, P. Manivasakan, and V. Rajendran, "Electrospun MgO/nylon 6 hybrid nanofibers for protective clothing," *Nano-Micro Letters*, vol. 6, pp. 46-54, 2014.

[76] U. T. Hielscher. *UP200H / UP200S – Ultrasonic Power for the Lab*, 2014. Available: http://www.hielscher.com/200s_p.htm . [Online; accessed 3 April 2014].

[77] M. Kole and T. K. Dey, "Effect of prolonged ultrasonication on the thermal conductivity of ZnO-ethylene glycol nanofluids," *Thermochimica Acta*, vol. 535, pp. 58-65, 2012.

[78] D. Devices, Inc. KD2 Pro thermal properties analyzer operator's manual version 4, Decagon Devices, Pullman, WA, 5 May 2015. Available: http://www.decagon.com/education/kd2-pro-manual/. [Online; accessed 6 June 2015].

[79] F. P. Incropera and D. P. DeWitt, *Introduction to Heat Transfer*. New York, USA: John Wiley & Sons, 1996.

[80] G. F. Hewitt, *Heat Exchanger Design Handbook 2008: Physical Properties*. New York, USA: Begell House, 2008.

[81] R. Saleh, N. Putra, R. E. Wibowo, W. N. Septiadi, and S. P. Prakoso, "Titanium dioxide nanofluids for heat transfer applications," *Experimental Thermal and Fluid Science,* vol. 52, pp. 19-29, 2014.

[82] B. H. Salman, H. A. Mohammed, K. M. Munisamy, and A. S. Kherbeet, "Characteristics of heat transfer and fluid flow in microtube and microchannel using conventional fluids and nanofluids: a review," *Renewable and Sustainable Energy Reviews*, vol. 28, pp. 848-880, 2013.

[83] R. S. Figliola and D. E. Beasley, "Theory and design for mechanical measurements," 3rd ed.: John Wiley & Sons, 2000.

[84] I. M. Mahbubul, S. A. Fadhilah, R. Saidur, K. Y. Leong, and M. A. Amalina, "Thermophysical properties and heat transfer performance of Al2O3/R-134a nanorefrigerants," *International Journal of Heat and Mass Transfer*, vol. 57, pp. 100-108, 2013.

[85] Y. Xuan, "Heat transfer enhancement of nanofuids," *International Journal of Heat and Fluid Flow*, vol. 21, pp. 58-64, 2000.

[86] W. Yu, H. Xie, L. Chen, and Y. Li, "Enhancement of thermal conductivity of kerosene-based Fe3O4 nanofluids prepared via phase-transfer method," *Colloids and Surfaces A: Physicochemical and Engineering Aspects*, vol. 355, pp. 109-113, 2010.

[87] K. S. Suganthi and K. S. Rajan, "Temperature induced changes in ZnO-water nanofluid: zeta potential, size distribution and viscosity profiles," *International Journal of Heat and Mass Transfer*, vol. 55, pp. 7969-7980, 2012.

[88] S. M. S. Murshed, K. C. Leong, and C. Yang, "Investigations of thermal conductivity and viscosity of nanofluids," *International Journal of Thermal Sciences*, vol. 47, pp. 560-568, 2008.

[89] M. S. Liu, M. C. C. Lin, C. Y. Tsai, and C. C. Wang, "Enhancement of thermal conductivity with Cu for nanofluids using chemical reduction method," *International Journal of Heat and Mass Transfer*, vol. 49, pp. 3028-3033, 2006.

[90] K. S. Hong, T. K. Hong, and H. S. Yang, "Thermal conductivity of Fe nanofluids depending on the cluster size of nanoparticles," *Applied Physics Letters*, vol. 88, no. 031901, pp. 1-3, 2006.

[91] D. G. Kleinbaum, L. L. Kupper, A. Nizam, and K. E. Muller, *Applied regression analysis and other multivariable methods*, 4th ed.: Thomson Books/Cole, 2008.

[92] C. H. Chon, K. D. Kihm, S. P. Lee, and S. U. S. Choi, "Empirical correlation finding the role of temperature and particle size for nanofluid (Al_2O_3) thermal conductivity enhancement," *Applied Physics Letters*, vol. 87, no. 153107, pp. 1-3, 2005.

[93] Y. A. Cengel, *Heat and Mass Transfer: A Practical Approach.* New York: McGraw-Hill, pp 854 - 862, 2006.

[94] C. T. Ragsdale, *Managerial Decision Modeling*, 6th ed.: South-Western, 2011.

[95] P. Kennedy, *A Guide to Econometrics*, 6th ed.: Blackwell, 2008.

Appendix A: Uncertainty analysis

A.1 Introduction

An uncertainty analysis is conducted on the thermal conductivity ratio of both MgO-glycerol and α-Al_2O_3-glycerol nanofluids.

A.2 Uncertainty of the thermal conductivity ratio

The thermal conductivity ratio of nanofluids (TCR) is not directly measured but calculated from the measurable variables as provided in the formula below:

$$TCR = \frac{k_{eff}}{k_f} \tag{A.1}$$

where k_{eff} and k_f are the effective thermal conductivity of the nanofluid and the thermal conductivity of the base fluid. The uncertainty propagation of TCR is given:

$$u_{TCR} = \pm\sqrt{\left(u_{k_{eff}} * \frac{\partial TCR}{\partial k_{eff}}\right)^2 + \left(u_{k_f} * \frac{\partial TCR}{\partial k_f}\right)^2} \tag{A.2}$$

$$u_{TCR} = \pm\sqrt{\left(\frac{\partial TCR}{\partial k_{eff}}\delta k_{eff}\right)^2 + \left(\frac{\partial TCR}{\partial k_f}\delta k_f\right)^2} \tag{A.3}$$

$$u_{TCR} = \pm\sqrt{\left(\frac{\delta k_{eff}}{k_f}\right)^2 + \left(\frac{-k_{eff}}{[k_f]^2}\delta k_f\right)^2} \tag{A.3}$$

where $k_{eff}, k_f, \delta k_{eff}, \delta k_f$ are the effective thermal conductivity of nanofluid, the thermal conductivity of glycerol, the standard deviation of the effective thermal conductivity of nanofluid and the standard deviation of glycerol respectively.

Appendix B: Regression analysis

B.1 Introduction

In order to identify the significant relationship between the thermal conductivity ratio of nanofluid and one or more of the predictors' variables, a regression analysis is used.

B.2 Guidelines for a good regression model

The guidelines for a good regression model [91, 94, 95] are as follows:

1. The regression model must strongly fit the data.

2. Most of the independent variables should be significant to explain the dependent variable, i.e. the t-test of most of the predictors or independent variables should be significant (p-value < 0.05 for 95% confidence).

3. The independent variables should be jointly significant to influence the dependent variable. The F-test of the model and t-test of most of the predictors should be significant at 95% confidence, i.e. p-value < 0.05.

4. Residual criteria: The residuals are not correlated, residuals must follow the normal distribution and residuals must be homoscedastic, i.e. the variance of residuals from the model must be constant.

B.3 Regression models

The target of regression analysis is to estimate the population regression model from the sample regression model [91, 94, 95].

B.3.1 Simple linear regression

The population regression model of a single predictor variable is written as follows:

$$Y = \alpha + \beta_1 X_1 + \varepsilon_1 \quad \text{(B.1)}$$

where α, β_1 and ε_1 are the intercept, slope or regression coefficient and error term respectively.

The sample regression model of a single predictor variable is written as follows:

$$Y = a + b_1 X_1 + \varepsilon_1 \quad \text{(B.2)}$$

Where a, b_1 and ε_1 are the intercept, slope or regression coefficient and error term respectively.

The coefficients a and b_1 are determined mathematically to minimise the sum of squared deviations (SSE) between the predicted value and measured experimental data of TCR. The linear regression analysis will test if the linear model is statistically significant. At 95% confidence, the null hypothesis H_0 (b_1 = 0) is accepted when the associated p-value of F-statistic is > 0.05, which means that there is no linear relationship between the dependent variable and the independent variable. The best model is either a naive model, which is the average value of the dependent variable, or a non-linear model. Otherwise, reject the null hypothesis and accept the alternative hypothesis H_a ($b_1 \neq 0$) [94]. The R-square is also computed to determine the proportion of variability of independent variable explained by the dependent variable.

B.3.2 Multiple regression analysis

The thermal conductivity ratio of nanofluids is likely to be influenced by some combination of several parameters. The multiple regression can precisely evaluate the effect of combined parameters on the TCR. The measured parameters (predictors) are

particle volume fraction, temperature and particle size. The population regression model of three predictor variables is written as follows:

$$Y = \alpha + \beta_1 X_1 + \beta_2 X_2 + \beta_3 X_3 + \varepsilon \quad \text{(B.3)}$$

where α, β_k and ε are the intercept, partial slope or partial regression coefficient and error term respectively.

The sample regression model of three predictor variables is written as follows:

$$Y = a + b_1 X_1 + b_2 X_2 + \cdots + b_k X_k \quad \text{(B.4)}$$

where a and b_k are the sample estimate of α and the sample estimate of β_k respectively, b_k is a change in Y for each one increment change in X_k.

The coefficients a and b_k are determined mathematically to minimise the sum of squared deviations (SSE) between the predicted values and measured experimental data of TCR [94].

The null hypothesis is H_0: $\beta_1 = \beta_2 = \cdots = \beta_k = 0$, whereas the alternative hypothesis is H_a: most $\beta_k \neq 0$. In addition to the F-statistic, the t-statistic of all the β_k must be determined and statistically analysed at 95% confidence interval as presented in Section B.2. The adjusted R-square is also computed to determine the proportion of independent variable explained by the dependent variables jointly.

Equation (B.5) [95] is inherently linear since it can be rewritten in the form B.6:

$$Y = AX_1^B X_2^C X_3^D \quad \text{(B.5)}$$

$$ln(Y) = ln(A) + Bln(X_1) + Cln(X_2) + Dln(X_3) \quad \text{(B.6)}$$

$$Y^* = A^* + BX_1^* + CX_2^* + DX_3^* \quad \text{(B.7)}$$

The multiple regression linear is applied to equation (B.7).

B.3.3 Multicollinearity

Multicollinearity describes the situation where there is a high correlation between two or more predictor variables. It should be avoided in a regression model as it increases the uncertainty associated with the parameter estimates (b_k). The variance inflation factor (VIF) verifies the collinearity of X_j in the model:

$$VIF_j = \frac{1}{(1 - R_j^2)} \tag{B.8}$$

where R_j^2 is multiple R square of X_j independent variable. X_j is correlated to the other independent variable when $VIF > 10$ [91, 95]. The residual criteria are similar to the linear regression analysis presented in Section B.2.

B.4 New model of the thermal conductivity of glycerol-based nanofluids

Equation 2.13 is the generalised form of the Corcione model [55].

$$\frac{k_{eff}}{k_f} = 1 + F * Re^A Pr^B \phi^C \left(\frac{T}{T_{fr}}\right)^D \left(\frac{k_p}{k_f}\right)^E \tag{B.9}$$

where A, B, C, D, E and F are constant.

The parameters $Re, Pr, T, T_{fr}, k_p, k_f$ and k_{eff} are defined in Section 4.7.

The Corcione model is inherently linear since it can be transformed in equation

$$ln\left(\frac{k_{eff}}{k_f}-1\right)=ln(F)+Aln(Re)+Bln(Pr)+Cln(\phi)+Dln\left(\frac{T}{T_{fr}}\right)+Eln\left(\frac{k_p}{k_f}\right) \quad \text{(B.10)}$$

$$k_{eff}^{*}=F^{*}+ARe^{*}+BPr^{*}+C\phi^{*}+D\left(\frac{T}{T_{fr}}\right)^{*}+E\left(\frac{k_p}{k_f}\right)^{*} \quad \text{(B.11)}$$

where k_{eff}^{*} is $ln\left(\frac{k_{eff}}{k_f}-1\right)$, F^{*} is $ln(F)$, $Re^{*}$is $ln(Re)$, $Pr^{*}$is $ln(Pr)$, $\phi^{*}$is $ln(\phi)$, $\left(\frac{T}{T_{fr}}\right)^{*}$ is $ln\left(\frac{T}{T_{fr}}\right)$ and $\left(\frac{k_p}{k_f}\right)^{*}$ is $ln\left(\frac{k_p}{k_f}\right)$

The multiple regression linear is applied to equation (B.11).